Durham University

Durham E-Theses

Development of a Novel In Vitro Bioengineered Human Breast Ductal Mucosal Model to Investigate the Invasive Properties of Breast Cancer During its Development.

WEBB, ETHAN,JAMES

How to cite:

WEBB, ETHAN,JAMES (2023) *Development of a Novel In Vitro Bioengineered Human Breast Ductal Mucosal Model to Investigate the Invasive Properties of Breast Cancer During its Development.*, Durham theses, Durham University. Available at Durham E-Theses Online: http://etheses.dur.ac.uk/15267/

Use policy

The full-text may be used and/or reproduced, and given to third parties in any format or medium, without prior permission or charge, for personal research or study, educational, or not-for-profit purposes provided that:

- a full bibliographic reference is made to the original source
- a link is made to the metadata record in Durham E-Theses
- the full-text is not changed in any way

The full-text must not be sold in any format or medium without the formal permission of the copyright holders.

Please consult the full Durham E-Theses policy for further details.

Academic Support Office, The Palatine Centre, Durham University, Stockton Road, Durham, DH1 3LE
e-mail: e-theses.admin@durham.ac.uk Tel: +44 0191 334 6107
http://etheses.dur.ac.uk

Higher Degree Entry Form

This form should be submitted to the Curriculum, Learning and Assessment Service along with two soft-bound copies of the thesis.

Personal Details:

DEGREE FOR WHICH THESIS IS BEING SUBMITTED:	MSc by Research
STUDENT ID:	000964883
SURNAME (Block Capitals):	WEBB
FORENAMES (Block Capitals):	ETHAN JAMES
RCUK FUNDED (Yes / No):[1]	NO
DEPARTMENT:	BIOSCIENCES
COLLEGE:	Grey College
ADDRESS TO WHICH ALL CORRESPONDENCE SHOULD BE SENT:	3 Parkway, Shudy Camps, Cambridge, CB21 4RQ
NON-DURHAM EMAIL ADDRESS:	ethan.webb@btinternet.com

Candidate Declaration:

I understand that:

1. if award of the degree is approved following examination of my thesis, I will be required to deposit with the University one electronic copy of the thesis which will be listed in on-line catalogues and databases.
2. in the interests of scholarship, the electronic copy will be made available in the University's digital repository to a wide variety of people and institutions – including automated agents – via the World Wide Web.
3. an electronic copy may also be included in the British Library Electronic Thesis On-line Service (EThOS)
4. I own the copyright in my work and am free to publish the thesis in its present or future versions. The University is granted non-exclusive rights to make the thesis available as described.
5. to ensure preservation and accessibility via future computer systems, the University may need to amend the storage format of the electronic copy.
6. I may request an embargo not exceeding three years on public access to my work for the protection of patent applications or other intellectual property or third party rights; it is not usual for access to theses to be withheld and good reason for the request must be provided.

I confirm that:

7. the thesis conforms with the prescribed word length set out in the **Core Regulations for Research Degrees by thesis or composition** OR I have approval on behalf of my Academic Department to submit a thesis which exceeds the prescribed length.
8. no part of the material offered has previously been submitted by me for a degree in this or any other University.
9. if material has been generated through joint work, my independent contribution has been clearly indicated.
10. I have exercised reasonable care to ensure that the thesis is original and does not to the best of my knowledge infringe any third party's copyright or other intellectual property right. Material from the work of others has been acknowledged and quotations and paraphrases suitably indicated.
11. I wish to request that public access to my thesis is withheld for ……. years and I have completed and attached the form '**Restricting access to my thesis'.**[1]

Signature:	ETHAN JAMES WEBB (SIGNED ELECTRONICALLY)
Date:	20/03/23

Supervisor's endorsement:

I certify that the above amend student has completed the required period of study for the award for which s/he wishes to be examined.

Supervisor's signature[2]:	
Date:	21st March 2023

This form must be completed by the candidate and returned to PG Administration, Curriculum, Learning and Assessment Service, Palatine Centre, Durham University, Stockton Road, Durham, DH1 3LE

August 2019

[1] Under RCUK rules and regulations, students who have received RCUK funding may apply for access to their thesis to be withheld for **no more than 12 months**.

[2] Only one member of the supervisory team is asked to endorse the HDE. An email can be accepted in lieu of a supervisory signature, if necessary.

Development of a Novel *In Vitro* Bioengineered Human Breast Ductal Mucosal Model to Investigate the Invasive Properties of Breast Cancer During its Development.

Ethan Webb
Grey College
MRes SAP Lab
Supervisor: Professor Stefan Przyborski

i. Abstract

Breast cancer is one of the mostly commonly diagnosed cancers globally, where it poses a significant healthcare burden in both developed and developing countries. Over recent years, it has become increasingly apparent that the tumour microenvironment is a major driver of the adoption of specific migratory phenotypes in breast cancer. However, *in vitro* models investigating breast cancer invasion often do not recapitulate this important aspect of breast cancer biology, thereby reducing their physiological relevance and predictive power.

This project aimed to develop novel three-dimensional (3D) migration assays, based on available Alvetex® technologies, that account for the tumour microenvironment. Their effectiveness at recapitulating *in vivo* behaviours was then compared against conventional 2D invasion assays and the literature. Through the use of three immortalised breast cancer cell lines: MCF-10A, MCF-7, and MDA-MB-231's, the three main stages of ductal breast cancer were able to be simulated, namely: Healthy tissue, Ductal Carcinoma *In Situ* (DCIS), and Invasive Ductal Carcinoma (IDC), respectively.

Initially the impact of a 3D geometric space on breast cancer invasion characteristics was investigated using Alvetex® Strata. Despite the increase in *in vivo*-like characteristics of each cell line in this platform, the physiological relevance of these models was limited due to the lack of presence of Extracellular Matrix (ECM) constituents and stromal cells. Using Co-culture techniques, optimised in the Przyborski lab, Human Neonatal Dermal Fibroblasts (HDFn's) were cultured in Alvetex® Scaffold with the immortalised cell lines to create and optimise a complex 3D breast cancer invasion model. The physiological relevance of these models was then assessed using immunostaining and histological analysis to confirm the presence of *in vivo* characteristics and reproducibility of this platform. This led to the creation of a novel reproducible 3D invasion assay for breast cancer that accounts for a physiologically relevant mammary microenvironment. The modular nature of this model was then explored, testing its compatibility with primary mammary fibroblast and epithelial cells to further increase physiological relevance, while also exploring the potential for patient personalised Alvetex® models.

Although physiological relevance is important in invasion models, so is the compatibility of a platform with anti-migratory compounds, as treatments of *in vitro* models with known inhibitors is a cornerstone for increasing our understanding of invasive processes, as well as identifying novel compounds. Thus, each model platform (2D, Alvetex® Strata, Alvetex® Scaffold) was treated with a known migration inhibitor, Caffeic Acid Phenyl-Ethyl Ester (CAPE), to demonstrate their compatibility with these pipelines.

Together, the data presented in this thesis demonstrates the ability of this novel 3D Co-culture system to recapitulate the migratory behaviour of breast cancer cells in its distinct developmental stages; in a platform that is compatible with both drug treatment protocols and the use of primary cell lines.

ii. Acknowledgements

A variety of people contributed personally and professionally to the completion of this thesis. In particular, I want to mention Professor Stefan Przyborski for giving me this amazing opportunity to pursue my interests in an academic setting and being the ultimate enabler of my goals and aspirations. I would also like to mention Dr Lucy Smith, for endlessly proofreading my work, answering my many questions, and guiding me through this project. Without you both, this project would not have been possible. My appreciation also goes out to the following people who also contributed to this project, be it through support or knowledge:

- Dr. Henry Cain
- Dr. Henry Hoyle
- Claire Mobbs
- Jess Simpson
- Jenny and Iain from Breast Cancer Now
- The rest of the Przyborski lab

Most importantly I would like to thank my friends and family for all their support during my studies, without them I would not be where I am today.

iii. Declaration

This work described herein was carried out in the Department of Biosciences, at Durham University between October 2021 and September 2022. All of the work is my own, except otherwise stated. No part has previously been submitted for a degree at this or other university. For full access to the data generated during this period, contact the Przyborski Lab in the Department of Biosciences, Durham.

iv. Statement of Copyright

The copyright of this thesis rests with the author. No quotation from it should be published without the prior written consent and information derived from it should be acknowledged.

Contents

i. Abstract 4
ii. Acknowledgements 5
iii. Declaration 5
iv. Statement of Copyright 5
1. Introduction 13
1.1. Epidemiology of Breast Cancer 13
1.2. Types of Breast Cancer 13
1.2.1. Hormone Receptor Positive Breast Cancer 15
1.2.2. HER2 Amplification Positive Breast Cancer 17
1.2.3. Triple Negative Breast Cancer 19
1.3. Staging of Breast Cancer 20
1.4. Risk Factors 22
1.4.1. Modifiable Risk Factors 23
1.4.2. Non-Modifiable Risk Factors 24
1.5. Treatment of Breast Cancer 26
1.5.1. Treatment of Hormone Receptor Positive Breast Cancer. 27
1.5.2. Treatment of HER2-type Breast Cancer. 28
1.5.3. Treatment of TNBC 29
1.5.4. Barriers to improving treatment. 30
1.6. Invasion Potential Differs between Breast Cancer Subtypes. 31
1.7. Adoption of migratory phenotypes is driven by a complex interplay between cancer cells and their microenvironment. 32
1.8. Molecular mechanisms driving cancer cell migration. 34
1.9. Cell Lines commonly used to understand Breast Cancer Invasion. 36
1.10. In Vitro Platforms for Investigating Breast Cancer Invasion and Their Limitations 37
1.10.1. 2D Cell Culture 39
1.10.2. Animal Models 42
1.10.3. 3D Cell Culture 43
1.11. Alvetex® As a Platform for Building a Physiologically Relevant Breast (Cancer) Model 47
1.11.1. Advantages of Alvetex® 47
1.11.2. Previous Alvetex® Models: Why a Breast Cancer Invasion Model is Feasible 48
2. Hypothesis 50
3. Aims 50
4. Objectives 50
5. Materials and Methods 51
5.1. 2D Cell Culture 51
5.1.1. MCF-7 Epithelial Cells 51
5.1.2. MDA-MB-231 Epithelial Cells 52
5.1.3. MCF-10A Epithelial Cells 53
5.1.4. Neonatal Human Dermal Fibroblast Cells 53
5.1.5. Primary Mammary Fibroblast Cells 54
5.1.6. Primary Healthy Mammary Epithelial Cells 55
5.1.7. 2D Invasion Assay 56
5.2. 3D Cell Culture. 58

5.2.1. Preparation of Alvetex® Membranes. 58
5.2.2. Basic 3D Invasion Assay using Alvetex® Strata. 59
5.2.3. Formation of Stromal Compartment using HDFn's in Alvetex® Scaffold. 59
5.2.4. Formation of Stromal Compartment using Primary Mammary Fibroblasts in Alvetex®. 60
5.2.5. Formation of Full Thickness Co-Culture Models with Fibroblast (HDFn & MF) Derived Stromal Compartments and Breast Cancer Derived Cell Lines 60
5.3. Processing of Samples 62
5.3.1. Harvesting Alvetex® Models 62
5.3.2. Fixing 62
5.3.3. Dehydration and Embedding 62
5.3.4. Sectioning 62
5.4. H&E Staining 63
5.5. Immunostaining 63
5.5.1. 3D Immunostaining 64
5.5.2. 2D Immunostaining 65
5.5.3. Imaging of Fluorescently Stained Samples 66
5.5.4. Imaging Co-Culture 3D Invasion Assay using Alvetex® Scaffold. 67
6. Results 69
6.1. Commercially available breast cancer cell lines display the behaviours correlating with the three distinct timepoints of breast cancer development in 2D culture. 69
6.1.1. Commercially available breast cancer cell lines differ in their invasive potential when grown in 2D. 74
6.1.2. Treatment Of Commercially Available Breast Cancer Cell Lines with a Known Migration Inhibitor Stopped Cell Invasion in 2D. 78
6.2. The Introduction of a Basic 3D Growth Environment Altered the Invasive Potential of Breast Cancer Cell Lines. 79
6.2.1. Treatment of Commercially Available Breast Cancer Cell Lines with CAPE Inhibited Penetration Into Alvetex® Strata. 83
6.3. The Introduction of a Complex and Relevant 3D Microenvironment Through Co-Culture of Breast Cancer Cell Lines with HDFn's Led to the Adoption of Enhanced In Vivo Characteristics. 91
6.3.1. The MCF-10A Cells Formed Structures and Invasion Patterns That Highly Represent Healthy Mammary Tissue. 93
6.3.2. The MCF-7 Cells Formed Structures and Invasion Patterns That Highly Represent DCIS Lesions. 95
6.3.3. The MDA-MB-231 Cells Formed Structures and Invasion Patterns That Highly Represent IDC Lesions. 97
6.3.4. Quantification of the Invasion Capabilities of the Commercially Available Breast Cancer Cell Lines in 3D Co-Culture Showed Significant Differences in Invasive Potential. 99
6.3.5. Addition of the CAPE Inhibitor to the MDA-MB-231 Models Inhibited their Invasion in 3D Co-Culture. 100
6.4. Physiological Relevance of the Alvetex® Scaffold Models was Increased Through the Seeding of Primary Healthy Breast Epithelium Cells with Human Dermal Fibroblasts 103
6.5. Growth of Breast Cancer Cell Lines in Alvetex® Scaffold as a co-culture system with Mammary Fibroblasts to Make Models More Representative of Mammary Tissue. 105
6.5.1. Seeding of Immortalised Epithelial Cell Lines Onto the MF Stromal Compartment Maintained The Enhanced In Vivo Characteristics Observed in HDFn Co-Culture. 107
6.6. Growth of pME in a Co-culture system with Mammary Fibroblasts to demonstrate the intrinsic modularity of Alvetex® Scaffold. 113
7. Discussion 115

7.1. In 2D Breast Cancer Cell Lines Show Graded Invasion that is Consistent with the Literature 116
7.1.1. Physiological Relevance is Limited in 2D. 117
7.2. The introduction of a basic 3D growth environment by Alvetex Strata maintained invasion characteristics of cell lines while enforcing new in vivo-like characteristics. 118
7.2.1. Limitations of the Alvetex® Strata Models 120
7.3. The introduction of physiologically relevant microenvironment constituents led to adoption of highly representative in vivo characteristics. 122
7.3.1. MCF-10A cells seeded onto HDFn-derived stromal compartments displayed key features of Healthy Mammary Tissue. 123
7.3.2. MCF-7 cells seeded onto HDFn-derived stromal compartments displayed enhanced DCIS features. 124
7.3.3. The deposition of an ECM physically blocked cell migration in the MCF-7 and MCF-10A models, but not in the MDA-MB-231 model 125
7.3.4. MDA-MB-231 cells seeded onto HDFn-derived stromal compartments display enhanced IDC features 126
7.3.5. The Compatibility of the CAPE inhibitor with the Alvetex® models. 126
7.3.6. Overcoming key limitations of the Alvetex® Scaffold model. 128
7.3.7. Advantages and Potential Uses of Alvetex® Strata derived Breast Cancer Invasion Models 129
7.3.8. Advantages and Potential Uses of Alvetex® Scaffold derived Breast Cancer Invasion Models 130
7.3.9. Future Directions 132
7.3.10. Alvetex® Strata Models: Modelling Metastasis of Complex Tumour Structures. 132
7.3.11. Alvetex® Scaffold Models: Increasing Complexity and Physiological Relevance to Better Model Tumour Microenvironments. 133
8. Conclusion 133
9. References 135

List of Figures

Figure 1: A Figure demonstrating the different localisation types of breast cancer.] 14
Figure 2: A figure demonstrating the different types of estrogenic signalling pathways 17
Figure 3: Overview of the metastatic cascade: The five key steps of metastasis include invasion, intravasation, circulation, extravasation, and colonization. 33
Figure 4: Fibrblasts cultured in 2D and 3D environments. 41
Figure 5: A diagram demonstrating the interplay of external microenvironment factors with a cell. 41
Figure 6: Measuring Scratch Assay Data in ImageJ. 58
Figure 7: Measuring Strata Invasion Assay Images in ImageJ. 67
Figure 8: Measuring Scaffold Co-Culture Invasion Assay Images in ImageJ. 68
Figure 9: Phase-contrast images of MCF-7 cells grown in 2D.. 69
Figure 10: Phase-contrast images of MCF-10A cells grown in 2D.. 71
Figure 11: Phase-contrast images of MDA-MB-231 cells grown in 2D.. 72
Figure 12: 2D Characterisation of Immortalised Mammary Epithelial Cell Lines using Phase Contrast and Immunofluorescence Microscopy. 74
Figure 13: Phase Contrast Images of Cell Lines during 2D Scratch Assays at T=0 and T=48 hours.. 76
Figure 14: Graphical Representation of the Invasion Capabilities of the MCF-10A, MCF-7, MDA-MB-231 Cell Lines in 2D. 77

Figure 15: Growth of Immortalised Breast Epithelial Cell Lines on Alvetex® Strata at 4, 7, and 14 days. 80
Figure 16: x40 Magnification of MCF-10A Growth in Alvetex® Strata..... 81
Figure 17: x40 Magnification Image of the growth of MDA-MB-231 cell line in Alvetex® Strata. 82
Figure 18: % Depth Penetration of Immortalised Breast Epithelial Cell Lines grown on Alvetex® Strata membrane at 14 days. 83
Figure 19: The Invasion Capabilities of MCF-10A ‘s when seeded onto Alvetex® Strata. 85
Figure 20: The Invasion Capabilities of MCF-7 ‘s when seeded onto Alvetex® Strata. 87
Figure 21: The Invasion Capabilities of MDA-MB-231’s when seeded onto Alvetex® Strata.. 89
Figure 22: Characterisation of the HDFn-derived stromal compartment in Alvetex® Scaffold. 92
Figure 23: Characterisation of the MCF-10A Full Thickness Model in Alvetex® Scaffold. 94
Figure 24: Characterisation of the MCF-7 Full Thickness Model in Alvetex® Scaffold. 96
Figure 25: Characterisation of the MDA-MB-231 Full Thickness Model in Alvetex® Scaffold. 98
Figure 26: A graph illustrating the % Depth Penetration of the three immortalised cell lines when cultured on the Alvetex® Scaffold platform.. 100
Figure 27: Immunostained images of the MDA-MB-231 HDFn full thcikness models treated with the CAPE inhibitor. 101
Figure 28: A graph illustrating the % Depth Penetration of the MDA-MB-231 Alvetex® Scaffold model following treatment with 10 µM and 20 µM of the CAPE inhibitor. 102
Figure 29: Characterisation of the pME Full Thickness Model in Alvetex® Scaffold. 104
Figure 30: Figure 31: Characterisation of the MF-derived stromal compartment in Alvetex® Scaffold. 106
Figure 32: Characterisation of the MCF-7 cells grown on the MF derived stromal compartment in Alvetex® Scaffold. 108
Figure 33: Characterisation of the MDA-MB-231 cells when grown on an MF-derived stromal compartment in Alvetex® Scaffold 110
Figure 34: Characterisation of the MCF-10A cells grown on an MF-derived stromal compartment in Alvetex® Scaffold. 112
Figure 35: Characterisation of the pME cells seeded onto a MF-derived stromal compartment in Alvetex® Scaffold. 114
Figure 36: A) Ductal carcinoma in situ with clear cell features. B) Growth of the MCF-7 Cell Lines on Alvetex® Strata for 14 days x20 magnification. 119
Figure 37: A) Invasive Ductal Carcinoma with clear cell features. B) Growth of the MDA-MB-231 Cell Lines on Alvetex® Strata for 14 days x20 magnification. 120
Figure 38: A) Histology section of healthy mammary ductal Magnification, ×20. B) Growth of the MCF-10A Cell Lines on Alvetex® Strata for 4 days x20 magnification. 120

List of Tables

Table 1: A Table demonstrating the different marker profiles of breast cancer subtypes. 15
Table 2: A Table showing the grading criteria for N values of tumours, according to the TNM system. Table taken from Kalli et al, (2019)[30] 21
Table 3: A Table showing the grading criteria for N values of tumours, according to the TNM system. Table taken from Kalli et al, (2019)[30] 21
Table 4: A Table showing the grading criteria for N values of tumours, according to the TNM system. Table taken from Kalli et al, (2019)[30] 22

Table 5: A Table showing the staging criteria for breast tumours. Table adapted from Kalli et al, (2019)[30] 22

Table 6: A table showing the overall survival and disease-free survival (as % of the study population) of the different molecular subtypes of breast cancer. Results were generated from all consenting female cases with primary, non-metastatic, unilateral breast cancer treated at the Heidelberg Breast Care Unit between 01 January 2003 and 31 December 2012, n=3454. Data sourced from the following paper(s): [40] 26

Table 7: A table highlighting the differences between proteolytic dependent and proteolytic independent migration mechanisms. 34

Table 8: A Table describing the advantages and disadvantages of clinically relevant breast cancer research platforms. 38

Table 9: Table of primary antibodies utilised, their dilutions, supplier, and relevant product code. 64

Table 10: Table of secondary antibodies utilised, their dilutions, supplier, and relevant product code. 65

Table 11: Table showing the Tukey's Post-hoc test for the One-way ANOVA undertaken between the control groups of each cell line during 2D scratch assays. 77

Table 12: Table showing the Tukey's Post-hoc test for the One-way ANOVA undertaken between each cell line during Alvetex® Strata experiments. 83

Table 13: Tukey's Post Hoc test for multiple comparisons on full thickness model invasion data. 100

Abbreviations

Abbreviation	Description
2D	Two Dimensional
3D	Three Dimensional
ADCC	Antibody-Dependent Cellular Cytotoxicity
Akt Kinase	Protein Kinase B
ATR	Ataxia Telangiectasia
AURKA	Aurora Kinase A
BL1	Basal-Like 1
BL2	Basal-Like 2
BMI	Body Mass Index
BRCA	Breast Cancer Gene
CAF	Cancer Associated Fibroblasts
cAMP	Cyclic Adenosine Monophosphate
CAPE	Caffeic Acid Phenethyl Ester
c-Cbl	Ubiquitin Ligase
CDH1	Cadherin-1
CDX	Cell-Derived Xenograft
CK4/6	Cyclin-Dependent Kinase 4 And 6
CK8	Cytokeratin 8
DCIS	Ductal Carcinoma In Situ
dH_2O	Deionised Water
DMEM	Dulbecco's Modified Eagle's Medium
DMEM:F12	Dulbecco's Modified Eagle Medium/Nutrient Mixture F-12
DMSO	Dimethyl Sulfoxide
ECM	Extracellular Matrix
EDTA	Ethylenediaminetetraacetic Acid
EGF	Epidermal Growth Factor
EMT	Epithelial-Mesenchymal Transition
EpCAM	Epithelial Cellular Adhesion Molecule

ER	Estrogen Receptor
ERE	Estrogen Responsive Elements
ERα	Estrogen Receptor Alpha
ERβ	Estrogen Receptor Beta
EtOH	Ethanol
FBS	Foetal Bovine Serum
FGF	Fibroblast Growth Factor
FGF-2	Fibroblast Growth Factor-2
FHS	Family History Scores
FOXA1	Forkhead Box A1
H&E	Haematoxylin And Eosin
HDFn	Neonatal Human Dermal Fibroblast
HER2/Neu	Human Epidermal Growth Factor Receptor 2
HR	Hormone Receptor
HRT	Hormone Replacement Therapy
IDC	Invasive Ductal Carcinoma
IGF1R	Insulin Like Growth Factor 1
IHC	Immunohistochemical
IM type	Immunomodulatory
Ki67	Kiel 67 Protein
LAR	Luminal Androgen Receptor
LCIS	Lobular Carcinoma In Situ
LIC	Lobular Invasive Carcinoma
M type	Mesenchymal-Like
MAPK / MEK	Mitogen-Activated Protein Kinases
MET	Mesenchymal-Epithelial Transition
MF	Mammary Fibroblast
MK167	Marker Of Proliferation Kiel 67
MMP-14	Matrix Metallopeptidase-14
MMP-2	Matrix Metallopeptidase-2
MMP-9	Matrix Metallopeptidase-9
MMPs	Matrix Metallopeptidase’s
MSL	Mesenchymal Stem-Like
NCS	Neonatal Calf Serium
NF-κB	Nuclear Factor Kappa-Light-Chain-Enhancer of Activated B Cells
NGF	Nerve Growth Factor
NK	Natural Killer
OS	Ovarian Suppression
P13	Phosphoinositide 3-Kinases
PBS	Phosphate Buffered Saline
PD-L1	Programmed Cell Death-Ligand 1
PDX	Patient Derived Xenograft
PFA	Paraformaldehyde
PKD	Protein Kinase D
pME	Primary Mammary Epithelial Cells
PR	Progesterone Receptor
PTEN	Phosphatase and Tensin Homolog Deleted on Chromosome 10
Raf	Rapidly Accelerated Fibrosarcoma
RAS	Rat Sarcoma
RPMI-1640	Roswell Park Memorial Institute-1640
SERDs	Selection Estrogen Down-Regulators
SERMs	Selective Estrogen Receptor Modulators
Smad	Suppressor of Mothers Against Decapentaplegic

STATs	Signal Transducers And Activator Of Transcription
STK11	Serine/Threonine Kinase 11
TGFβ	Transforming Growth Factor-Beta
TGFβ1	Transforming Growth Factor Beta-1
TNBC	Triple Negative Breast Cancer
TP53	Tumour Protein 53
Vim	Vimentin
Wnt	Wingless-related Integration Site
α-SMA	Alpha-Smooth Muscle Actin

1. Introduction

1.1. Epidemiology of Breast Cancer

Breast cancer is one of the most common malignancies globally, where its incidences account for 10.4% of all cancer diagnoses [1]–[3]. In addition to being one of the most commonly diagnosed malignancies, breast cancer is also the leading cause of death in women worldwide. In 2020 alone, 2.3 million new cases were diagnosed worldwide and resulted in 684,996 deaths [4], [5].

This high-volume of diagnoses and mortalities resulting from breast cancer are further exacerbated by the presence of a substantial disparity in the outcome of the disease between developed and developing countries. For example, although incidence rates of breast cancer are higher in developed regions than developing regions, death rates are counterintuitively higher in developing countries [4]. This starts to show the current wealth barrier surrounding current treatment regimens for breast cancer, where women who develop breast cancer in high-income countries are more likely to survive, while women in most low-income and many middle-income countries are financially isolated from treatment and thereby suffer higher death rates from this malignancy.

The high global incidence rate of breast cancer shows that this disease poses a huge healthcare burden in both developing and developed countries. Furthermore, when combined with the distribution of death rates, global data shows a real wealth disparity in the survival of breast cancer and a global need for the development of cost-effective treatments to help solve this. However, breast cancer is a highly heterogenous malignancy with mechanisms of progression and routes of treatment differing between not only the different stages of breast cancer, but also the different molecular sub-types of the disease.

1.2. Types of Breast Cancer

The highly heterogenous nature of breast cancer complicates its treatment and our understanding of the disease, as different subtypes carry differential clinical

outcomes, pathological progression, and varied therapeutic responses to treatment protocols [6]. Thus, to allow cost-effective and efficient care of patients with breast cancer, treatment protocols are grouped based on tumour histopathology and immunohistochemical markers (IHC) associated with the individual breast cancer cells composing the tumour.

Initially, histopathological analysis of early breast cancer tumours divides these malignancies into four broad types based on their localisation (Figure 1): Lobular Carcinoma *In Situ* (LCIS), Lobular Invasive Carcinoma (LIC), Ductal Carcinoma *In Situ* (DCIS), and Invasive Ductal Carcinoma (IDC) [7], [8]. Clinically LCIS tumours have their proliferation centred in the terminal ductal lobular units and consists of cancerous cells that fill >50% of the glandular acini [9]. On the other hand, DCIS malignancies have their proliferation centred in the ductal region [10]. In both cases once the cells have breached past their respective boundaries, they become LIC and IDC respectively [9], [10].

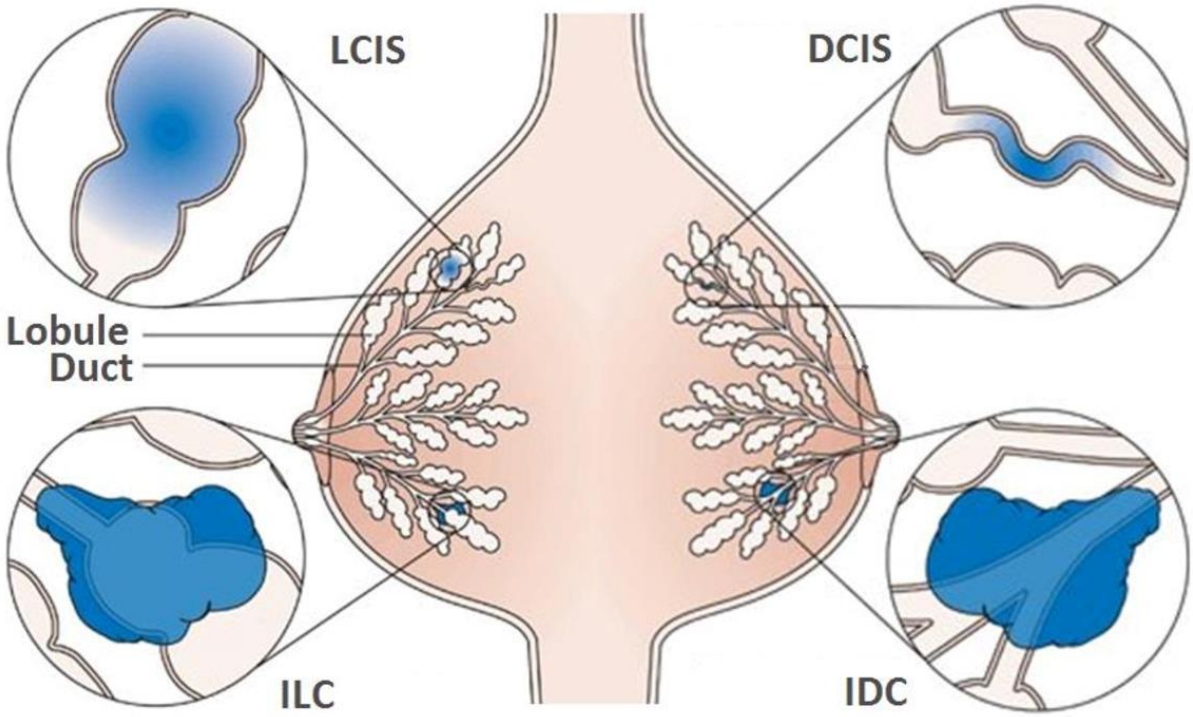

Figure 1: A Figure demonstrating the different localisation types of breast cancer. There are two broad localisation types of breast cancer: Lobular and Ductal. Lobular breast cancer refers to have their proliferation centred in the terminal ductal lobular units of mammary tissue. Once the cancer cells have breached past the lobular ductal units, it is then known as Lobular Invasive Cancer (LIC). Ductal breast cancer has its proliferation centred in the ductal region, like LIC once the cells have breached past the ductal tissue, it is known as Invasive Ductal Carcinoma (IDC). Figure adopted from Petridis, 2018 and CRUK.org [11]

Following this, IHC analysis of these tumours then informs clinicians on the molecular subtype of the tumour and in turn what drugs it will likely be susceptible to. This is achieved through comparisons of the expression of hormone receptors (Estrogen [ER+] and/or Progesterone [PR+]), the expression of the proliferation marker Ki67, and epidermal growth factor receptor 2 (HER2/Neu) status [3], [12]. Specifically, tumours are categorised into five molecular subtypes: Luminal A-like, Luminal B/HER2 negative-like, Luminal B/HER2 positive-like, HER2-type, and Triple Negative. The different marker profiles of these sub-types are summarised in Table 1 [3], [6], [12].

Table 1: A Table demonstrating the different marker profiles of breast cancer subtypes.

Breast Cancer Sub-Type	**ER/PR (+/-)**	**Ki67 (+/-)**	**HER2 (+/-)**
Luminal A-like	**+**	**-**	**-**
Luminal B/HER2 Negative	**+**	**+**	**-**
Luminal B/HER2 Positive	**+**	**+**	**+**
HER2	**-**	**+**	**+**
Triple Negative	**-**	**+**	**-**

1.2.1. Hormone Receptor Positive Breast Cancer

Hormone receptor positive (HR+) breast cancer refers to tumours that express either the estrogen receptor (ER), progesterone receptor (PR), or both [13]. HR+ breast cancers generally encompass the Luminal A-like and Luminal B/HER2 negative-like molecular subtypes and accounts for around 70% of all breast cancer diagnoses' [14]. While both Luminal A and B tumours express ER to a similar degree, they do have key differences that result in better prognosis for Luminal A breast cancer patients than Luminal B patients [5], [6], [14]. Specifically, Luminal A breast cancers have low expression of proliferation-related and luminal-regulated pathways, meaning they are slow growing and less likely to metastasise and migrate to other regions of the body [5], [6]. On the other hand, Luminal B breast cancer tumours have high expression of proliferation-related such as MKI67 and AURKA and have

lower expression of genes or proteins typical for luminal epithelium such as PR and FOXA1, resulting in faster growth, Epithelial-Mesenchymal Transitions that promote progression and migration to other regions of the body, and overall worse prognosis [5].

1.2.1.1. *Molecular Mechanisms driving HR+ Breast Cancer Development*

Due to the high expression of ER's, both cytoplasmic and membrane bound, in this type of breast cancer, tumorigenic processes are driven through increased ER activation and the resulting cross talk that disrupts cell cycle processes and leads to the abnormal production of growth factors. Typically, estrogen will bind to ER's creating a high affinity complex that can bring about cellular changes through two distinct pathways: the nuclear pathway, and the non-nuclear pathway (Figure 2) [5].

The nuclear pathway involves cytoplasmic ER's, such as ERα and ERβ, which act as ligand-activated transcription factors once they bind to estrogen that has entered the cell [15]. When estrogen binds to cytoplasmic ER's a conformational change is evoked that promotes receptor dimerization and allows translocation to the nucleus, where the complex binds to specific chromatin sequences known as ERE's (Estrogen Responsive Elements) [15], [16]. HR+ breast cancer have increased availability of cytoplasmic ER's, due to increases in expression during tumorigenesis, that leads to increased binding to ERE's and transcription of their chromatin sections via the nuclear pathway, thereby dysregulating a broad range of cellular processes that drive tumour development in this molecular sub-type.

Activation of gene transcription by ER complexes can also be non-nuclear, or indirect, whereby ER complexes bind to other transcription factors through protein-protein interactions and promote the increased expression of non-ERE containing chromatin sequences [1], [15], [16]. Indirect gene transcription by ER's is largely orchestrated by membrane bound ER's which drive second messenger interactions when extracellular estrogen binds to them [15], [16]. There are four main protein-kinase cascades that membrane-bound ER's act through: the phospholipase C/ protein kinase C pathway, 2) the Ras/Raf/MAPK cascade, 3) the phosphatidyl

inositol 3 kinase/Akt kinase cascade, and 4) the cAMP/protein kinase A signalling pathway [15]. Thus, by activating these protein-kinase cascades, membrane-bound ER interactions are able to indirectly regulate gene transcription at DNA response elements distinct from ERE's [15].

Thus, when combined with the action of cytoplasmic ER's, the increased ER stimulation brought about by extracellular estrogen compounds with this and initiates dysregulation of genomic signalling in areas distinct to ERE's, thereby broadening the disruption to genomic transcription profiles, further driving tumorigenesis in the HR+ molecular sub-types.

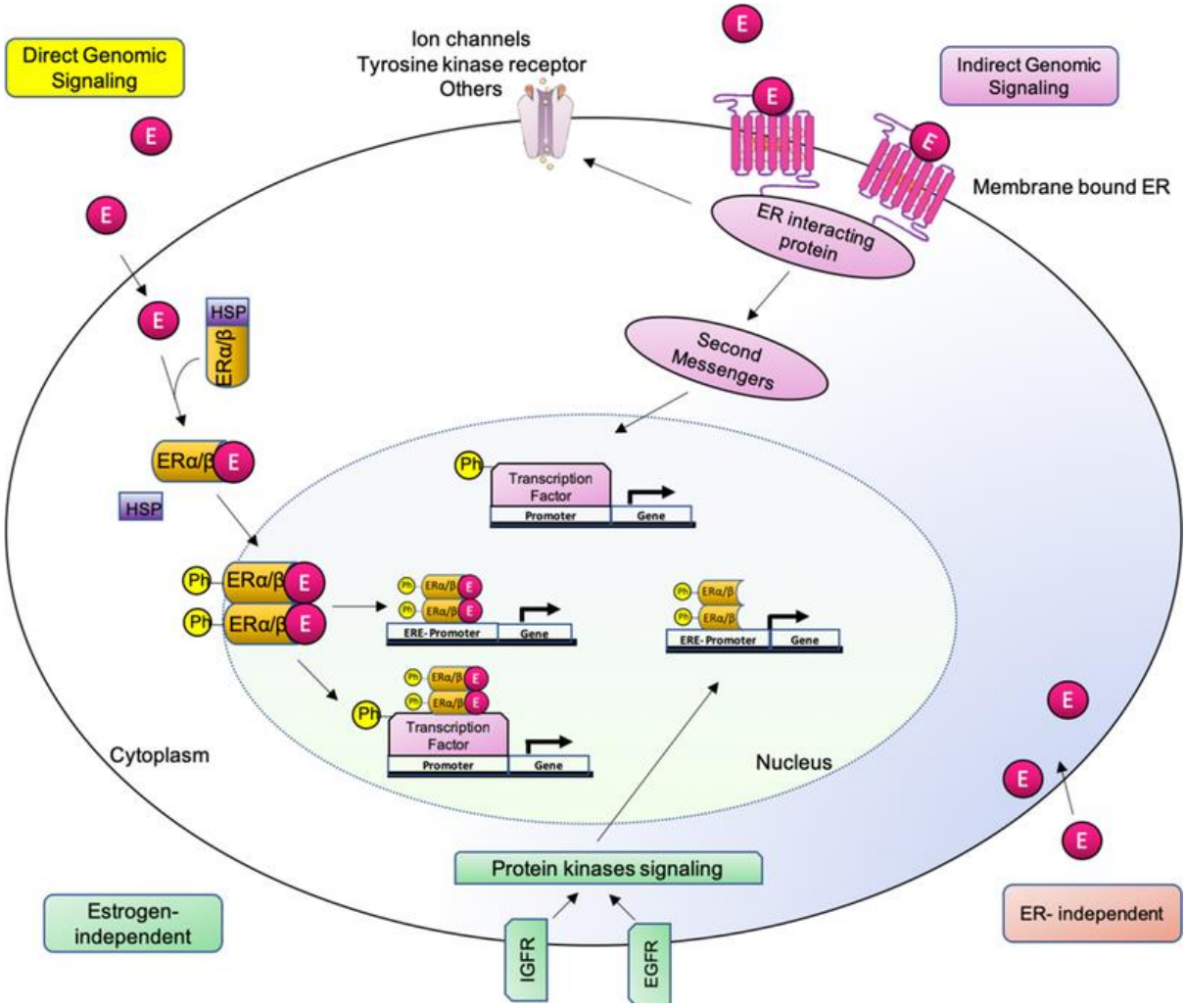

Figure 2: A figure demonstrating the different types of estrogenic signalling pathways. Figure adopted from Fuentes, 2019 [15].

1.2.2. HER2 Amplification Positive Breast Cancer

Human epidermal growth factor receptor-2 (HER2) is a membrane-bound tyrosine kinase that is overexpressed and amplified in roughly 20% of breast cancers [17]. Immunohistochemical analysis has revealed that HER2 levels can reach up to two million receptors per cell, a 100x increase when compared to healthy breast epithelial cells [17], [18]. This substantial increase in HER2 receptors in HER2+ tumours leads to a marked increase signalling along the HER2 pathway, driving multiple downstream pathways that bring about tumorigenic properties such as increased cell proliferation, survival, and invasion in this breast cancer sub-type [17], [18]. The pathways controlled by HER2, combined with the total increase in signalling, results in a more aggressive subtype that carries the second-poorest clinical prognoses among the breast cancer subtypes [17], [19].

1.2.2.1. *Molecular Mechanisms driving HER2 Breast Cancer Development*

The mechanisms driving HER2 breast development via HER2 pathway disruption can be split into three main steps: 1) Activation of membrane bound HER2. 2) Signal transduction to the nucleus. 3) Increased transcription of HER2 regulated genes that alter cell function and expression profiles leading to tumorigenesis [17].

HER2 activation occurs in two main ways: homodimerization with other HER2 proteins in the membrane space; or heterodimerization with another HER protein isoforms (HER1-3) [18]. Both dimerization scenarios result in transphosphorylation of tyrosine residues on the HER2 intracellular domains, which drives docking with intracellular protein kinases and initiation of step two of the HER2 pathway, signal transduction. The overexpression of HER2 during breast cancer pathogenesis drives tumour development by increasing both the available amount of HER2 for dimerization, and the amount of activated dimer complexes present in the cell membrane space. This, in turn, results in increased protein kinase docking and increased signal transduction to the nucleus. It is also important to note that HER2 homodimers have higher catalytic activity than HER2 heterodimers and thereby stronger signalling activity. Thus, amplification of HER2 in breast cancer not only increases signal output via increased dimer formation, but also increases signal

strength by raising the proportion of HER2 homodimers present in the membrane space.

The phosphorylated tyrosine residues allow binding with a wide range of second messengers, but the most common protein kinase systems that HER2 dimers interact with are the PI3K/AKT, RAS/MEK/MAPK, and STATs kinase cascades[17], [18]. These cascades then bring about tumorigenic properties of affected cells by allowing activation of transcription factors that drive increased expression of proliferation, migration, differentiation, and angiogenic pathways, while inhibiting apoptotic pathways.

1.2.3. Triple Negative Breast Cancer

Triple negative breast cancer (TNBC) accounts for 15-25% of all breast cancers and refers to malignancies that lack ER/PR expression and HER2 molecular markers [20]. Due to the lack of common conventional markers in this sub-type of breast cancer, the malignancy can be grouped by the tumours' general cell behaviours into 6 molecular subtype: mesenchymal stem-like (MSL), mesenchymal-like (M), basal-like 1 and 2 (BL1, BL2), immunomodulatory (IM), luminal androgen receptor expression (LAR)[20]–[22]. The lack of common targets and the broad heterogeneity of this sub-type, TNBC is considered the most aggressive breast cancer sub-type with the worst prognosis among breast cancer patients.

1.2.3.1. *Molecular Mechanisms Driving TNBC Development*

The molecular mechanisms of TNBC development are highly dependent on the subtype. BL1 tumours develop through disruption of cell cycle and DNA repair pathways [22]–[24]. Disruption of DNA repair pathways is a result of alterations to ATR/BRCA activity, which are proteins responsible for the recruitment of DNA repair proteins. During BL1 TNBC, *BRCA1* and *BRCA2* may become mutated and result in the cell being unable to initiate homologous recombination of DNA strands to repair double strand breaks [25], [26]. Furthermore, Ki67 is overexpressed in BL1 tumours, this protein is heavily involved in cell cycle modulation where it stabilizes and maintains the mitotic spindle [27]. Increased Ki67 primes cells and allows increased

proliferation, this coupled with increased accumulation of DNA mutations is a factor that drives tumour progression, heterogeneity, and worsens prognosis for TNBC. The molecular mechanisms driving BL2 tumour development differ slightly to the BL1 sub-type. Where dysregulation is centred around metabolic pathways, such as gluconeogenesis and glycolysis, and changing growth factor signalling such as: EGF, NGF, MET, Wnt/beta-catenin, and IGF1R [24]. This has the effect of altering metabolic conditions to drive uncontrolled proliferation of this TNBC sub-type.

Our understanding of the remaining sub-types of TNBC is highly limited due to their intrinsic heterogeneity. However, we do know that the M and MSL subtypes adopt mesenchymal characteristics and are associated with increased cell motility and interference with Actin-regulated pathways [22], [23]. Furthermore, the IM subtype mainly progresses through disruptions to immune cell and cytokine signalling and is characterized by alterations in helper T-cell immune responses, as well as the activity of natural killer cells. Finally, the LAR subtype develops through disruption of genes involved in hormone regulation.

1.3. Staging of Breast Cancer

Staging of breast cancer is initially determined through the use of the TNM system which uses anatomical features of tumours to grade: the size of the primary tumour and its invasion into other tissues (T), status of lymph nodes (N), and metastasis status [28]–[30]. The T grade of a tumour ranges from T0-T4. Where T0 indicates that there is no tumour present, then T1-4 show progressive enlargement and invasiveness of the tumour. The specific grading criteria for T values are shown in Table 2. N values are used to describe lymph node involvement of the tumour. N0 indicates no regional nodal spread, while N1-N3 show progressive spread of the tumour into the lymph nodes, with progressively distal spread from N1 to N3[28]–[30]. The specific grading criteria for N values are shown in Table 3. M values are used to identify the presence of distant metastases of the primary tumour. A tumour is classified as M0 if no distant metastasis is present and M1 if there is evidence of distant metastasis [28]–[30]. The specific grading criteria for M values are shown in Table 4.

Table 2: A Table showing the grading criteria for N values of tumours, according to the TNM system. Table taken from Kalli et al, (2019)[30]

T Category	T Criteria
TX	Primary tumor cannot be assessed
T0	No evidence of primary tumor
Tis (DCIS)	Ductal carcinoma in situ
Tis (Paget)	Paget disease not associated with invasive carcinoma or DCIS
T1	Tumor size ≤ 20 mm
T1mi	Tumor size ≤ 1 mm
T1a	Tumor size > 1 mm but ≤ 5 mm
T1b	Tumor size > 5 mm but ≤ 10 mm
T1c	Tumor size > 10 mm but ≤ 20 mm
T2	Tumor size > 20 mm but ≤ 50 mm
T3	Tumor size > 50 mm
T4	Tumor with direct extension to the chest wall and/or the skin with macroscopic changes
T4a	Tumor with chest wall invasion
T4b	Tumor with macroscopic skin changes including ulceration and/or satellite skin nodules and/or edema
T4c	Tumor with criteria of both T4a and T4b
T4d	Inflammatory carcinoma

Table 3: A Table showing the grading criteria for N values of tumours, according to the TNM system. Table taken from Kalli et al, (2019)[30]

cN Category	cN Criteria
cNX	Regional nodes cannot be assessed (previously removed)
cN0	No regional nodal metastases
cN1	Metastases to movable ipsilateral level I and/or level II axillary nodes
cN1mi	Micrometastases
cN2	Metastases to fixed or matted ipsilateral level I and/or level II axillary nodes; or metastases to ipsilateral internal mammary nodes without axillary metastases
cN2a	Metastases to fixed or matted ipsilateral level I and/or level II axillary nodes
cN2b	Metastases to ipsilateral internal mammary nodes without axillary metastases
cN3	Metastases to ipsilateral level III axillary nodes with or without level I and/or level II axillary metastases; or metastases to ipsilateral internal mammary nodes with level I and/or level II axillary metastases; or metastases to ipsilateral supraclavicular nodes
cN3a	Metastases to ipsilateral level III axillary nodes with or without level I and/or level II axillary metastases
cN3b	Metastases to ipsilateral internal mammary nodes with level I and/or level II axillary metastases
cN3c	Metastases to ipsilateral supraclavicular nodes

Table 4: A Table showing the grading criteria for N values of tumours, according to the TNM system. Table taken from Kalli et al, (2019)[30]

M Category	M Criteria
M0	No clinical or imaging evidence of distant metastases
cM0(i+)	No clinical or imaging evidence of distant metastases, but with tumor cells or deposits measuring ≤0.2 mm detected in circulating blood, bone marrow, or other nonregional nodal tissue in the absence of clinical signs and symptoms of metastases
cM1	Distant metastases on the basis of clinical or imaging findings
pM1	Histologically proven distant metastases in solid organs; or, if in nonregional nodes, metastases measuring >0.2 mm

The TNM system helps to establish the anatomic extent of the disease, and the combination of the three factors can serve to define the overall stage of the tumour. This method allows for simplification, with cancers staged from I-IV, with stage IV being the most severe stage. Table 5 lists these stages in more detail.

Table 5: A Table showing the staging criteria for breast tumours. Table adapted from Kalli et al, (2019)[30]

Clinical Stage	**Criteria**
Stage 0	Indicates carcinoma in situ. Tis, N0, M0.
Stage I	Localized cancer. T1-T2, N0, M0.
Stage II	Locally advanced cancer, early stages. T2-T4, N0, M0.
Stage III	Locally advanced cancer, late stages. T1-T4, N1-N3, M0.
Stage IV	Metastatic cancer. T1-T4, N1-N3, M1.

1.4. Risk Factors

As Breast Cancer is a pathology that typically effects patients in adulthood, the cause of this disease becomes a unique blend of risk factors that combines modifiable risk factors, and non-modifiable risk factors [5].

1.4.1. Modifiable Risk Factors

1.4.1.1. *Alcohol and Smoking*

During both active and passive smoking, carcinogens enter the blood stream and are transported around the body. From a breast cancer perspective, these carcinogens accumulate in breast tissue and increase the rate of mutations, and in turn the increase chance of mutations within oncogenes and tumour suppressor genes to initiate breast cancer development [5].

Excessive alcohol consumption is also a factor that enhances the risk of breast cancer. It is not the alcohol accumulation within the body that increases the risk of breast cancer, but rather the physiological imbalances caused by excessive consumption. For example, excessive alcohol intake has been shown to increase physiological estrogen levels, creating hormonal imbalances that can increase the risk of carcinogenesis in females [5], [31]. One study found that Alcohol consumption increased the risk of estrogen-positive breast cancers in particular [5], [32]. Furthermore, alcohol intake often results in excessive fat gain and increases in BMI, which as mentioned in section 1.4.1.3, compounds the increased risk of breast cancer.

1.4.1.2. *Exogenous Estrogen*

The main sources of exogenous estrogen in woman are hormonal contraceptives and hormone replacement therapy (HRT). In terms of hormonal contraception, an estimated 140 million women worldwide use hormonal contraception [33]. In 2017, a Danish study reported that women who were using or had recently stopped using oral combined hormone contraceptives were 1.24 times more likely to develop breast than women who have never used oral contraceptives [33]. Many studies have found that this increased risk of breast cancer returns to normal immediately after discontinuation in women who have used hormonal contraceptives for short periods of time, whereas women who have used these contraceptives for longer periods of time are at an increased risk of developing breast cancer for at least 5 years after discontinuation [33]–[35].

1.4.1.3. *Diet and BMI*

Diet, and by extension, BMI are also key modifiable risk factors of breast cancer. For example, when people have large caloric surpluses, their bodies accumulate adipose tissue and their BMI increases. Adipose tissue is a major site in the body where androstenedione is converted to estrone and other estrogens [36]. The increased conversion of physiological steroid hormones thereby increases the circulating levels of estrogens, creating hormone imbalances that, as previously mentioned, may activate breast cell growth and carcinogenesis [5], [35], [36]. Furthermore, increased BMI and fat volume BMI are also associated with more aggressive tumour types including a higher percentage of lymph node metastasis and greater tumour size [5]. Overall, individuals with greater BMI's and poorer diets are at a higher risk of breast cancer than those who have healthy BMI's and lower fat volumes.

1.4.2. Non-Modifiable Risk Factors

1.4.2.1. *Genetic Mutations and Family History*

A major risk factor of breast cancer is the presence of a family history of breast cancer. In one study, it was found that 12.9% of women diagnosed with breast had one or more first-degree relatives with a history of breast cancer [37]. Using family history scores (FHS) of first-degree relatives diagnosed with breast cancer, that account for the expected number of family cases based on the family's age-structure and national cancer incidence rates, another study found that the risk of breast cancer significantly increases with an increasing number of first-degree relatives affected. Where participants with the highest FHS where 3.5 times more likely to develop breast cancer than those without familial histories of breast cancer.

Family history is such a pertinent risk factor in the development of breast cancer because high risk genetic abnormalities, combinations, and mutations are likely to be shared by family members. Furthermore, because breast cancer effects patients later in life, typically after reproduction, it is likely that the high-risk genetics have been passed on to the next generation before diagnosis.

There are several genetic mutations that are highly associated with an increased risk of breast cancer development. Two major genes that are passed in an autosomal dominant manner are the BRCA1 (located on chromosome 17) and BRCA2 (located on chromosome 13) genes. Other highly penetrant breast cancer genes include TP53, CDH1, PTEN, and STK11 [1], [5], [12].

1.4.2.2. *Sex, Ethnicity, and Age*

Female sex constitutes one of the major factors associated with an increased risk of breast cancer, primarily because of their enhanced use and sensitivity to hormonal stimulation. Unlike men who present insignificant estrogen levels, women have elevated estrogen levels in their body. Increased estrogen can interact with cancer cells, driving their proliferation and metastasis through the pathways mentioned previously. Furthermore, females have a higher number of mammary cells in their body, which are highly sensitive to changes in estrogen and progesterone. These cells' intrinsic sensitivity to estrogen and progesterone, paired with the high number in females, means that a tumorigenic event is more likely to occur in the mammary tissue of females than males.

Age is also a key non-modifiable risk factor of breast cancer. Currently, about 80% of patients with breast cancer are individuals aged >50 [5]. As patients get older, as does their risk of developing breast cancer, which as of writing stands at <1.5% before 40, 1.5% risk at 40, 3% at 50, and >4% at age 70 [5]. This, in part, can be explained by the alterations to physiological levels of sex hormones during menopause, a process that occurs in older women, which results in a higher risk of breast cancer in postmenopausal women than premenopausal women due to the physiological imbalances of estrogen the process onsets [2], [5]. Furthermore, as we age our bodies accumulate mutations across our genome, which increase the chances of a tumorigenic event and the development of breast cancer. Although there is a clear correlation in terms of age and breast cancer incidence, there is also a relationship between molecular subtype of breast cancer and a patient's age. TNBC is more prevalent in younger patients, while in older patients, the most common breast cancer type is HR+ [5], [38].

When comparing the ethnicity of breast cancer patients and their respective outcomes, there are wide disparities and a general lack of understanding of the mechanisms that drive breast cancer development and the different trends observed between ethnicities. [5], [39]. For example, breast cancer incidence rates remain the highest among White women, while mortality rates and overall survival rates are worse in Black women [39]. It is important that these differences observed between ethnicities are not solely a result of differences in genetics between populations, but instead are a complex convergence of socioeconomic factors, genetics, and environmental factors.

1.5. Treatment of Breast Cancer

As standard, treatment protocols for breast cancer patients are based around surgical intervention and the utilisation of systemic therapies in order to: shrink the tumour prior to surgery; maintain tumour stability if non-operable; and maintain remission after surgical intervention [8]. However, different molecular sub-types and stages of breast cancer have highly variable responses to treatments and thus require targeted systemic therapies and surgical approaches. This requirement for different treatment procedures between molecular sub-types of breast cancer drastically affects the overall survival of breast cancer patients, as shown in **Table 6**.

Table 6: A table showing the overall survival and disease-free survival (as % of the study population) of the different molecular subtypes of breast cancer. *Results were generated from all consenting female cases with primary, non-metastatic, unilateral breast cancer treated at the Heidelberg Breast Care Unit between 01 January 2003 and 31 December 2012, n=3454. Data sourced from the following paper(s):* [40]

	HR+ Breast Cancers		**HER2+ Breast Cancers**		**Triple negative Breast Cancers**
	Luminal A-like	**Luminal B/HER2 neg.-like**	**Luminal B/HER2 pos.-like**	**HER2-type**	
Overall Survival %	95.1	88.7	92.5	85.6	78.5
Disease Free Survival %	92.2	80.1	79.0	77.0	69.1

1.5.1. Treatment of Hormone Receptor Positive Breast Cancer.

Treatment of HR+ breast cancers follow similar regimens to many other cancers, whereby surgical intervention, chemotherapy, and radiotherapy are used to initially treat this disease [40]. However due to the highly conserved impact of ER signalling in HR+ breast cancer development, existing treatment strategies can be augmented by including drugs that target aspects of the nuclear and non-nuclear pathways. These treatment strategies work by either reducing activation of ER complexes (endocrine therapy) or by preventing the function of the protein-kinase cascades mediated by membrane-bound ER (specific inhibitors). By adding these strategies to standard treatment protocols, clinical outcome has been largely improved, reducing reoccurrence and providing treatment options for patients who may not be suitable for surgical intervention or chemotherapy due to tumour progression or pre-existing health conditions [41].

Endocrine therapies typically target the nuclear pathway of ER activation in HR+ breast cancers. These therapies currently consist of ovarian suppression (OS), selective estrogen receptor modulators (SERMs) and down-regulators (SERDs), and aromatase inhibitors[41], [42]. These approaches have two main themes: reducing physiological estrogen concentrations; and preventing direct activation of ER complexes. OS and aromatase inhibitors adopt the former, where OS utilises compounds to prevent the overall physiological production of androgens, while aromatase inhibitors inhibit the processes by which androgens are converted to estrogen. On the other hand, SERMs and SERDs are inhibitors that prevent direct activation of ER complexes and the subsequent downstream processes that occur as a result. SERDs bind directly to estrogen, forming complexes that cannot activate ER receptors, while SERMs bind to nuclear ER’s and prevent their activation [41].

Specific inhibitors are also used in conjunction with endocrine therapies and other conventional approaches to target the non-nuclear pathways elicited by ER’s. Typically, these therapies will target the protein kinase cascades brought about during signal transduction in the non-nuclear pathway. This in turn prevents the overstimulation of transcription factors by the non-nuclear pathway and slows tumour

development and progression. The most common specific inhibitors are CK4/6 inhibitors such as palbociclib, ribociclib, and abemaciclib [43].

Overall endocrine therapies and specific protein kinase inhibitors work to reduce progression and recurrence of HR+ breast cancer in patients by counteracting the increase in ER-related signalling, and initiation of tumorigenic events, present in this molecular sub-type of breast cancer.

1.5.2. Treatment of HER2-type Breast Cancer.

Much like HR+ breast cancers, Treatment regimens for HER2-type breast cancers are mainly based around augmenting conventional treatment strategies with drugs that target the HER2 pathway. In particular drugs are used to reduce the effective concentration and dimerization of HER(2) proteins in the breast cancer cells. The most common of these HER2 drugs is Trastuzumab, a monoclonal antibody that interacts with HER2 in three main ways: 1) HER2 degradation. 2) Antibody-dependent cellular cytotoxicity. 3) MAPK and PI3K/Akt interference.

HER2 degradation mediated by Trastuzumab occurs when the drug binds to HER2 proteins present in the cell membrane space. The binding of Trastuzumab to membrane-bound HER2 induces a conformational change that promotes the internalisation of the protein and the binding of tyrosine kinase – ubiquitin ligase (c-Cbl). C-Cbl then ubiquitinates HER2 and marks it for degradation, thereby reducing the effective concentration of HER2, the amount of dimerized HER2, and in turn decreases the amount of dysregulated signalling in HER2 tumours [19], [44]. This has the effect of reducing activation of tumorigenic pathways and slowing tumour development, while also encouraging apoptotic pathways that regress tumour size.

The binding of Trastuzumab also induces Antibody-dependent cellular cytotoxicity (ADCC), a mechanism by which the binding of Trastuzumab to HER2 encourages the attraction of immune cells to tumour sites and marks the ‘bound’ cells for programmed cell death [19], [45]. Essentially, the binding of Trastuzumab to HER2 on tumour cells makes a portion of the antibody, known as the Fc fragment, available to immune cells, such as Natural Killer (NK) cells, which contain a complimentary Fc

gamma receptor[19], [45], [46]. The more HER2 receptors on a cell, the more Trastuzumab that binds, increasing the strength of binding of complimentary immune cells to HER2 enriched areas (HER2-type tumours), ultimately directing immune cells and cascades to degrade bound tumour cells [17], [19], [45].

The final mechanism by which trastuzumab interacts with HER2+ breast cancer cells during treatment is through the inhibition of the MAPK, STATs, and PI3K/Akt protein kinase pathways. Trastuzumab blocks tyrosine kinase activity and the transphosphorylation that the enzyme mediates, thereby preventing the formation of dysregulated second messenger signals via these pathways. This then leads to an increase in cell cycle arrest, the suppression of cell growth and proliferation, and induces cell apoptosis.

Overall, by binding to HER2 receptors, HER2-specific therapies are able to: supress tumorigenic pathways that result from dysregulated HER2 signalling, while also marking tumour cells for degradation. By combining these specific therapies with other conventional therapies, clinicians have been able to drastically increase prognosis and disease outcome of this more aggressive cancer type.

1.5.3. Treatment of TNBC

The lack of common markers or pathogenic pathways in TNBC patients has meant that conventional treatment strategies are not able to be augmented, and their standalone use has remained the standard treatment protocol for this sub-type of breast cancer [47], [48]. The chosen regimen of these treatments is independent of metastatic status: whereby operable non-metastatic tumours have protocols that use chemotherapy as a neoadjuvant therapy to reduce tumour size and improve the chance of a positive post-surgical outcome; while non-operable and advanced tumours are exposed to chemotherapy and radiotherapy to stabilise tumour progression and prolong patient life. This lack of augmentation to TNBC treatment strategies, often means that advanced and non-operable tumours usually have short-lived responses to treatment and are typically followed by rapid relapse and fatal metastasis, due to the high heterogeneity and mutational rates of TBNC which allow TBNC tumours to become resistant to treatment [48].

To counteract the poor prognosis of TNBC, clinical studies and genetic profiling are being used to find common targets and pathways that drive TNBC development. Recent studies have shown that this sub-type is more immunogenic and contains a larger proportion of tumour-infiltrating lymphocytes than other breast cancer subtypes [48], [49]. It is thus becoming apparent that TNBC tumours in particular modulates immune cells, and their pathways, in order to avoid degradation and continue development [49].

Novel treatment protocols are thus being formulated to target immune checkpoints, in particular T-cell checkpoints, altered by this breast cancer sub-type. For example, TNBC tumour cells have been found to display a high level of programmed cell death-ligand 1 (PD-L1) expression, a cell surface protein which suppresses immune cells in the tumour microenvironment. This novel conserved pathway was targeted as part of the IMpassion130 trial which utilised Atezolizumab, an anti-PD-L1 antibody, to relieve the suppression of TIL's onset by PD-1. When Atezolizumab was utilised in combination with current chemotherapy regimens, notable increases in overall survival and progression-free survival when compared to control groups[47], [48], [50]. However, it is important to note that the specific mechanisms driving PD-L1 mediated immune suppression are not well understood.

Overall, TBNC treatment still relies on conventional cancer treatments due to its intrinsic heterogeneity. However, it is becoming apparent that like HER2-type and HR+ tumours, TNBC also relies on common interactions with the surrounding tumour microenvironment, immune cells, and immune pathways to avoid degradation. Thus, as our understanding of these interactions and processes increases, our ability to augment conventional cancer treatments will increase, and as will the effectiveness of treatment strategies for TBNC.

1.5.4. Barriers to improving treatment.

It is evident that treatment of breast cancer from patient-to-patient is highly variable and has varied outcomes based on staging, molecular sub-type, and individual patient characteristics. One way in which this has been counteracted is through

improvements in diagnostic technologies and strategies that allow the detection of breast cancer in the early phases of the disease, where surgical intervention is more likely to be successful. Screening programmes and their coupling with surgical intervention and systemic therapies have meant that since the late 1980s the number of associated deaths as a result of breast cancer has declined [51]. Despite this decline in mortality, this pre-emptive model of treatment carries its own negatives that need to be addressed in order to further improve treatment of this disease. For example, only 30-40% of DCIS cases are likely to progress to invasive and metastatic carcinomas [52]. Thus, it is often the case that screening programmes lead to over-diagnosis and over-treatment of low-risk and benign tumours, which in turn carries negative impacts on patient wellbeing, patient quality of life, and incurs higher healthcare costs for providers, and in some cases, patients themselves [51]. Furthermore, where screening programmes fail or are not implemented, such as in developing countries, late detection of breast cancer still carries very poor prognoses and 5-year outcomes for patients.

These problems associated with poor prognosis, over-diagnosis, over-treatment, and the varying effectiveness of treatment options is a result of two main factors. First, we do not fully understand the specific molecular mechanisms that drive breast cancer migration and invasion; the integral components of metastasis, the major cause of death in cancer patients [53]. Second, a lack of understanding of how tumours interact within their microenvironment during metastasis and development [54].

1.6. Invasion Potential Differs between Breast Cancer Subtypes.

Breast cancer cell invasion and associated metastasis is not a random process, although all breast cancer sub-types have the potential to metastasise, there is a clear pattern in the rates and locations of tumour spread between breast cancer sub-types [52], [55]. The site in which a tumour metastasises to is a substantial indicator on patient survival, whereby metastasis and associated organ disruption to the brain, liver, and lungs, is much more severe than bone metastasis. Furthermore, different metastatic sites carry differences in treatment options and efficacy. For example,

when cancers metastasise to the brain, they are harder to access, drug effectiveness decreases due to the blood brain barrier, and disruption to the brain by the cancer cells themselves is more fatal. On the other hand, metastasis to bone is often more easily accessible, organ disruption is less fatal, and drug effectiveness is maintained.

Studies comparing the differences in metastatic characteristics between breast cancer sub-types have found that TNBC and HER2+ breast cancers have higher rates of metastasis than HR+ breast cancers [55]. Furthermore, when investigating the site of metastasis between sub-types, it is evident that there is a clear preference in terms of their site of metastasis. Specifically, HR+ breast cancers preferentially metastasis to bone; TNBC preferentially metastasis to the lungs; and HER2+ breast cancer preferentially metastasise to the brain and liver [55]–[59].

Although these trends have been observed, the molecular mechanisms driving cancer cell invasion are a complex interplay between cell-intrinsic processes and the associated signalling between tumour cells and their surrounding microenvironment.

1.7. Adoption of migratory phenotypes is driven by a complex interplay between cancer cells and their microenvironment.

All cells have differential migratory properties linked to their function in the body, for example immune cells are much more migratory than epithelial cells. Thus, not all cancer cells will have migratory properties as part of their native gene profile, yet advancement of the vast majority of cancers ultimately leads to metastasis and migration to distinct secondary sites (Figure 3). Adoption of migratory phenotypes and subsequent invasion of cancer cells can be brought about by two distinct mechanisms: 1) Genetic mutations drive the adoption of migratory phenotypes via disruption to tumorigenic pathways mentioned previously. 2) Changes in microenvironment conditions and associated signalling between tumour cells and their microenvironment can drive changes in gene, transcriptomic, and metabolic profiles that lead to the adoption of migratory phenotypes in cancer cells.

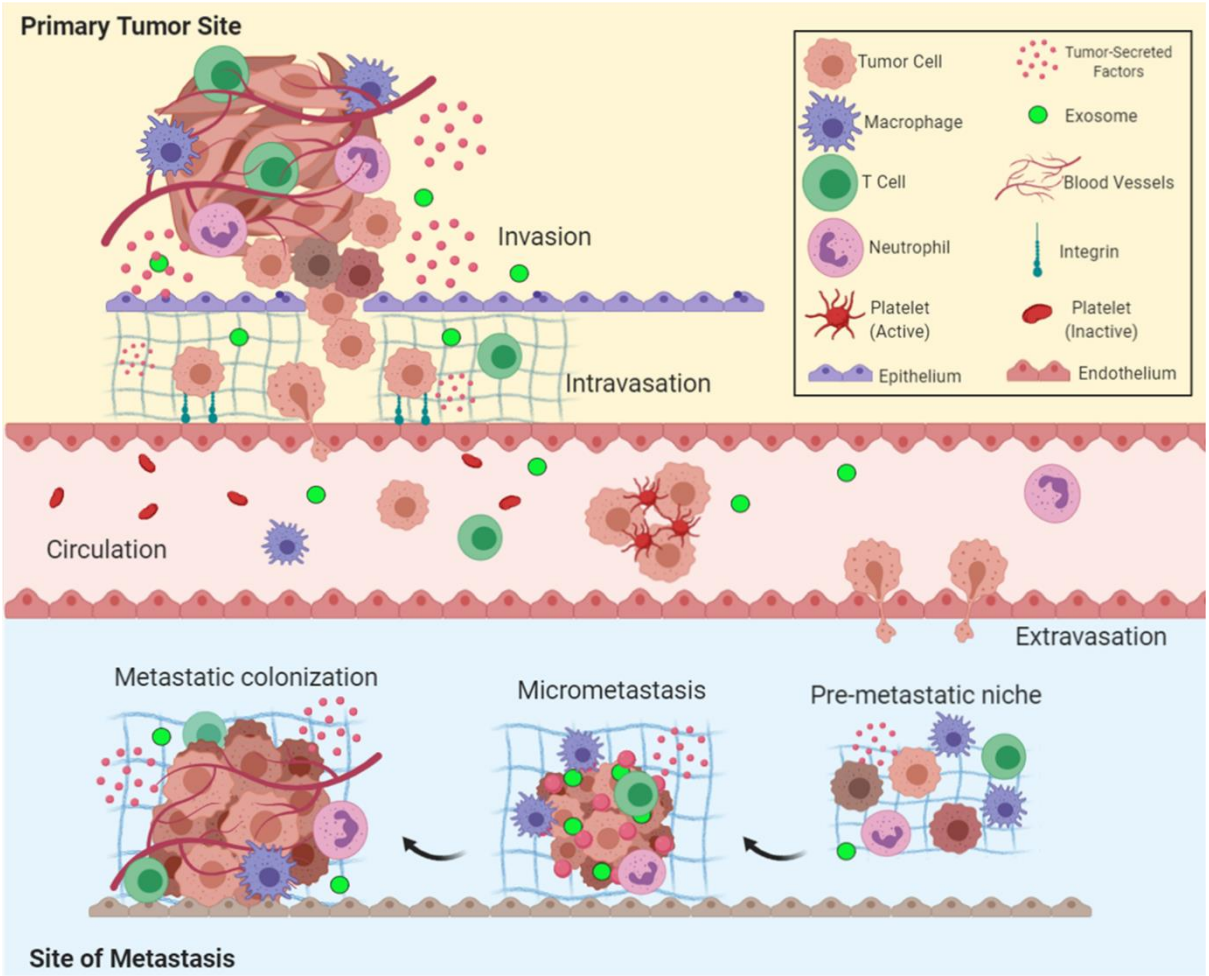

Figure 3: Overview of the metastatic cascade: The five key steps of metastasis include invasion, intravasation, circulation, extravasation, and colonization. Figure adopted from Fares et al, 2020 [60].

These changes in microenvironment conditions are driven by tumour cells and their development. During tumorigenesis, tumour cells acquire the ability to ignore the normalising queues present in the surrounding microenvironment. This allows tumour growth to continue occurring unhindered, and leads to remodelling of the surrounding microenvironment [61]. For example, as tumour growth continues, cancer cell populations grow past the carrying capacity of their local microenvironments. This lowers oxygen availability and creates nutrient depleted environments, thereby providing a selection pressure for proliferating cancer cells. This selection pressure leads to the preferential selection of cells with high invasive potential, and thereby the adoption of migratory phenotypes in response to the remodelled microenvironment, as these cells can move to nutrient rich areas and proliferate [61], [62].

This adoption of migratory phenotypes can also be driven by resident cell populations, such as cancer associated fibroblasts, in the remodelled microenvironment. Cancer associated fibroblasts (CAFs), generated in response to microenvironment remodelling or tumour cell (trans) differentiation, mediate the adoption of migratory phenotypes. It has been found that CAFs have differential cytokine profiles than normal fibroblasts. For example, CAFs release increased amounts of transforming growth factor-β (TGFβ). TGFβ binds to form a complex of transmembrane receptor serine/threonine kinases on cancer cells and induces their trans-phosphorylation. Once phosphorylated, type I receptors phosphorylate Smad2/3 which complexes with the common-mediator Smad (co-Smad) Smad4 to form activated Smad complexes [63]. Activated Smad complexes translocate into the nucleus of the cancer cell, where they modulate gene transcription to drive the acquisition of a mesenchymal phenotypes, and in turn the increased migratory potential associated with this cell class [63].

1.8. Molecular mechanisms driving cancer cell migration.

Once migratory phenotypes have been adopted by cancer cells, they can either invade as individual cells, or as highly coordinated collectives. Individual cancer cell invasion and migration can be split into two main mechanisms: proteolytic dependent migration, or proteolytic independent migration. The differences between these two mechanisms have been summarised in Table 7.

Table 7: A table highlighting the differences between proteolytic dependent and proteolytic independent migration mechanisms.

Characteristic	**Proteolytic Dependent Migration**	**Proteolytic Independent Migration**
Secretion of MMP's + Protease Loaded Vesicles	+	-
Cytoskeletal Contractility	+	+
Morphology	Rounded, Amoeboid	Elongated, Mesenchymal
Alignment to ECM fibres	+	-
Adhesions	Strong	Weak, Dynamic

During proteolytic dependent invasion mechanisms, individual cancer cells exhibit elongated mesenchymal morphologies and move away from tumour sites by generating traction force via cytoskeletal contractility and integrin-mediated ECM-adhesion [53], [64]. However due to the dense packing of the ECM, internally generated traction force is not high enough to force cells through the surrounding matrix. To counteract this, cancer cells align their contractile fibres with that of the ECM and secrete protease-loaded vesicles in the direction they are migrating [65]. This degrades ECM fibres in front of the cell and allows cancer cells to generate paths away from the initial tumour site [66]. Then by aligning with the surrounding ECM fibres, cancer cells are essentially able to pull themselves along the fibres in the desired direction of migration [53], [65], [67].

Conversely, proteolytic-independent mechanisms, also known as amoeboid-like migration mechanisms, see cancer cells assume more rounded and deformable morphologies. This difference in morphology allows cancer cells to traverse the pores of the ECM without the need for proteolytic enzymes and instead through their own internally generated traction forces [64], [66]. During this type of movement, the cells do not align with ECM fibres, but instead create protrusions driven by actomyosin contractions, and traverse the tumour microenvironment quickly by maintaining weak and dynamic cell adhesions to the surrounding ECM [53], [65]. This strategy of movement allows cancer cells adopting this migration type to selectively navigate through tissues via pores of appropriate size using internally generated traction forces [65], [67].

Distinct to single cell migration mechanisms, cancer cells can also migrate as a highly coordinated collective [53]. Grouped cancer cell movement incorporates aspects of both proteolytic dependent and independent single cell migration. The cell collectives use signalling to partition migratory functions across heterogenous cell populations to achieve highly coordinated grouped migration. This is allowed through the retention of cell-cell connections, coordination of cell movement via cell polarisation and actin dynamics, integrin-based ECM adhesion, and proteolytic cleavage of the surrounding ECM to create pathways for movement [53], [66], [67]. The cells composing these multicellular units are polarised into a leading edge and

trailing edge [53], [68]. Cells at the leading edge have vastly different gene expression profiles and morphological characteristics than cells at the trailing edge allowing highly coordinated and efficient movement of the multicellular collective [53], [68], [69]. At the cellular level, there are many similarities between collective migrating cells and proteolytic-dependent single migrating cells For example, alignment of the collective unit with ECM fibres and overexpression of MMP-14 and cathepsin B proteases allows the leader cells to generate ECM tracks which the trailing cells can follow [53], [69].

1.9. Cell Lines commonly used to understand Breast Cancer Invasion.

It is evident that cancer cell migration is a complex process that is further complicated by the heterogeneity of tumour cells themselves, as well as the interactions they undertake with their surrounding microenvironment. When surveying the literature, *in vitro* models have helped us understand standalone processes driving breast cancer migration through the use of three main immortalised cell lines: MCF-7's, MCF-10A, MDA-MB-231.

The MCF7 epithelial line (ECACC 86012803) is an immortalised cell line that was originally derived from the pleural effusion of a 67 year old Caucasian Female suffering from breast adenocarcinoma [70]. The cell line is a well characterised and has been used in a wide variety of *in vitro* studies surrounding breast cancer research showing that this cell line is robust and reliable. The cells exhibit some features of differentiated mammary epithelium including oestradiol synthesis and formation of domes, while also expressing ER and PR receptors which allow them to represent hormone receptor positive breast cancer [71], [72]. Furthermore, the MCF-7 cell-line is a poorly aggressive and non-invasive cell line with low metastatic potential, making it an ideal candidate for modelling HR+ and DCIS lesions *in vitro*. The cell line has also been used in a range of *in vitro* invasion models [72]–[74].

The MCF 10A is an epithelial cell line (ATCC CRL-10317), that immortalised spontaneously without defined factors [75]. The cell line was originally isolated from the mammary gland of a White, 36-year-old female donor with fibrocystic breasts.

Furthermore, the cell line is non-tumorigenic and lacks oestrogen receptor expression [75]. The non-tumorigenic nature of the MCF-10A cell line makes it ideal for producing a reproducible, breast cancer invasion models that are representative of healthy mammary tissue. The MCF-10A cell line has also been used previously in the literature in *in vitro* invasion models [51], [75].

The MDA-MB-231 epithelial cell line is an immortalised cell line that was originally derived from the from a pleural effusion of a 51-year-old woman with metastatic breast cancer [93]. MDA-MB-231 is a TNBC cell line that lacks hormone receptor expression, as well as HER2 amplification [76]. These factors make the cell line highly aggressive, invasive, and poorly differentiated. Furthermore, the highly aggressive and invasive nature of the cell line makes it an ideal candidate for modelling IDC lesions *in vitro*. The MDA-MB-231 line has also been used previously in the literature in *in vitro* invasion models [76]–[78].

1.10. In Vitro Platforms for Investigating Breast Cancer Invasion and Their Limitations

Experimental models, *in vivo* and *in vitro*, are vital tools for scientists to understand the cellular and molecular biology driving different pathologies, as they provide a platform to analyse properties such as the biochemistry, functionality , and morphology of diseased and wild-type cells in a controlled environment [79], [80]. While the cell lines mentioned previously have been imperative in the formation of robust and reliable models for investigating breast cancer invasion, they often lack physiological or clinical relevance. For example, in recent years it has become increasingly apparent that a cells surrounding microenvironment plays a substantial role in cellular morphology, behaviour, and therefore, their function. This is because the external signals provided by the microenvironment can influence cell-cell interactions, cell signalling, and in turn gene expression. This accounting for wider tumour architecture and the microenvironment a tumour develops in is often mis-represented or missing from breast cancer invasion models in the literature, and even the ones those that do try to account for this aspect of tumour development either suffer from problems in reproducibility, or incorrect composition of the tumour microenvironment.

The platform for building clinically relevant models is a major determining factor of a cell system's microenvironment. There are three main platforms for building clinically relevant models for breast cancer research: 2D Cell Culture, Animal Models, and 3D Cell culture. Each of these have been used to recapitulate the breast cancer biology, however they each carry their own advantages and disadvantages in terms of their physiological relevance, cost, and reproducibility. Table 8 summarises these advantages and disadvantages.

Table 8: A Table describing the advantages and disadvantages of clinically relevant breast cancer research platforms.

Model Platform	**Advantages**	**Disadvantages**
2D	• Low cost. • Simple maintenance. • High degree of experimental control.	• Altered cell morphologies. • Lack of microenvironmental cues • Lack of ability to recapitulate tumour structures. • Limited translatability of research to *in vivo.*
Animal Models	• Accurate *in vivo* microenvironment that accounts for interactions with other organs in a functioning organism. • Compatibility with primary cell samples to increase understanding of tumour heterogeneity.	• High cost. • Complicated maintenance. • Requires immunocompromised mice. • Limited translatability of research to humans due to physiological differences.

Hydrogels	• Accurately reflect tissue soft tissues and mechanical features. • Tuneable mechanical characteristics. • A representative microenvironment that promotes the formation of *in vivo* characteristics.	• Batch-Batch Variability • Limited physiological relevance • Rely on the supplementation with exogenous proteins to form physiologically relevant microenvironments
Organoids	• Creation of self-organising tumour-like structures. • The potential to better understand organ development and function on a tissue-wide scale.	• Lack of reproducibility • In vivo characteristics are limited. • Limited investigative potential for migratory characteristics.

1.10.1. 2D Cell Culture

Traditional cell culture, also referred to as 2D cell culture, refers to the growth of cell lines as a monolayer in a culture flask or petri dish [79]. With respect to breast cancer, these models have been vital in understanding which families of genes and signalling molecules contribute to breast cancer processes and development. For example, by transfecting MCF-7 cells (an immortalised cancer cell line which represents the ER+/PR+ molecular subtype of breast cancer) with vectors instructing the overexpression of growth factors and growth factor receptors, it was found that Fibroblast Growth Factor-4 and -1 (FGF-4 & FGF-1) were implicated with the acquisition of invasive phenotypes seen in late breast cancer development [81]. The ability to manipulate gene expression in a controlled environment, coupled with the low cost of maintenance is a major advantage of 2D cell culture.

Although this type of platform is a cost-effective way to screen and identify potential pathways involved with disease development, the monolayer nature of the cells in 2D means there are substantial limitations to this platform for building *in vitro* models. For example, cell structure does not represent those found in native tumour structures, the cells become more flattened which leads to altered cell-cell adhesions and cell-plastic interactions. This is well demonstrated in Figure 4, where during 2D cell culture fibroblasts adopt a wildly different morphology and fibronectin organisation than when they are in a 3D environment. These differences are further summarised in Figure 2, which shows the extent of *in vivo* factors and microenvironmental cues that 2D cell culture misrepresents, uniquely expresses, or does not account for. For example, although you can alter mechanical stiffness of the plastic substrate utilised during 2D culture, it is typically not representative of tissue flexibility and stiffness *in vivo*, thus skewing the microenvironment and potentially causing an abnormal cellular response.

These misrepresentations and unique microenvironmental cues found in 2D cell culture lead to cellular responses that can alter gene expression profiles, developmental routes adopted, metabolic activity [79]. This often means that when trying to translate research, such as drug effectiveness, ‘hits’ found in 2D Cell Culture do not perform when pursued further down the research pipeline, such as in human trials, due to differences in cell morphology, metabolism, and gene profile brought about by the substantially different microenvironment.

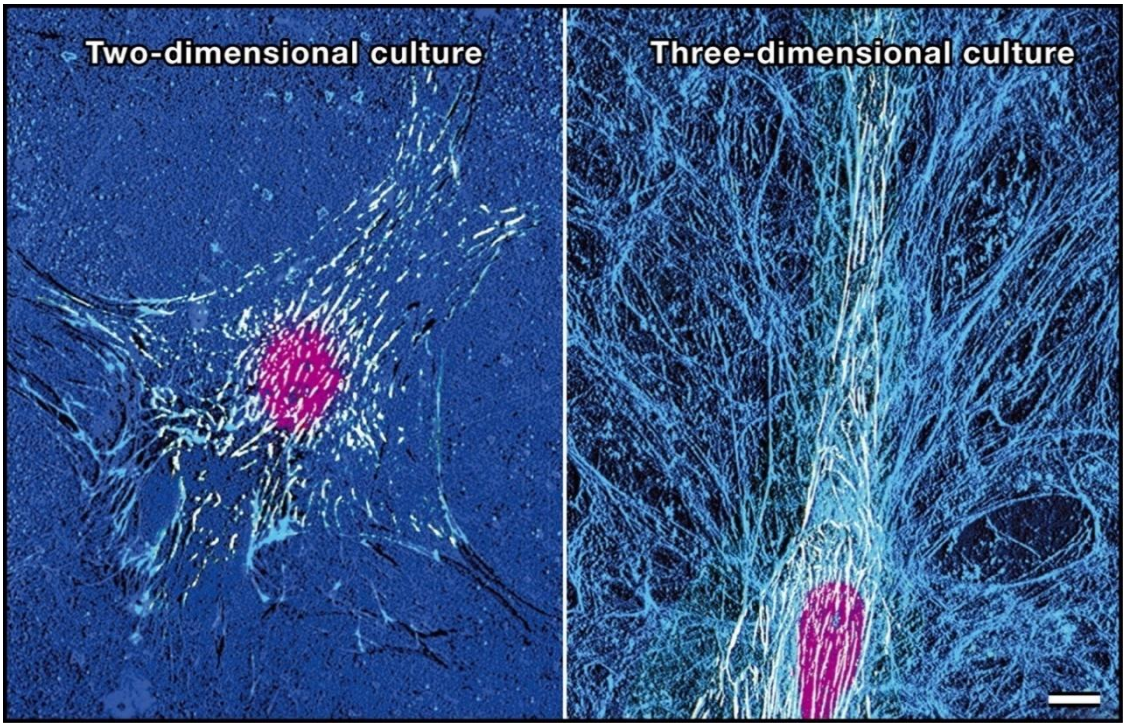

Figure 4: Left panel: Fibroblasts cultured on planar fibronectin. Right Panel: Fibroblasts cultured as part of a mesenchymal cell-derived three-dimensional (3D) matrix. Fibronectin matrix = blue, α5 integrin-positive adhesion structures = white; nuclei are magenta. Scale bar = 10 μm. Figure and legend sourced from: Yamada and Cukierman (2007) [82]

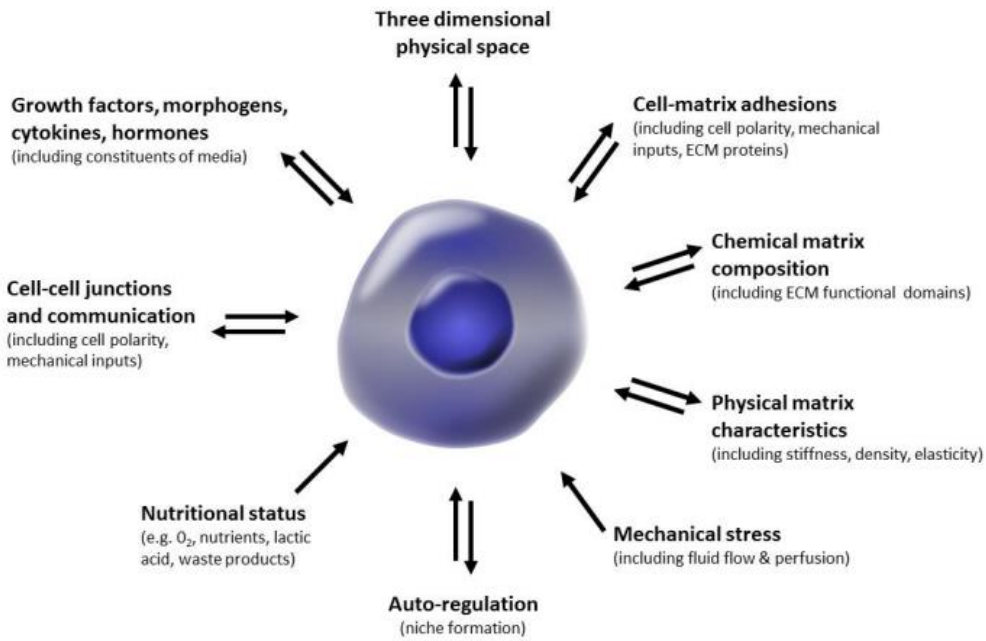

Figure 5: A diagram demonstrating the interplay of external microenvironment factors with a cell. Sourced from a Figure provided by Stefan Przyborski, adapted from Yamada & Cukierman (2007)[82].

1.10.2. Animal Models

It is evident that 2D cell culture does not account for key *in vivo* characteristics such as nutritional distribution, mechanical stress, and chemical matrix composition, ultimately meaning that 2D culture is not able to achieve the same complexity as *in vivo* microenvironments. One way to circumvent this has been to utilise animal models, such as immunodeficient mice. For example cell-derived xenografts (CDX) on immunodeficient mice, whereby breast cancer cell lines such as: MCF-7's and MDA-MB-231's, are implanted subcutaneously and their development monitored, have been particularly useful in allowing both the validation of target genes involved in breast cancer metastasis, and the identification of potential breast cancer therapeutics [83]. For example, Borges *et al.,* injected MDA-MB-231 cells (a cell line that represents triple negative breast cancer) into the mammary glands of immunodeficient mice and used progression tissue microarrays to show that a switch towards expression of Protein Kinase D (PKD) 3 occurs in aggressive cancers [73]. This was taken a step further by knocking down PKD3 which resulted in a decrease in cancer cell proliferation, migration and invasion in the murine models [73]. A similar effect was observed when using CRT0066101, a PKD3 inhibitor, ultimately allowing the identification of a potential novel therapeutic for triple negative breast cancer based around PKD3 inhibition [73]. This ability for murine models to predict the effectiveness and toxicity of novel compounds, makes them very attractive in breast cancer research as they can give insights not only on a tissue-wide scale, but also on an organism-wide scale that cannot be achieved in other conventional cell culture platforms.

There is a limitation when utilising CDX's in murine models, in that immortal cancer cell lines, such as MDA-MB-231's and MCF-7's, are derived from highly aggressive malignant tumours or plural effusions [83]. This makes these cell types less useful for modelling the early stages of development of breast cancer. Furthermore, there is the added problem of heterogeneity in breast cancer diagnoses and treatment, where there isn't just variation between patients, but also between cells composing actual tumours. These cell lines do not generate tumours with the same variability as that observed in patients [54].

These problems have been addressed, in part, through the use of patient-derived-xenograft (PDX) murine models, which allow the integration of patient samples / primary cells into immunodeficient murine models [84]. This is especially important during drug development where CDX and genetically modified murine models often lead to mis-predications for novel drugs which carries huge costs to developers [85]. The ability for PDX models to mimic patient heterogeneity could be one way to reduce costs of drug development as it could reduce the likelihood of a misidentification. Furthermore, these models could be vital for both increasing our understanding of the extent of heterogeneity in breast cancer treatment, and how cell types transform during the course of the pathology.

Overall, murine models allow observations and data to be collected in a 3D microenvironment with an organism-wide physiological context that cannot be achieved in 2D cell culture, whereby features such as toxicity and tumour advancement can be assessed in a controlled manner [86]. Despite this, murine models do carry their own disadvantages. For example, immune cells and their interactions with cells and the microenvironment is nullified in these models, as the mice must be immunodeficient. Immune cells play a role in cancer development and metastasis through cell-cell interactions and secreted factors; thus, these models are reduced in their predictive capacity. Furthermore, the upkeep, low take rate of engrafted tumours, and maintenance of these models also poses a large cost to their use in pre-clinical trials. Finally, mice are physiologically not humans, they have their own biology, differing from humans in terms of their gene expression patterns, alleles, and protein types. This means that while these models can be indicative, they will never be able to provide conclusive results for direct use in humans. It is evident that there is a need for reproducible and cost-effective models that can better recapitulate human tissues in order to effectively advance our understanding of breast cancer biology.

1.10.3. 3D Cell Culture

3D cell culture has the potential to solve some of these disparities produced by murine and 2D models. First, they have the potential to supply researchers with highly reproducible models that are cheaper than animal studies, Secondly, these

models contain features that will enhance their physiological relevance, when compared to 2D and murine model systems. For example, the ability to utilise human cells to recreate the structure of native tissues will make results more translatable to human conditions. Furthermore, these models can also account for the microenvironmental cues, making 3D models more similar to the conditions experienced *in vivo*. There are multiple formats of 3D cell culture, which can be broadly split into 3 categories: hydrogels, organoids, and scaffolds. Each of these culture systems carry their own advantages and disadvantages when analysing their use as breast cancer models.

1.10.3.1. *Hydrogels*

One route for creating 3D matrices in which cells can grow is through the use of hydrogels. Hydrogels are crosslinked polymer chains that contain high water contents and allow diffusion of soluble factors, oxygen, waste, and nutrients through their matrices [87]. Furthermore, they accurately recapitulate the nature of many soft tissues, making hydrogels an attractive option for replicating the extracellular matrix and in turn, the breast tumour microenvironment in terms of model stiffness and the effect this has on mechano-transduction to seeded cells [87].

The benefits of hydrogels as a platform for creating 3D breast cancer models is highlighted by Vantangoli *et al.,* who utilised non-adhesive agarose hydrogels and seeded MCF-7 cells into them [88]. In this study, seeded MCF-7's formed microtissues that represented breast luminal structures and secreted carbohydrate-positive material into the luminal spaces [88]. The formation of these microtissues, shows how hydrogels can be used to form a microenvironment that encourages the formation of *in vivo*-like characteristics. The positives of hydrogel-based systems are further exemplified by the work by Wang *et al.,* who found that when MCF-7 cells are cultured in their hydrogel system the breast cancer cells better retained and exhibited their malignant phenotype than in 2D [89]. In addition to improving cell behaviour and histology, hydrogel systems also have advantages in terms of their ease of use. For example, Huang *et al*., formed hydrogels using H9E peptides. This hydrogel can be diluted, and its structure disrupted to allow easy isolation of cells cultured in 3D [90]. Furthermore, the H9E hydrogel allows effective diffusion of the

drug Cisplatin throughout its matrix, potentially meaning that during drug studies you could easily expose a cell population to a drug in 3D, then easily isolate them for downstream analysis [74].

It is evident that hydrogels have large advantages in terms of ease of use and the provision of physiologically relevant microenvironments that produce morphologies and cellular behaviours that are more representative of those found *in vivo*. Despite this, there are drawbacks to hydrogels as a platform for building 3D clinical models. For example, although naturally derived hydrogels can be advantageous in promoting cellular proliferation, differentiation, and adoption of *in vivo*-like characteristics, they are often ill-defined and suffer from batch-batch variability which makes results difficult to reproduce from experiment to experiment [87]. Although synthetic hydrogels overcome these problems through, their composition poses different limitations. Specifically, synthetic hydrogels are made of polymers such as polyethene glycol which are not found *in vivo*. This means models created using synthetic hydrogels lack the presence of polymers and exogenous components such as collagens, fibronectins, polysaccharides, ECM proteins, thereby limiting their physiological relevance. Thus, synthetic hydrogels are not as easily able to recapitulate the stromal compartment of organs in this manner without exogenous additions of proteins, which often carry high degrees of batch-batch variability and reduces their reproducibility.

1.10.3.2. *Organoids*

Organoids are self-organising 3D culture systems that utilise stem cells (adult or embryonic), cell line progenitors, or tissue specific cell populations to form spheroid structures that are highly similar to human organ structures [91]. This self-organising nature of organoids, coupled with their generation from human stem cell lines, gives them huge potential as a 3D culture system to better understand organ development and function on a tissue-wide scale, in a more physiologically relevant setting than traditional 2D cell culture or murine models [91], [92]. Furthermore, when compared with traditional 2D culture systems, organoids also better resemble the native organ

they are trying to recapitulate in terms of their gene expression profiles, metabolic function, and recapitulation of *in vivo* structures [91], [93].

Organoids have huge potential for drug discovery and personalised medicine, where they could be used to augment current treatment strategies. For example, Bruna *et al*., have created a biobank of breast cancer explants to screen novel compounds for anti-cancer capabilities. This biobank utilises PDX onto immunodeficient mice, which as previously mentioned have drawbacks in terms of physiological relevance and cost [94]. Organoids could be used in a similar way, whereby generation of patient-derived organoids could be used to screen treatment options and novel compounds in a system that accounts for the tumour microenvironment and patient derived cell lines [95].

However, organoids do carry their own disadvantages when trying to utilise mammary epithelial cells to recapitulate the breast microenvironment. For example, these types of organoids are often hard to produce as suitable and compatible cell lines can be difficult to source. This reason is twofold, whereby cells composing breast tissue are highly differentiated, and the hierarchy of cells within the mammary breast epithelium is highly complex, making it hard to find a common progenitor to use for organoid generation. Furthermore when trying to recapitulate cancer pathologies as part of organoid studies, it is difficult to isolate and preserve progenitor breast cancer cells [96]. Recently, a subset of mammary epithelial cells that express basal surface markers (CD49+, EpCAM-) have been shown to form both basal and luminal cells *in vitro* and *in vivo,* however more work is required to make generation of breast organoids accurate and reproducible [96], [97]. Reproducibility of organoids is also a limiting factor of their use in wider research, where spheroids show large variations in diameter. This poses a problem because if organoids are too large the cells within can become necrotic reducing functional model yield, and if they are too small, they do not effectively recapitulate the relevant tissue structures they are trying to mimic [93], [98]

1.11. Alvetex® As a Platform for Building a Physiologically Relevant Breast (Cancer) Model

Overall, it is evident that hydrogels and organoid cell cultures have huge potential for recapitulating tissue-scale architecture and function. However, as previously mentioned, these types of 3D culture platform often lack the characteristics to investigate invasion effectively. For example, the structure of organoids means you cannot measure invasion, and hydrogels lack the ability to measure changes in the ECM that occur during invasion and metastatic processes. A scaffold-based 3D cell culture platform, Alvetex®, has the potential to overcome these problems, where it could be used to produce reproducible and physiologically relevant tissue models to advance our understanding of human pathologies. The growth of cells onto the scaffold itself means that invasion can be measured via cell depth penetration, and the ability to have ECM components supplemented in an endogenous manner, means that changes in these microenvironmental components can be accurately measured.

1.11.1. Advantages of Alvetex®

The preparation of Alvetex® carries many advantages for its use as a 3D cell culture system. For example, the scaffold is cut at a thickness of 200 µm to match the tissue diffusion limit. This, combined with the highly porous nature of the scaffold, means that much like hydrogels, media and other diffusible elements (O_2, CO_2, growth factors, etc…) can easily pass through the scaffold at this thickness to keep cells viable, which ultimately avoids the presence of necrotic cells often observed when utilising larger sized and more complex organoids, and therefore enables long-term cell culture in 3D.

In addition to this, the formulation of Alvetex® using polystyrene means that the scaffold itself is made from the same material as conventional 2D cell culture flasks. The use of polystyrene as part of the scaffold makes Alvetex® inert and well defined. This means it is unlikely for the scaffold to interfere with cellular chemistry and interactions, nullifying the batch-to-batch variability that can be observed when using natural hydrogels or supplemented synthetic hydrogels. Another major advantage of the Alvetex® platform is that it is highly compatible with current, and widely used, cell

culture formats such as 6-well and 12-well adherent plates. This lack of need for specialist equipment, alongside its manufacture using polystyrene, makes Alvetex® a cost-effective and easily adoptable technology when compared to other 3D cell culture platforms and *in vivo* models.

1.11.2. Previous Alvetex® Models: Why a Breast Cancer Invasion Model is Feasible

Previously, Alvetex® has been used to recapitulate a range of epithelial tissues, including intestinal and epidermal structures [99], [100]. These studies show how Alvetex® is able to effectively model epithelial tissues, and their microenvironments, through the generation of tissue specific stromal compartments, and the subsequent seeding of epithelial populations on top of these compartments. This proven ability for Alvetex®-based models to effectively recapitulate epithelial tissue architecture and function *in vivo,* as well as improve upon current 2D models, means this platform could have the potential to recapitulate mammary tissue and breast cancer *in vitro*.

The feasibility of an Alvetex®-based breast cancer invasion model is also part supported by the previous use of breast cancer cell lines in conjunction with Alvetex®. For example, MCF7 cells (ECACC 86012803) which represent hormone receptor positive (ER+/PR+) breast cancer phenotypes, were shown to not only effectively grow in the scaffold but they also expressed fewer stress related pathways and biomarkers [101]. Furthermore, MDA-MB-231 cells (ECACC 92020424) which represent triple negative breast cancer phenotypes, were grown in a Matrigel coated Alvetex® scaffold and migration assays were used to better understand how Wnt and PI3K/AKT pathways stimulate tumour metastasis and migration in triple negative breast cancer [76].

Both studies support the feasibility of an Alvetex®-based breast cancer invasion model as they not only show that breast epithelial cell lines are compatible and can grow as part of an Alvetex® scaffold, but that these cell lines express fewer stress pathways, adopt more *in vivo*-like characteristics and morphologies, and have been used to measure invasive potential, when used in conjunction with Alvetex®. Furthermore, both the MCF-7 and MDA-MB-231 cell lines have been used

extensively in both 2D and 3D *in vitro* models, as discussed in section 1.9, supporting their biocompatibility with this platform of *in vitro* model.

Both Alvetex® studies only grew these cells as mono-culture regimens without key microenvironmental constituents, showing that their use within this platform could be improved to build more accurate and physiologically relevant breast cancer invasion models. For example, the previous biocompatibility of these cell lines with Alvetex®, and the refined use of HDFn derived stromal compartments with other epithelial tissues, starts to elicit a direction where these models could be taken further. Specifically, a stromal compartment could be generated and then the biocompatible breast cancer cell lines (MCF-7 and MDA-MB-231's) could be seeded on top to create a robust 3D model that recapitulates and accounts for the microenvironment found *in vivo*. Furthermore, the commercial availability of MCF-10A cells (ATCC product ID: CRL-10317), an immortalised cell line of non-tumourgenic healthy breast cells, means that potential Alvetex®-based breast cancer invasion models could model the distinct pathological timepoints of the disease (namely: healthy, DCIS, and IDC), in a way that accounts for the tumour microenvironment. If successful, these models could ultimately be used to make better *in vivo* predictions about breast cancer biology during metastatic and invasion processes.

Overall, it is evident that not only are Alvetex®-based breast cancer models feasible, but they could also be used to advance our understanding of breast cancer migration and invasion as part of a breast cancer system. The presence of three extensively used immortalised cell lines (MCF-10A, MCF-7, MDA-MB-231) in the literature that represent the different sub-types, and developmental stages, of breast cancer presents clear options for the development of reproducible Alvetex®-based models. Furthermore, there is a clear need in the literature for models that account for the tumour microenvironment, which Alvetex®-based breast cancer models could account for. This thesis aims to develop a range of Alvetex®-based breast cancer invasion models, with variably complex microenvironments, that recapitulate the key pathological timepoints of breast cancer development and assess how these compare to conventional 2D invasion models of breast cancer.

2. Hypothesis

It is hypothesised that across cell culture platforms (2D, Alvetex® Strata mono-culture models, and Alvetex® Scaffold Co-Culture models) migratory potential will differ between immortalised cell lines, with MCF10A's representing healthy breast epithelial cells being the least migratory, and MDA-MB-231's representing the IDC pathological timepoint being the most migratory, while MCF-7's will act as a migratory intermediate of the two. Furthermore, it is hypothesised that as cell-culture complexity increases from 2D, to 3D monoculture, to 3D Co-culture, migration results for each cell line will still differ, but will change to better represent their *in vivo* counterparts. During co-culture in the Alvetex® scaffold platform we also hypothesise that culture of breast cancer derived cell lines (MCF-7's, MDA-MB-231's, MCF-10A's) with HDFn's will allow the formation of a robust and reproductible model for investigating breast cancer migration in a system that accurately represents and recapitulates its *in vivo* counterpart. This ability to represent and recapitulate *in vivo* characteristics will be assessed through anatomical and functional characterisation of the model. Furthermore, we hypothesise that the model can be improved through the incorporation of primary mammary fibroblast and epithelial cells.

3. Aims

- To develop and assess the effectiveness of an Alvetex®-based 3D Co-culture and monoculture model for investigating the invasive properties of breast cancer cells through treatment with a known migration inhibitor and comparing with other invasion platforms (2D scratch assays)

4. Objectives

- Determination of Invasion Characteristics in 2D.
- To assess cell-line standalone migratory potential in 3D monoculture using Alvetex® strata and measuring depth penetration of each cell line.
- Creation of initial breast mucosal co-culture equivalents that represent each pathological timepoint of breast cancer through the seeding immortalised breast cancer derived cell lines onto a HDFn stromal compartment.
- Determination of invasion characteristics of immortalised cells in 3D Co-culture models.

- Incorporation of primary mammary derived fibroblasts into Co-Culture models with immortalised cell lines to increase physiological relevance.
- Incorporation of Primary Healthy Epithelial Cells with primary mammary cells and HDFns to create a healthy mammary mucosal model.

5. Materials and Methods

5.1. 2D Cell Culture

5.1.1. MCF-7 Epithelial Cells

5.1.1.1. *Cell Line Maintenance*

MCF-7 epithelial cells were maintained in Dulbecco's Modified Eagle's Medium (DMEM, ThermoFisher Scientific), supplemented with 10% foetal bovine serum (FBS, Thermofisher Scientific, 49 Massachusetts, USA), 2mM L-glutamine (ThermoFisher Scientific) and 5% Penicillin and Streptomycin (ThermoFisher Scientific) at 37 °C, in a 5% CO_2 humidified environment. Henceforth, assume this is the media used in conjunction with the MCF-7 cell line unless otherwise stated.

5.1.1.2. *Revival, Passage, and Cryopreservation*

During the revival procedure, the MCF-7 cells were rapidly transferred from -150 °C storage into a 37 °C waterbath to thaw. Once a small ice crystal remained, the cells were then transferred into a 75cm^2 BD Falcon culture flask (BD Falcon, Erembodegem, Belgium) containing 13 mL of media at a seeding density of 27,000 cells/cm^2. The newly seeded flask was then incubated at 37°C, in a 5% CO_2 humidified environment overnight, where the following day the cells were media changed with 13 ml Media to remove any dimethyl sulfoxide (DMSO, Sigma-Aldrich, Dorset, UK) leftover from cryopreservation.

Once 70-80% confluent, typically in 5-7 days, the cells were routinely passaged into a new 75cm^2 culture flask (BD Falcon) at a ratio of 1:4 or a seeding density of 27,000 cells/cm^2. When passaging this cell line, the 70-80% confluent T75 cm^2 flasks were aspirated of their media and washed in approximately 5 mL PBS. The cells were then trypsinised using 2 mL 0.25% Trypsin EDTA (ThermoFisher Scientific)

and incubated for 5-10 minutes at 37°C, in a 5% CO_2 humidified environment. Once the cells were detached, the Trypsin was neutralised using an equivalent volume of media. After neutralisation of the trypsin, the detached cells were then transferred to a 15 mL falcon tube (Greiner Bio-One) and underwent centrifugation at 1000rpm for 3 minutes to form a cell pellet. A viable cell count was then performed using a trypan blue (Sigma-Aldrich) exclusion assay in which the cells were counted using a haemocytometer. After cell counts the cells would be seeded into a T75 cm^2 at a seeding density of 27,000 cells/cm^2 and topped up with Media to 13 mL

For cryopreservation, the cells were passaged as previously described. The cells were then counted and made up into a 5 mL cell suspension, using Media supplemented with 10% dimethyl sulfoxide (DMSO, Sigma-Aldrich, Dorset, UK), that contained 10 million cells. This cell suspension was then aliquoted into 5 cryovials (ThermoFisher Scientific), each containing 1 mL of the DMSO-supplemented cell suspension and 2 million cells per cryovial. Cryovials were then frozen down at a rate of -1 °C per minute at -80 °C using isopropanol chambers. Once frozen, the cell stocks were transferred to a -150 °C freezer or liquid nitrogen for long term storage.

5.1.2. MDA-MB-231 Epithelial Cells

5.1.2.1. *Cell Line Maintenance*

MDA-MB-231 epithelial cells were maintained in Dulbecco's Modified Eagle's Medium (DMEM, ThermoFisher Scientific), supplemented with 10% foetal bovine serum (FBS, Thermofisher Scientific), 2mM L-glutamine (ThermoFisher Scientific) and 5% Penicillin and Streptomycin (ThermoFisher Scientific) at 37 °C, in a 5% CO_2 humidified environment. Henceforth, assume this is the media used in conjunction with the MDA-MB-231 cell line unless otherwise stated.

5.1.2.2. *Revival, Passage, and Cryopreservation*

MDA-MB-231 cells were revived following the same method outlined in section 5.1.1.2 for the MCF-7 cell line. However, once 70-80% confluent, typically in 3-5 days, the cells were passage into a new 75cm2 culture flask (BD Falcon) at a 1:6 ratio or a seeding density of 27,000 cells/cm^2.

Cryopreservation and cell passage also followed the same procedures outlined in section 5.1.1.2 for the MCF-7 cell line.

5.1.3. MCF-10A Epithelial Cells

5.1.3.1. *Cell Line Maintenance*

MCF-10A Epithelial cells were maintained in Dulbecco's Modified Eagle Medium/Nutrient Mixture F-12 (DMEM:F12, ThermoFisher Scientific), supplemented with 10% foetal bovine serum (FBS, Thermofisher Scientific), Hydrocortisone (0.5mg/mL Sigma), Human Insulin (10µg/mL, Sigma), Human EGF (20ng/mL, Peprotech), Isoprenaline (100 nM, Tocris) and 5% Penicillin and Streptomycin (ThermoFisher Scientific) at 37 °C, in a 5% CO_2 humidified environment. Henceforth, assume this is the media used in conjunction with the MCF-10A cell line unless otherwise stated.

5.1.3.2. *Revival and Cryopreservation*

MCF-10A cells were revived following the same method outlined in section 5.1.1.2 for the MCF-7 cell line. However, once 70-80% confluent, typically in 2-3 days, the cells were passage into a new 75cm^2 culture flask (BD Falcon) at a 1:6 ratio or a seeding density of 27,000 cells/cm^2.

Cryopreservation and cell passage also followed the same procedures outlined in section 5.1.1.2 for the MCF-7 cell line, except for the use of 0.05% Trypsin EDTA.

5.1.4. Neonatal Human Dermal Fibroblast Cells

Primary Dermal Fibroblast Normal; Human, Neonatal (HDFn), lot number #34 (ATCC PCS-201-010) is a cell line isolated from a primary neonatal foreskin donor.

5.1.4.1. *Cell Line Maintenance*

HDFn fibroblast cells were maintained in Dulbecco’s Modified Eagle’s Medium (DMEM, ThermoFisher Scientific), supplemented with 10% foetal bovine serum

(FBS, Thermofisher Scientific), 2mM L-glutamine (ThermoFisher Scientific) and 5% Penicillin and Streptomycin (ThermoFisher Scientific) at 37 °C, in a 5% CO_2 humidified environment. Henceforth, assume this is the media used in conjunction with this cell line.

5.1.4.2. *Revival, Passage, and Cryopreservation*

HDFn cells were revived following the same method outlined in section 5.1.1.2 for the MCF-7 cell line. However, once 70-80% confluent, typically in 5-7 days, the cells were passage into a new 175cm^2 culture flask (BD Falcon) at a seeding density of 2900 cells/cm^2. All HDFn cells were derived from Lot #34 and were only used until their 7th passage.

Cryopreservation and cell passage also followed the same procedures outlined in section 5.1.1.2 for the MCF-7 cell line.

5.1.5. Primary Mammary Fibroblast Cells

Primary mammary fibroblast (MF) cells were sourced from Breast Cancer Now, in which the cells were harvested during a normal reduction mammoplasty of patient LS14-3137. During processing at Breast Cancer Now, the harvested tissue was chopped into small pieces and digested for 12 to 16 hours at 37˚C in RPMI-1640 medium plus 25mM Hepes, supplemented with 5% foetal bovine serum (FBS), penicillin (100U/ml), streptomycin (0.1mg/ml) and amphotericin-B (5µg/ml) containing 1mg/ml collagenase 1A and hyaluronidase on a rotary shaker.

The digested tissue was then centrifuged at 380g for 20 minutes and washed in media three times to remove excess enzymes. The tissue isolates were then sedimented three times at 1g for 30 mins to collect the denser organoids. The supernatants containing the fibroblasts are centrifuged (380g x 3 minutes) and the cell pellets re-suspended and cultured in DMEM:F12 supplemented with 10% FBS, hydrocortisone, transferrin, insulin, EGF, penicillin/streptomycin and amphotericin-B (Breast Culture Medium, BCM).

5.1.5.1. *Cell Line Maintenance*

MF cells were maintained in DMEM:F12 (DMEM:F12, ThermoFisher Scientific), supplemented with 10% foetal bovine serum (FBS, Thermofisher Scientific), and 5% Penicillin and Streptomycin (ThermoFisher Scientific) at 37 °C, 5% CO_2 in a humidified environment. Henceforth, this media formulation will be referred to as MF culturing media when referring to media used in conjunction with this cell line.

5.1.5.2. *Revival, Passage and Cryopreservation.*

MF cells were revived following the same method outlined in section 5.1.1.2 for the MCF-7 cell line. However, once 70-80% confluent, typically in 5-7 days, the cells were passage into a new 175cm^2 culture flask (BD Falcon) at a seeding density of 2900 cells/cm^2.

Cryopreservation and cell passage also followed the same procedures outlined in section 5.1.1.2 for the MCF-7 cell line.

5.1.6. Primary Healthy Mammary Epithelial Cells

Primary mammary epithelial cells (pME) were sourced from Breast Cancer Now and matched to the fibroblasts that were also sourced by them. The cells were harvested during a normal reduction mammoplasty of patient LS14-3137. During processing at Breast Cancer Now, the harvested tissue was chopped into small pieces and digested for 12 to 16 hours at 37˚C in RPMI-1640 medium plus 25mM Hepes, supplemented with 5% foetal bovine serum (FBS), penicillin (100U/ml), streptomycin (0.1mg/ml) and amphotericin-B (5µg/ml), 1mg/ml collagenase 1A , and hyaluronidase on a rotary shaker.

The digested tissue was then centrifuged at 380g for 20 minutes and washed in medium three times to remove enzymes. The tissue isolates were then sedimented three times at 1g for 30 mins to collect the denser organoids (ductal tree containing TDLUs and ducts). The organoids were then centrifuged at 380g for 3minutes.

The isolated organoids were then digested using trypsin, and DNAse to ensure the cells were single. The cells were then counted before adding fluorescently

conjugated antibodies for EpCAM, allowing screening and isolation of epithelial cells through passage of the cells through a FACS machine. The fraction containing epithelial cells was then centrifuged (380g x 3minutes) and the cell pellet re-suspended and cultured in DMEM:F12 supplemented with 10% FBS, hydrocortisone, transferrin, insulin, EGF, penicillin/streptomycin and amphotericin-B (BCM), on collagen coated tissue culture plates. pME cells were then grown for 1 passage and frozen down at 300,000 cells per vial, where they were then shipped to the Durham Lab.

5.1.6.1. *Cell Line Maintenance*

pME cells were maintained in DMEM:F12 (DMEM:F12, ThermoFisher Scientific), supplemented with 10% foetal bovine serum (FBS, Thermofisher Scientific), 0.5 µg/ml hydrocortisone (H0888, Sigma), 10 µg/ml apo-transferrin (T1147, Sigma), 10 ng/ml EGF (E9644, Sigma), 5 µg/ml insulin (I9278, Sigma) and 5% Penicillin and Streptomycin (ThermoFisher Scientific) at 37 °C, 5% CO_2 in a humidified environment. Henceforth, assume this media formulation is used in conjunction with the pME cells.

5.1.6.2. *Revival, Passage and Cryopreservation*

pME cells were revived following the same method outlined in section 5.1.1.2 for the MCF-7 cell line. However, once 70-80% confluent, typically in 7-9 days, the cells were passage into a new 175cm^2 culture flask (BD Falcon) at a seeding density of 2900 cells/cm^2.

Harvesting pME cells follows the same procedure as the MCF-10A cell line (section 5.1.3.2) as they are trypsin sensitive.

5.1.7. 2D Invasion Assay

Immortalised epithelial cells (MCF-10A, MCF-7, MDA-MB-231's) were grown to confluency in 12-well adherent cell culture plates (83.3921, Sarstedt) following the cell seeding densities stated previously for each cell-line. Plates were media changed every 2 days until fully confluent. Once fully confluent, the cells were serum

starved, by adding culturing media without FBS, for 24 hours to synchronise the cells. Following synchronisation, the cells were treated with Mitomycin C, a mitotic inhibitor, for two hours prior to scratching. Once treated with Mitomycin C, the cells were washed with PBS twice and media changed to remove excess Mitomycin C. A scratch was then made vertically along the middle of each well using a 10 µL pipette tip. Once the scratch has been made, the cell culture plate was transferred to the Zeiss Cell Observer.

5.1.7.1. *Imaging*

Imaging was undertaken using the Zeiss Cell observer, a widefield fluorescence microscope system which allows for the visualisation of living organisms and intracellular processes, over set time periods and across multiple plate positions. All cell images were taken using the Zeiss 20x LD Plan NEOFLUAR PH2 Korr, N.A 0.4, lens on the phase contrast setting. Each well was imaged at 3 distinct points across the scratch, with images being taken every 15 minutes for 48 hours.

5.1.7.2. *Measuring Scratch Distance*

To measure the images generated by the Zeiss Cell Observer, the image processing software ImageJ (imagej.nih.gov) was used. Each scratch measurement had two images isolated in ImageJ, T=0 and T=48 hours. The images were then split into equal horizontal grids, separating the image into 8 equal partitions using the grid function in ImageJ (Figure 6). Measurements were taken along these partitions at T=0 and T=48 hours (Figure 6), the following formula was used to derive the % Width Migrated of each cell line $\frac{Width\ of\ scratch\ at\ T{=}48}{Width\ of\ scratch\ at\ T{=}0} \times 100$.

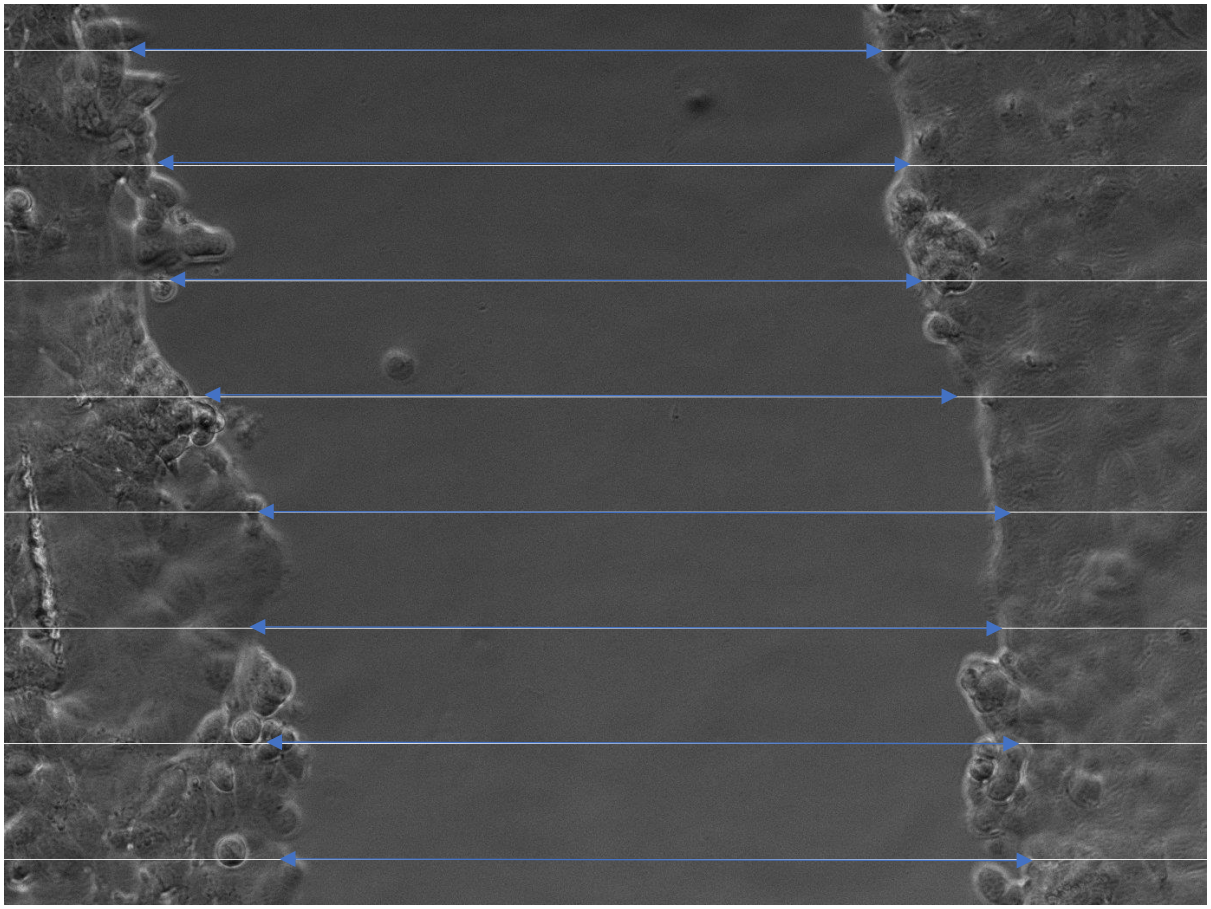

Figure 6: Measuring Scratch Assay Data in ImageJ.

5.2. 3D Cell Culture.

5.2.1. Preparation of Alvetex® Membranes.

Alvetex® membranes (Reprocell Europe Ltd, Sedgefield, UK) were used in this work for the culture of cells in a 3D microenvironment. Two forms of Alvetex® were used: Scaffold and Strata. Both variants are 200 µm thick, porous membranes made from polystyrene, the variants only differ in terms of their pore sizes. Alvetex® Scaffold is a highly porous version of the Alvetex® platform with average pore sizes of 38 µm. This cell culture platform is conventionally used in the lab for the generation of co-culture full-thickness models [99]. Alvetex® Strata, is a more porous version of the scaffold, with smaller average pores which are on average 13 µm in size. This variant of Alvetex® is mainly used for mono-culture 3D migration assays.

Both variations of Alvetex® are prepared for routine cell culture in the same way. The scaffolds are first rendered hydrophilic by soaking inserts in 70 % EtOH for 10

minutes. The scaffolds were then inserted into a 12-well plate (Sarstedt, 83.3921) and washed twice in PBS. After aspirating the second PBS wash, 1 mL of cell-specific culture medium was added to the well in preparation for cell seeding.

5.2.2. Basic 3D Invasion Assay using Alvetex® Strata.

Following preparation of Alvetex® Strata as per section 5.2.1, epithelial cells were harvested as per their respective sections. Once harvested, 750,000 cells were seeded onto each 12-well membrane in a volume of 100 µL. The volume was then carefully distributed across the whole surface of the membrane. The cells were then left to adhere for 2 hours at 37 °C, in a 5% CO_2 humidified environment. Once adhered, the relevant epithelial media was added to the outer compartment, and when the media reached the bottom of the scaffold ~0.5mL was gently added to the inner compartment. With the inner compartment filled, the outer compartment was then filled to the maximum level.

The newly seeded Alvetex® Strata inserts were then cultured for 3, 7, 11, and 14 days with media changes twice a week. The strata models were then processed and harvested as per section 5.3.1.

5.2.3. Formation of Stromal Compartment using HDFn's in Alvetex® Scaffold.

Alvetex® Scaffold 24-well inserts were prepared as per section 5.2.1 and placed into a 12-well plate and covered with 3 mL of HDFn culturing media. The media was aspirated from the wells and 170,000 HDFn cells were seeded in 50 µl of HDFn culturing medium onto the Alvetex® inserts (HDFn cells were harvested as per section 5.1.1.2). The newly seeded wells were then placed in an incubator for two hours to allow the cells to adhere.

Once adhered, 3 mL of HDFn culturing media was then added with the addition of 100 µg/ml of ascorbic acid and 5 ng/mL TGFβ1. The plates were placed back in the incubator and cultured for 14 days. Media changes were performed the day after seeding, including replacing the 12-well plate to remove cells which had not adhered.

Further media changes were carried out twice weekly. All media changes when forming the HDFn derived stromal compartments contained the additional ascorbic acid and TGFβ1 mentioned previously. However, once epithelial cells were seeded on top of the HDFn compartments, the utilised media changed to the specific epithelial cell media formulations mentioned previously, without TGFβ1 and ascorbic acid.

5.2.4. Formation of Stromal Compartment using Primary Mammary Fibroblasts in Alvetex®.

Formation of MF derived stromal compartments followed the same procedure as the HDFn cell line in section 5.2.4, except with the use of MF culturing media instead of HDFn culturing media.

5.2.5. Formation of Full Thickness Co-Culture Models with Fibroblast (HDFn & MF) Derived Stromal Compartments and Breast Cancer Derived Cell Lines

5.2.5.1. *MCF-7*

Once the HDFn/MF derived stromal compartment had matured after 14 days of culture, MCF-7 cells were harvested as per 5.1.2.2. Once harvested, the stromal compartments were aspirated of their media in the outer and inner compartments. 1,500,000 MCF-7 cells, within a volume of 50 µL, were then seeded onto the top of matured stromal compartment, with the volume being evenly dispersed across the top of the membrane. The newly seeded compartments were then moved into the incubator for 2 hours to allow the cells to adhere. Once adhered the inserts were filled with media, their plates changed the day after, and media changed three times a week for 14 days. After the 14-day period the full thickness models were harvested and embedded as per section 5.3.1.

5.2.5.2. *MDA-MB-231*

Once the HDFn/MF derived stromal compartment had matured after 14 days of culture, MDA-MB-231 cells were seeded following the same procedure as the MCF-7's in section 5.2.5.1.

5.2.5.3. *MCF-10A*

Once the HDFn/MF derived stromal compartment had matured after 14 days of culture, MCF-10A cells were seeded following the same procedure as the MCF-7's in section 5.2.5.1.

5.2.5.4. *pME*

Once the HDFn derived stromal compartment had matured after 14 days of culture, pME cells were seeded following the same procedure as the MCF-7's in section 5.2.5.1.

5.3. Processing of Samples

5.3.1. Harvesting Alvetex® Models

5.3.2. Fixing

Following harvest, Alvetex® models were fixed by submerging the models in 4% PFA, for 2 hours at room temperature or overnight at 4°C. Once fixed, the PFA was removed from the samples, and they were washed twice in PBS to remove any excess PFA.

5.3.3. Dehydration and Embedding

Once samples are fixed, they are dehydrated by moving through increasing concentrations of EtOH:

- 30%, 50%, 70%, 80%, 90%, 95% - 10 minutes for each
- 100% - 30 minutes

Once dehydrated the samples were moved into labelled cassettes and submerged in Histoclear for 30 minutes. After 30 mins, molten wax was added to the beaker in a ratio of 1:1 and the beaker placed into a 65°C oven for 30 mins or until all the wax had melted. Once melted the Histoclear:wax mixture was poured away and the cassettes placed into 100% molten wax in a 65°C oven for an hour. Following this, the cassettes were removed from the wax and samples isolated, where they were placed into embedding moulds, filled with wax, and left overnight to harden.

5.3.4. Sectioning

Once embedded the blocks were sectioned using a Leica RM2125RT microtome (Leica Biosystems, Wetzlar, Germany). The blocks were clamped into the relevant holder and sectioned at a thickness of 5 µm. The sections were then floated onto a SuperFrost™ Plus microscope slide (Fisher Scientific) using a water bath set to 40 °C. Slides were then left to dry on a heated slide drying rack for a minimum of one hour.

5.4. H&E Staining

Haematoxylin and Eosin (H&E) staining was carried out as per the following protocol. Slides were deparaffinised in Histoclear (National Diagnostics) for 5 minutes. Once deparaffinised the slides were rehydrated through an EtOH series of decreasing concentration: 100 % EtOH for 2 minutes, 95 % EtOH for 1 minute, 70 % EtOH for 1 minute, and dH_2O for 1 minute. The rehydrated slides were then stained in Mayer's Haematoxylin (Sigma Aldrich) for 5 minutes, before washing in dH2O for 30 seconds, and incubating in alkaline alcohol for 30 seconds to blue the nuclei.

Once stained with Haematoxylin and the nuclei blued, the slides were dehydrated in an EtOH series of increasing concentrations: 70 % EtOH and 95 % EtOH for 30 seconds each. The newly dehydrated slides were then stained in Eosin for 1 minute before 2 washes in 95 % EtOH for 10 seconds. Slides were then dehydrated again in 100 % EtOH for 15 seconds, and then again in 100 % EtOH for 30 seconds. Once dehydrated, the slides were cleared twice in Histoclear for 3 minutes in each. To mount, excess Histoclear was carefully removed from the slides, and a small amount of Omni-mount (National Diagnostics) was placed on the slide, before a coverslip was added to the top. Slides were left to dry and set in the fume hood for at least 30 minutes before imaging on a Leica ICC50 HD brightfield Microscope.

5.5. Statistical Testing

The following statistical tests were utilised during the analysis of data in this thesis:

- One-way ANOVA. This was chosen as the sample groups are deemed independent of each other, allowing the testing for statistically significant differences present across the population of the study.
- Dunnets Post-hoc Test. This was utilised following One-way ANOVA when comparing the samples to a control group, identifying where statistically significant differences were present between groups.
- Tukeys Post-hoc Test. This was utilised when comparing cell groups, under identical conditions, to find areas of statistically significant difference between them.

To be deemed statistically significant, the result of any statistical test undertaken in this study had to return a P value of <0.05.

5.6. Immunostaining

5.6.1. 3D Immunostaining

Slides were deparaffinised in Histoclear for 15 minutes, before being run through the following rehydration series: 5 minutes in 100 % EtOH, 5 minutes in 95 % EtOH, 5 minutes in 70 % EtOH, and 5 minutes in dH2O. Antigen retrieval was performed by incubation in citrate buffer at 95 °C for 20 minutes. After antigen retrieval, slides were cooled through the addition of dH2O. Blocking buffer was prepared depending on whether intracellular markers or extracellular markers were being stained for.

For intracellular markers, slides were incubated with 20 % Neonatal Calf Serum (NCS, Sigma Aldrich) and 0.4 % Triton-X-100 in PBS. While extracellular markers were incubated in 20% NCS made up in PBS. Once prepared, a hydrophobic pen was used to draw around the separate samples, and 100 µL of blocking buffer was added. The samples were then incubated for 1 hour. Once blocked, primary antibody solutions were made up to their respective dilutions, listed in Table 9, and 100 µL of the given solution was added to the samples and incubated at 4°C overnight.

Table 9: Table of primary antibodies utilised, their dilutions, supplier, and relevant product code.

Antibody	**Dilution**	**Supplier**	**Product Code**
Cytokeratin 8	1:100	Abcam	ab59400
Vimentin	1:100	Santa Cruz	sc6260
Collagen I	1:100	Abcam	ab34710
Collagen IV	1:100	Abcam	ab6586
Collagen III	1:100	Abcam	ab7778
Fibronectin	1:100	Abcam	ab17808
Alpha Smooth Muscle Actin (ASMA)	1:100	Abcam	ab5694

After overnight incubation, slides were washed 3 times in PBS before addition of an appropriate fluorescently conjugated secondary antibody and the nuclear stain Hoechst 33342, diluted in blocking buffer at the concentrations listed in Table 10. 100 µL of secondary antibody solution was then added to the samples. Slides were

then incubated at room temperature for one hour before washing 3 times in PBS with 0.1 % Tween 20. Slides were mounted in Vectashield™ (Vector Labs, Peterborough, UK) and a cover slip placed on top, which was sealed around the edges using nail varnish. Slides were stored at 4 °C in the dark until imaging.

Table 10: Table of secondary antibodies utilised, their dilutions, supplier, and relevant product code.

Antibody	Dilution	Supplier	Product Code
Goat Anti-Mouse 488	1 in 1000	Invitrogen	A11001
Goat Anti-Mouse 594	1 in 1000	Invitrogen	A11005
Goat Anti-Rabbit 488	1 in 1000	Invitrogen	A11012
Goat Anti-Rabbit 594	1 in 1000	Invitrogen	A11012
Hoescht-33342	1 in 10,000	ThermoFisher Scientific	H3570

5.6.2. 2D Immunostaining

2D immunostaining was carried out on cells fixed to coverslips. Cells were seeded into a 12 well plate at their respective seeding densities stated previously. Once confluent, cells were fixed in 4% PFA for 20 minutes and washed three times with PBS to remove excess PFA. Coverslips were placed on ice and permeabilised in 0.1% Triton-X-100 in PBS for 15 minutes. Permeabilisation solution was removed from the well using a Pasteur pipette.

Once permeabilised, coverslips were then blocked in a buffer consisting of 10% NCS in 0.1% Tween20 in PBS solution for 1 hour. 50 µl of the desired primary antibody solution at the appropriate concentration (Table 9) was pipetted onto Parafilm (Fisher Scientific UK) in a plastic tray, coverslips were removed from the 12-well plate and placed on the Parafilm with the cells face-down in contact with the antibody solution. The coverslip was then incubated in the primary antibody solution for 1 hour.

Coverslips were then washed in blocking buffer by moving the facedown coverslips onto fresh 50 µl droplets of blocking buffer on the Parafilm, where they were incubated for 10 minutes. This was repeated 3 times. Coverslips were then placed

onto 50 µl droplets of the appropriate secondary antibody solution and Hoescht nuclear stain at the correct concentration (Table 10) for 1 hour, before washing again in 50 µL droplets of blocking buffer as previously described.

To mount the coverslips, a small amount of Vectashield™ was placed on a SuperFrost™ Plus slide, excess PBS carefully blotted from the coverslip, and the coverslip placed onto the Vectashield™ on the slide. The coverslips were sealed with nail varnish, allowed to dry, and stored at 4°C until imaging.

5.6.3. Imaging of Fluorescently Stained Samples

Once samples had been processed, they were then imaged on a Zeiss 800 Airyscan microscope with either a Zeiss 20x Plan-Apochromat 0.8NA or Zeiss 63x oil Plan-Apochromat 1.4 NA objective lens.

5.6.3.1. *Imaging of H&E Stained Samples*

Once the samples had been processed, embedded, and stained with H&E as per section 5.3., the samples were then imaged on a Leica ICC50 HD brightfield Microscope.

5.6.3.2. *Measuring Depth Penetration of Epithelial Cell Lines.*

To measure the images generated by the Leica ICC50 HD brightfield Microscope, the image processing software ImageJ (imagej.nih.gov) was used. The H&E images were then split into equal vertical grids, separating the image into 11 equal partitions using the grid function in ImageJ. Measurements were taken along these partitions, measuring the height of the Alvetex® (Figure 6, red arrow) and the depth penetrated of each epithelial cell line into the membrane (Figure 6, blue arrow). Once measured the following formula was used to derive the % Depth Penetrated of each cell line:

$$\frac{Height\ of\ Alvetex}{Depth\ Penetrated\ of\ the\ Epithelial\ Cell\ Lines} \times 100.$$

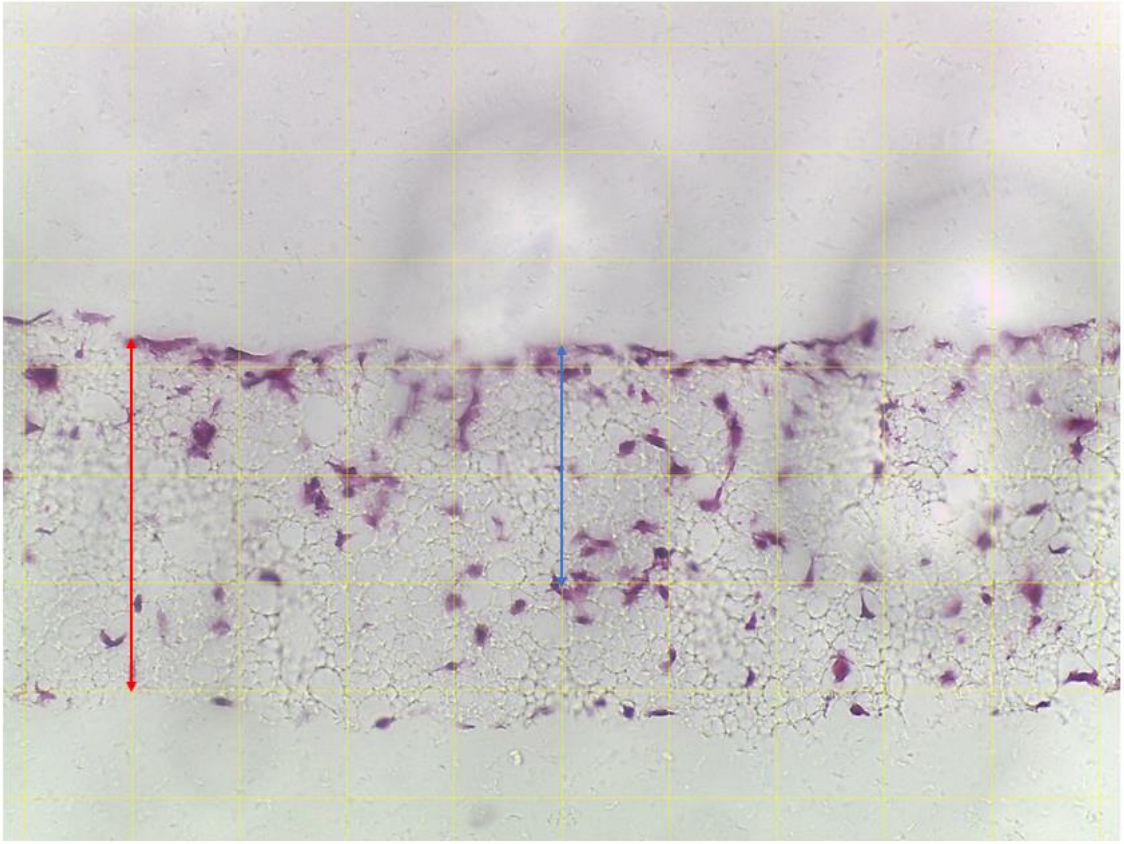

Figure 7: Measuring Strata Invasion Assay Images in ImageJ. The red line is measuring the height of the Alvetex® Strata membrane, the blue line is representing the depth penetrated by the epithelial cell line at that specific partition.

5.6.4. Imaging Co-Culture 3D Invasion Assay using Alvetex® Scaffold.

Once the samples had been processed, embedded, and stained cell line specific markers as per section(s) 5.6.1, the samples were then imaged on a Zeiss 800 Airyscan microscope with either a Zeiss 20x Plan-Apochromat 0.8NA or Zeiss 63x oil Plan-Apochromat 1.4 NA objective lenses.

5.6.4.1. *Measuring Depth Penetration of Epithelial Cell Lines.*

To measure the images generated by the Zeiss 800 Airyscan Microscope, the image processing software ImageJ (imagej.nih.gov) was used. The immunostained images were split into equal vertical grids, separating the image into 11 equal partitions using the grid function in ImageJ. Measurements were taken along these partitions, measuring the height of the Alvetex® scaffold (Figure 8, red arrow) and the depth penetrated of each epithelial cell line into the membrane (Figure 8, blue arrow).

Once measured the following formula was used to derive the % Depth Penetrated of each cell line: $\frac{Height\ of\ Alvetex\ model}{Depth\ Penetrated\ of\ the\ Epithelial\ Cell\ Lines} \times 100.$

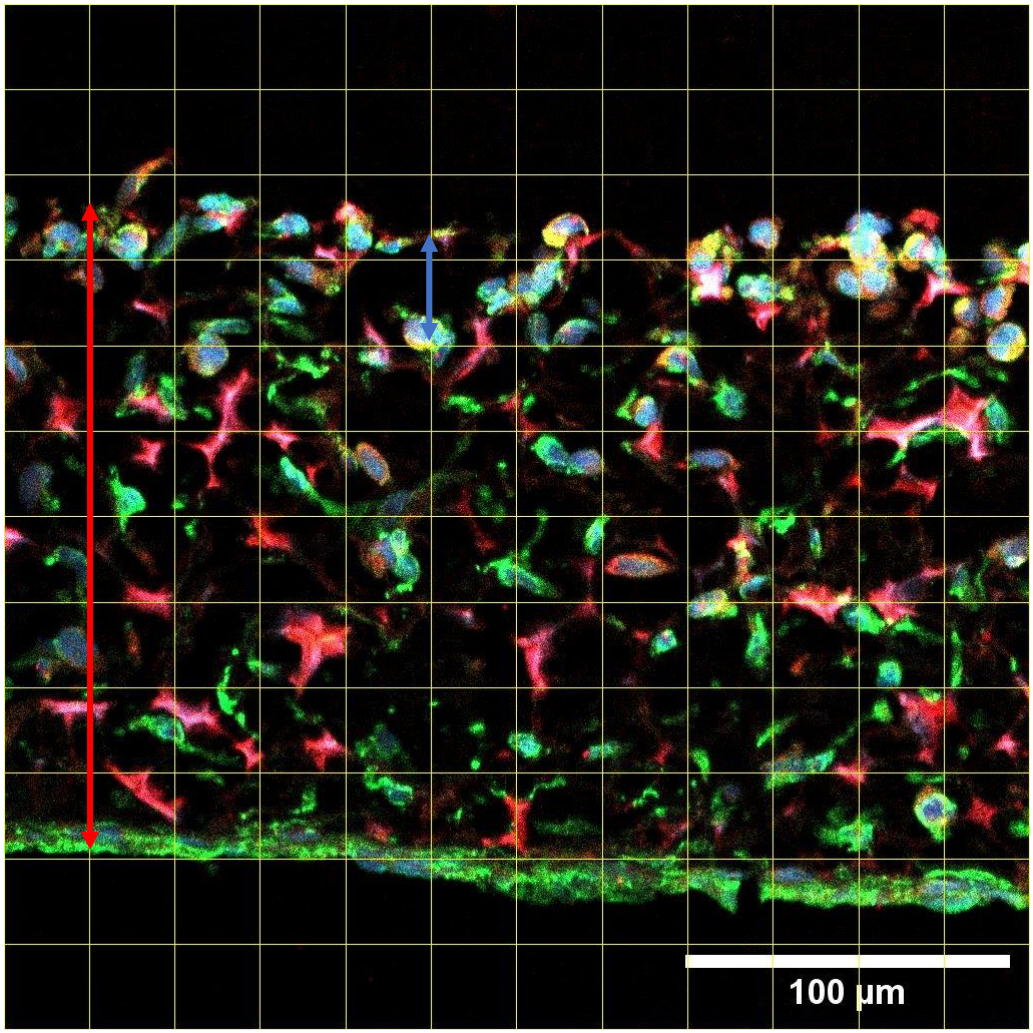

Figure 8: Measuring Scaffold Co-Culture Invasion Assay Images in ImageJ. The red line is measuring the height of the Alvetex® Scaffold membrane, the blue line is representing the depth penetrated by the epithelial cell line at that specific partition.

6. Results

6.1. Commercially available breast cancer cell lines display the behaviours correlating with the three distinct timepoints of breast cancer development in 2D culture.

As mentioned previously, the MCF-7 epithelial line is an immortalised cell line that was originally derived from the pleural effusion of a 67 year old Caucasian Female suffering from breast adenocarcinoma [70]. In 2D cell culture these cells adopt a cobblestone morphology and grow as islands of epithelial cells in low confluency, before forming an epithelial monolayer under high confluency (Figure 9).

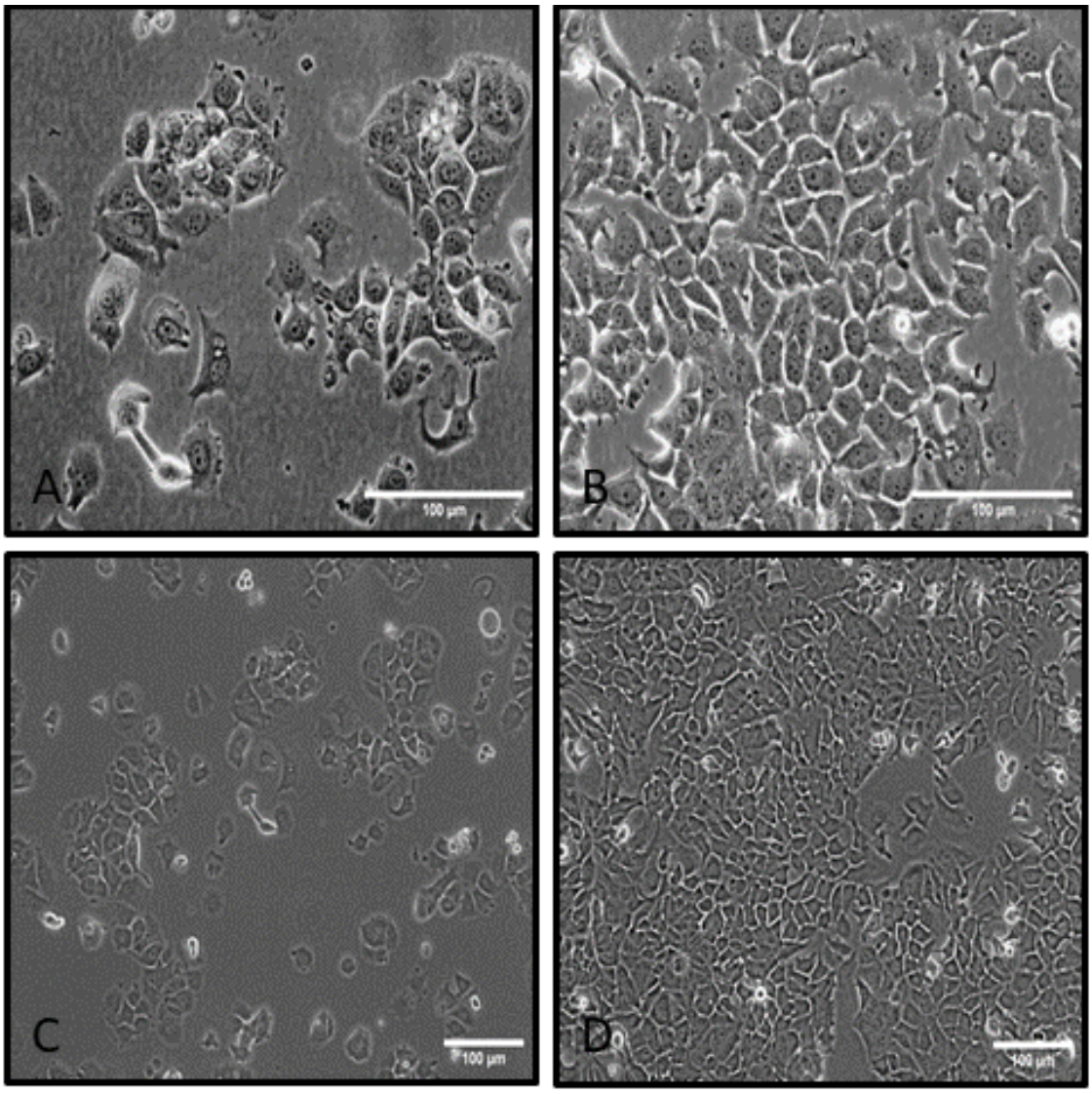

Figure 9: Phase-contrast images of MCF-7 cells grown in 2D. In 2D, MCF-7 cells grow with a cobblestone morphology and group together as islands of cells in low confluency (Left). Once high confluency is reached (right) a uniform monolayer is formed of cobblestone epithelia cells. Scale bars are 100 µm.

The MCF-7 cell line was selected due to the cell lines' native expression of hormone receptors, and derivation from HR positive breast cancer which makes this cell line ideal for producing breast cancer models that are: highly reproducible, due to the cell lines immortalised nature; physiologically relevant, due to its derivation from a human donor; and representative of the HR sub-type of breast cancer. Furthermore, the MCF-7 cell-line is a poorly aggressive and non-invasive cell line with low metastatic potential, which makes it an ideal candidate for modelling DCIS lesions *in vitro* [72]–[74].

The MCF-10A is an epithelial cell line, that immortalised spontaneously without defined factors [75]. The cell line was originally isolated from the mammary gland of a White, 36-year-old female donor with fibrocystic breasts. Furthermore, the cell line is non-tumorigenic and lacks oestrogen receptor expression [75]. Much like the MCF-7 cell line, the MCF-10A cell line is well characterised and has been used in a wide variety of in vitro studies surrounding breast cancer research showing that this cell line is robust and reliable [51], [75]. When grown in 2D, the MCF-10A cells form two distinct phenotypes depending on their confluency. Under low confluency the cells elongate and adopt a spindle-like morphology, then once high confluency is reached the cells condense into a cobblestone morphology (Figure 10). The non-tumorigenic nature of the MCF-10A cell line makes it ideal for producing a reproducible, full-thickness breast mucosal model that is physiologically relevant and representative of healthy mammary tissue.

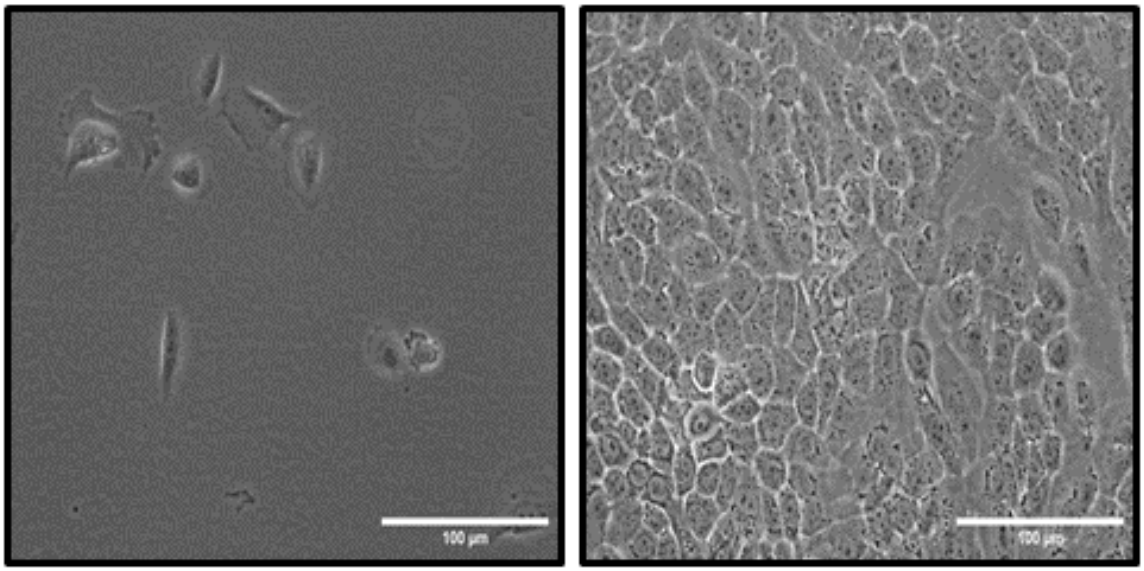

Figure 10: Phase-contrast images of MCF-10A cells grown in 2D. In 2D, MCF-10A cells grow with a spindle-like morphology under low confluence (Left). Once high confluency is reached (right) the cells adopt a cobblestone morphology, typical of epithelial cells, forming a monolayer across the cell culture plate. Scale bars are 100 µm.

The MDA-MB-231 epithelial cell line is an immortalised cell line that was originally derived from the from a pleural effusion of a 51-year-old woman with metastatic breast cancer [93]. MDA-MB-231 is a TNBC cell line that lacks hormone receptor expression, as well as HER2 amplification [76]. These factors make the cell line highly aggressive, invasive, and poorly differentiated. Much like the MCF-7 cell line, the MDA-MB-231 cell line is well characterised and has been used in a wide variety of in vitro studies surrounding breast cancer research showing that this cell line is robust and reliable [51], [76]. When grown in 2D, the MDA-MB-231 cells adopt mesenchymal-like behaviours and adopt spindle-like morphologies (Figure 11).

The MDA-MB-231 cell line was selected due to its derivation from metastatic breast cancer, the lack of HR and HER2 amplification, which makes this cell line ideal for producing a full-thickness breast mucosal model that is physiologically relevant and representative of this aggressive sub-type of breast cancer. Furthermore, the highly aggressive and invasive nature of the cell line makes it an ideal candidate for modelling IDC lesions *in vitro*.

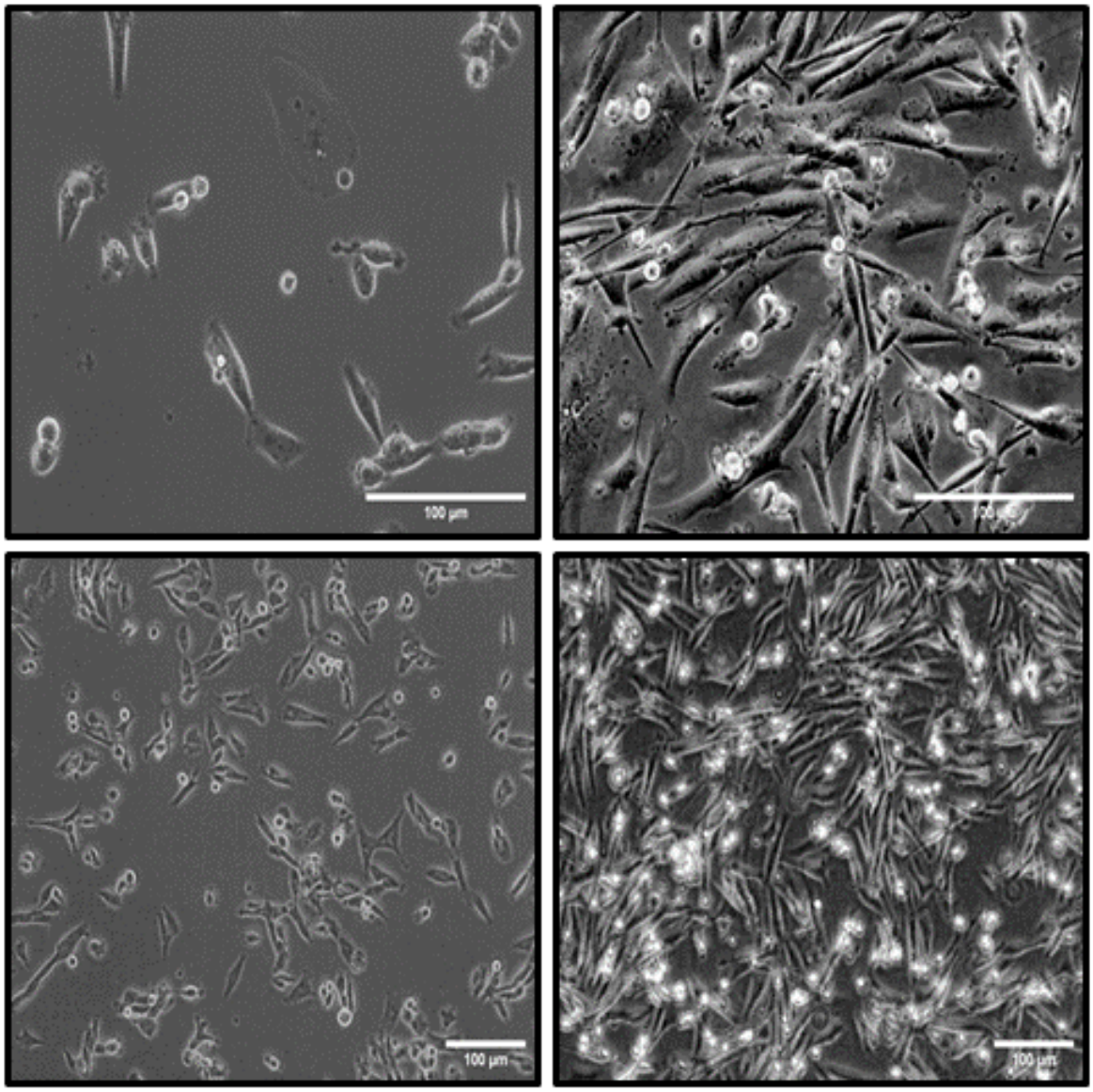

Figure 11: Phase-contrast images of MDA-MB-231 cells grown in 2D. In 2D, MDA-MB-231 cells grow with a spindle-like morphology under low confluence (Left). Once high confluency is reached (right) the cells montain the spindle-like morphology, however the cells overlap and form multilayer structures composed of the epithelial cells. Scale bars are 100 µm.

Previous literature has shown these cell lines to represent the invasive characteristics of breast cancer in its distinct pathological points. However, to assess the effectiveness of the novel 3D invasion assays generated in this thesis, baseline results of each cell lines' 2D characteristics within a well-established technology must be gathered to ensure they do show the desired characteristics observed in the literature. Initially, all three immortalised cell lines (MCF-10A, MCF-7, MDA-MB-231) were grown in 2D culture plates, to assess cell morphology, basic cell marker expression, and growth patterns.

Each cell line displayed unique morphological and proliferative characteristics when cultured on 2D plates. The MCF-10A cell line under phase contrast showed two distinct morphologies during low and high confluence cell culture. During low confluency the cells exhibit an elongated and sparse morphology (Figure 12B), then as the growth period of the cells progresses, they condense into a compact cobblestone morphology (Figure 12C) typical of healthy epithelial cell lines. The MCF-10A cell line also showed highly proliferative properties, where 70-80% confluency (Figure 12C) was reached within ~3 days of culture.

Similar to the MCF-10A's, the MCF-7 cell line also exhibited a cobblestone morphology typical of epithelial cells, however in contrast to the MCF-10A's this was maintained in both low confluency, where the cells would form islands of cells (Figure 12E), and high confluency (Figure 12F). Furthermore, the MCF-7 cell line showed the lowest proliferative properties, where 70-80% confluency was reached within ~7 days of culture.

In contrast to both the MCF-10A and the MCF-7 cell lines, the MDA-MB-231's displayed an elongated spindle morphology, typical of cells with mesenchymal properties, in both low (Figure 12H) and high (Figure 12I) confluency culture. The proliferative characteristics of the MDA-MB-231 cell line also differed to the other two cell lines, acting as an intermediatory of the two, whereby confluency was reached in ~5 days of culture.

Basic immunostaining was carried out for two conventional epithelial and mesenchymal markers, Cytokeratin 8 (CK8) and Vimentin (Vim) respectively. The MCF-10A cell line, showed two distinct sub-populations when immunostained. The first was a less prevalent CK8 positive population (Figure 12A, white triangles) and the second was a more prevalent Vim positive population (Figure 12A, white arrowheads). The MCF-7 cell line showed a uniform population of CK8 positive and Vim negative cells (Figure 12D). The MDA-MB-231 cell line also showed a uniform population, but instead these were CK8 negative and Vim positive (Figure 12G).

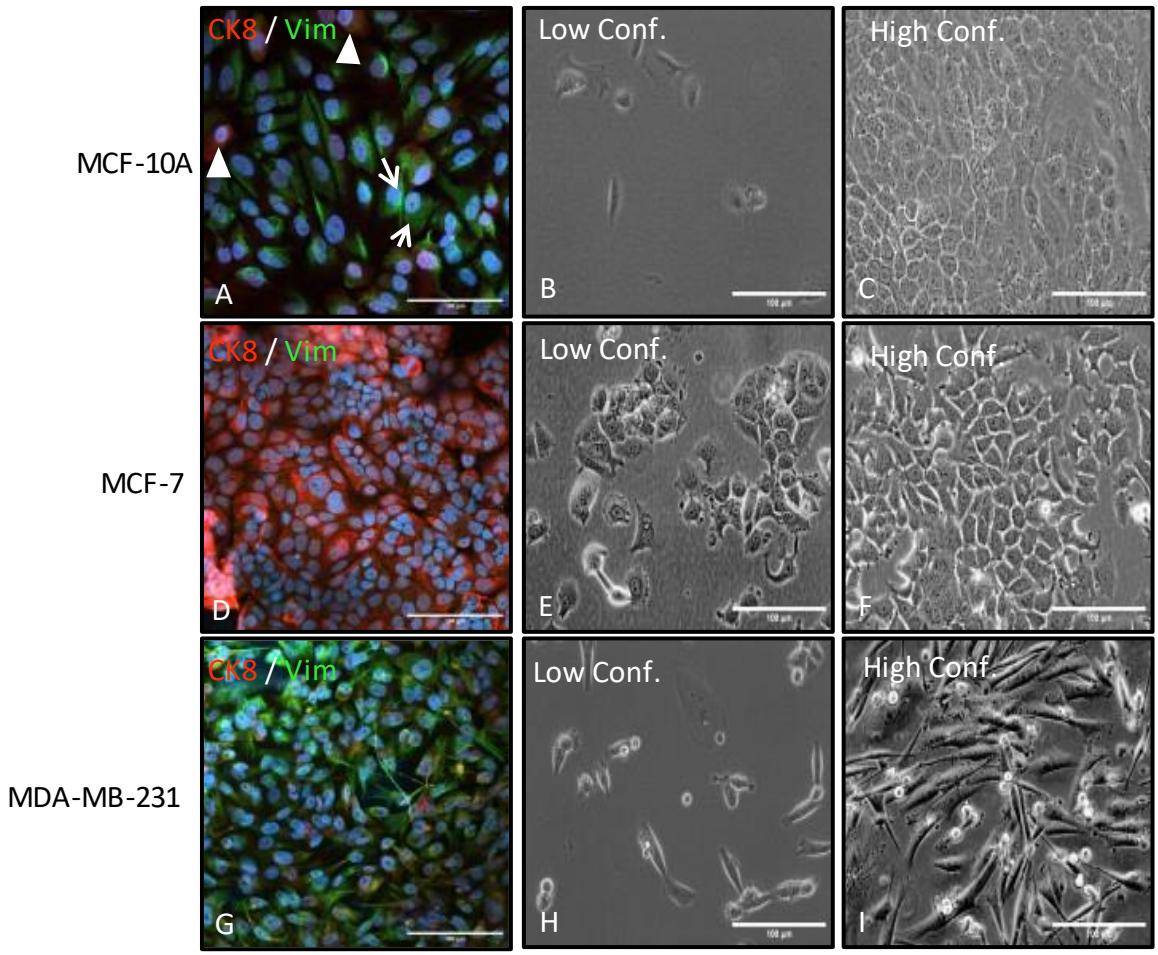

Figure 12: 2D Characterisation of Immortalised Mammary Epithelial Cell Lines using Phase Contrast and Immunofluorescence Microscopy. A) Immunostaining of confluent MCF-10A cells with Cytokeratin 8 (Red), Vimentin (Green), and nuclei with Hoechst (Blue) White triangles indicate Cytokeratin 8 positive sub-population of MCF-10A cells, White Arrowheads indicate Vimentin positive sub-population of MCF-7 cells. B) Phase Contrast images of MCF-10A cells during low confluency. C) Phase Contrast images of MCF-10A cells during high confluency D) Immunostaining of confluent MCF-7 cells with Cytokeratin 8 (Red), Vimentin (Green), and nuclei with Hoechst (Blue). E) Phase Contrast images of MCF-7 cells during low confluency. F) Phase Contrast images of MCF-7 cells during high confluency. G) Immunostaining of confluent MDA-MB-231 cells with Cytokeratin 8 (Red), Vimentin (Green), and staining of nuclei with Hoechst (Blue). H) Phase Contrast images of MDA-MB-231 cells during low confluency. I) Phase Contrast images of MDA-MB-231 cells during high confluency All scale bars represent 100µm.

6.1.1. Commercially available breast cancer cell lines differ in their invasive potential when grown in 2D.

Once cell characteristics had been ascertained in standard 2D cell culture, it was important to gain a baseline understanding of each cell lines' invasion capabilities in a well-established platform cell invasion platform. To achieve this understanding, scratch assays were performed as per 5.1.7.

2D scratch assays showed that the intrinsic invasion characteristics of each cell line differed in terms of the % width of the scratch migrated over 48 hours, where a larger

% of the width migrated shows higher cell motility and invasion characteristics (Figure 13 & Figure 14A). The MCF-10A cell line, representing a healthy mammary epithelium, exhibited the least invasive characteristics with the lowest mean % Width Migrated of 15.6% (Figure 13A & D, Figure 14A). Interestingly, in response to the scratch the cells would detach from the culture plate and would form migratory islands (Figure 13D, white triangle). In contrast to this, the MDA-MB-231 cell line, representing late stage invasive breast cancer epithelia, exhibited the most invasive characteristics with the highest mean % Width Migrated of 63.2% (Figure 13C & F, Figure 14A). As the MDA-MB-231 cells migrated they would elongate further in order to move across the scratch (Figure 14F, white triangle). The MCF-7 cell line, representing early stage *in situ* breast cancer epithelia, then acted as an intermediate of the two with a % Width Migrated of 27.2% (Figure 13B & E, Figure 14A). As the MCF-7 cells migrated across the scratch they maintained their rounded epithelial morphology (Figure 13E, white triangle).

Graphical analysis of migration results showed a lack of overlap between SEM error bars between cell lines (Figure 14A), suggesting that the differences in migration results are statistically significant. A one-way ANOVA revealed that there was a statistically significant difference in % Width Migrated between at least two of the cell lines ($F(2, 141) = 93.75$ $p = < 0.0001$). Tukey's HSD Test for multiple comparisons between groups found that the mean value of % width migrated was significantly different between all three cell lines ($p<0.01$), specific values are denoted in Table 11. Thus, in a simple and widely adopted 2D invasion assay, the cell lines show differential migration characteristics in line with the pathologies they are trying to emulate, as per the relevant literature: the MCF-10A's being the least invasive, matching the characteristics of healthy epithelia; the MCF-7's acting as an intermediate, as you would expect for early stage DCIS epithelia; and the MDA-MB-231's being the most invasive, which aligns with the characteristics of IDC breast cancer epithelia.

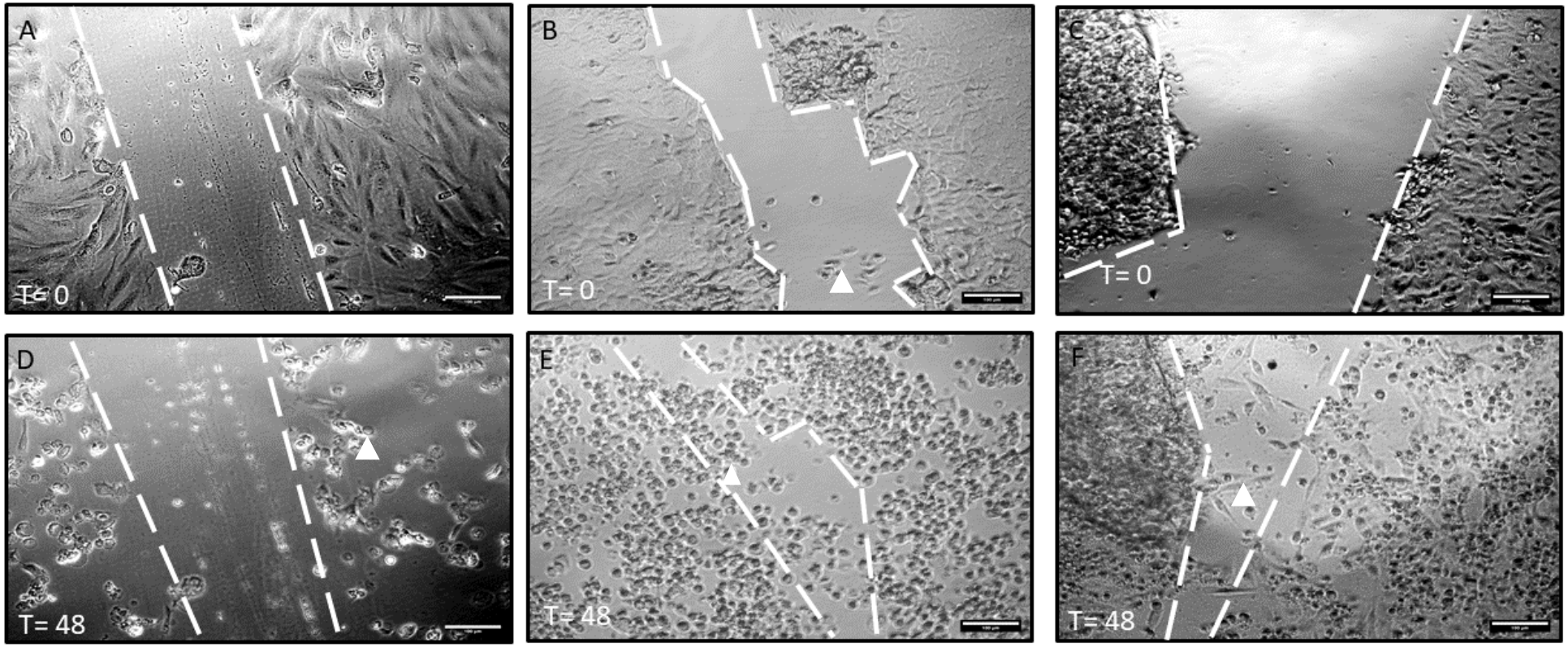

Figure 13: Phase Contrast Images of Cell Lines during 2D Scratch Assays at T=0 and T=48 hours. A & D) MCF-10A scratch assay images at the same location at T = 0 (A) and T = 48 (D). B & E) MCF-7 scratch assay images at the same location at T = 0 (B) and T = 48 (E). C & F) MDA-MB-231 scratch assay images at the same location at T = 0 (E) and T = 48 (F). Cells were grown to confluency and then treated with Mitomycin C for 2 hours, prior to scratching at T=0, the cells were then placed into a CO2 and temperature-controlled cell observer for imaging to occur. Scale bars represent 100 µm.

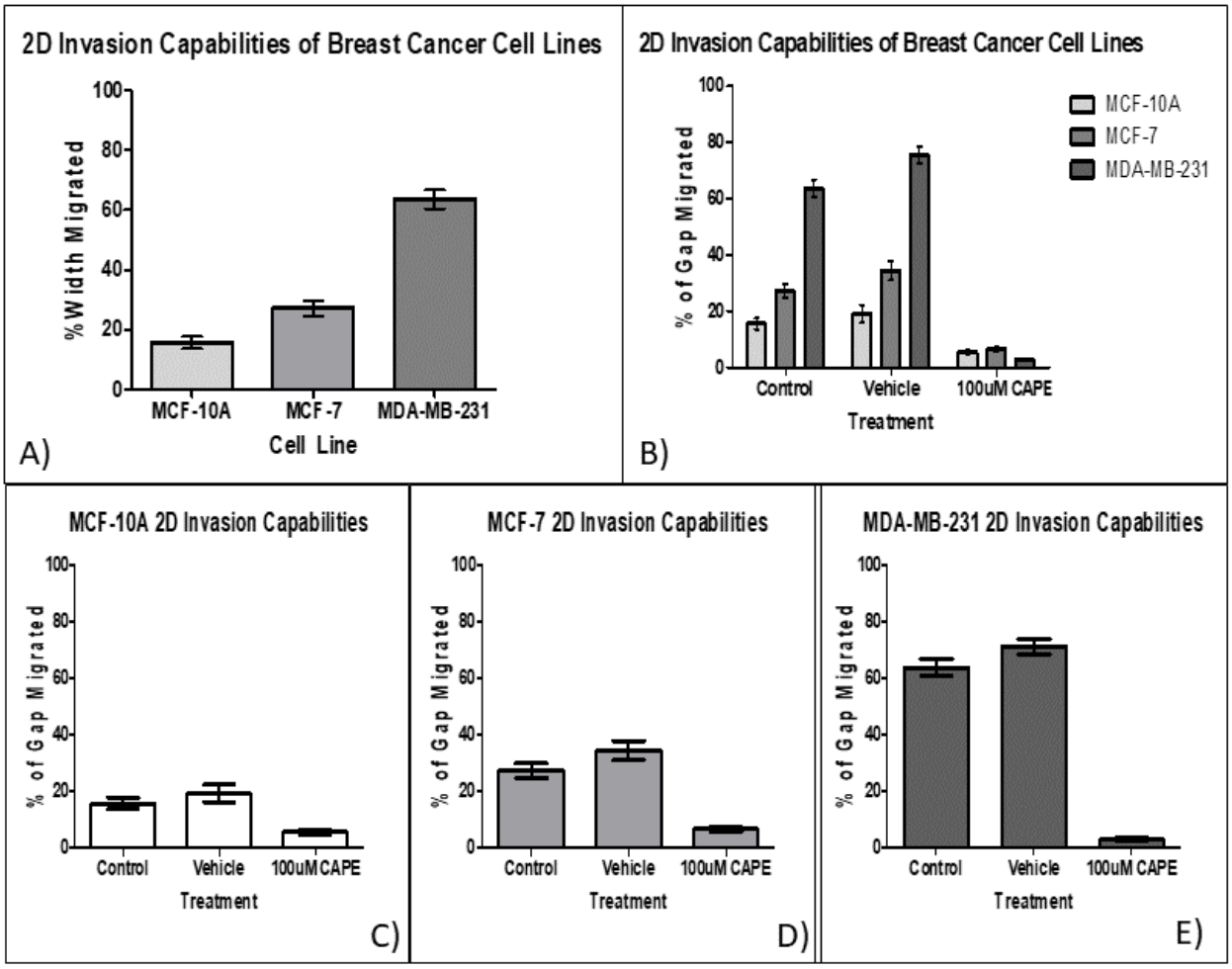

Figure 14: Graphical Representation of the Invasion Capabilities of the MCF-10A, MCF-7, MDA-MB-231 Cell Lines in 2D. Data was collected from 3 independent experimental repeats (N=3), with 3 technical model repeats per set up. 48 measurements were taken per condition across the 3 models (n=48).A) Comparison of 2D invasion capabilities between cell line control groups (N=3, n=48). B) Comparison of 2D invasion Capabilities of Cell Lines and their treatment with vehicle controls (DMSO), and 100 µM of the CAPE inhibitor (N=3, n=48). C) Comparison of the invasion capabilities of the MCF-10A Cell Line when treated with culture media (Control), culture media + 10 µL DMSO (Vehicle Control), and culture media + 100 µM CAPE inhibitor (100 µM CAPE). D) Comparison of the invasion capabilities of the MCF-7 Cell Line when treated with culture media (Control), culture media + 10 µL DMSO (Vehicle Control), and culture media + 100 µM CAPE inhibitor (100 µM CAPE). E) Comparison of the invasion capabilities of the MDA-MB-231 Cell Line when treated with culture media (Control), culture media + 10 µL DMSO (Vehicle Control), and culture media + 100 µM CAPE inhibitor (100 µM CAPE). Error bars show ± SEM.

Table 11: Table showing the Tukey's Post-hoc test for the One-way ANOVA undertaken between the control groups of each cell line during 2D scratch assays.

Tukey's Multiple Comparison Test	Mean Diff.	q	P Value	Summary	95% CI of diff
MCF-10A vs MCF-7	-11.61	4.487	<0.01	**	-20.29 to -2.927
MCF-10A vs MDA-MB-231	-48.02	18.56	<0.001	***	-56.70 to -39.34
MCF-7 vs MDA-MB-231	-36.41	14.07	<0.001	***	-45.09 to -27.73

6.1.2. Treatment Of Commercially Available Breast Cancer Cell Lines with a Known Migration Inhibitor Stopped Cell Invasion in 2D.

Following initial assessment of 2D invasion capabilities of each cell line, treatment with the CAPE inhibitor was used twofold: 1) To assess the drugs compatibility with a well-established platform for investigating cell migration. 2) To test whether CAPE inhibits the migratory capabilities, and by extension the invasion characteristics, of the cell lines selected to emulate breast cancer epithelia during its various disease states. To achieve these goals, scratch assays were carried out as previously mentioned, with the addition of the CAPE inhibitor solubilised in DMSO, and a vehicle control to form three treatment groups: Control, Vehicle (Media + 10 µL DMSO), 100 µM CAPE Treatment.

CAPE inhibits the migratory activity of cancer cells by interacting with and inhibiting the action of NF-κB, a potent factor in oncogenesis and cancer progression [77]. Furthermore, CAPE inhibits Fibroblast Growth Factor 2 (FGF-2) to inhibit cell migration [102].

For the MCF-10A cell line, treatment with CAPE decreased migration capabilities of the cell line by decreasing the % of the scratch closed by the cell line, while the vehicle treatment produced similar results to the control group (Figure 14B & C). One-way ANOVA testing revealed that there was a statistically significant difference in % Width Migrated between at least two of the treatment groups ($F(2, 141) = [10.86]$, $p = <0.0001$). Dunnett's Post-hoc Test for multiple comparisons against the control group found that the mean value of % Width Migrated was not significantly different when comparing the Control and Vehicle groups ($p = >0.05$) but was significantly different when comparing the Control group to the 100 µM CAPE treated group ($p = <0.0001$).

The MCF-7 cell line showed a similar trend to the 10A's whereby CAPE treatment reduced the % Width Migrated of the cells, and the vehicle control produced comparable results to the control group (Figure 14B & D). One-way ANOVA testing revealed that there was a statistically significant difference in % Width Migrated

between at least two of the treatment groups ($F(2, 140) = [34.64]$, $p = <0.0001$). Dunnett's Post-hoc Test for multiple comparisons between the control group confirmed that the mean value of % Width Migrated was not significantly different when comparing the Control and Vehicle groups ($p = >0.05$) but was significantly different when comparing the Control group to the 100 µM CAPE treated group ($p = <0.0001$).

In agreement with the other two cell lines, the MDA-MB-231 cell line showed the same decrease in % Width Migrated as the other two cell lines following treatment with the CAPE inhibitor and the vehicle control (Figure 14B & E). One way ANOVA testing revealed that there was a statistically significant difference in % Width Migrated between at least two of the treatment groups ($F(2, 141) = [247.3]$, $p = <0.0001$). Dunnett's Post-hoc Test for multiple comparisons between the control group found that the mean value of % Width Migrated was not significantly different when comparing the Control and Vehicle groups ($p = >0.05$) but was significantly different when comparing the Control group to the 100 µM CAPE treated group ($p = <0.0001$). These analyses show that the DMSO used to solubilise the CAPE inhibitor was not likely to have had a statistically significant effect on the migration capabilities of any of the three selected cell lines and any changes in migration were likely to be a result of the action of the CAPE inhibitor. Overall, these results show that not only is the use of the CAPE inhibitor compatible with this invasion platform, but also treatment with the CAPE inhibitor decreased cell motility, and invasion capabilities, across all three cell lines to a statistically significant degree in 2D, when compared to the control groups.

6.2. The Introduction of a Basic 3D Growth Environment Altered the Invasive Potential of Breast Cancer Cell Lines.

Having ascertained the 2D invasion characteristics of each cell line, the next step in model development was to investigate the effect of the introduction of a 3D growth environment. This was achieved through monoculture seeding of each of the epithelial cell lines onto Alvetex® Strata and observing their growth over 4, 7, and 14 days (Figure 15).

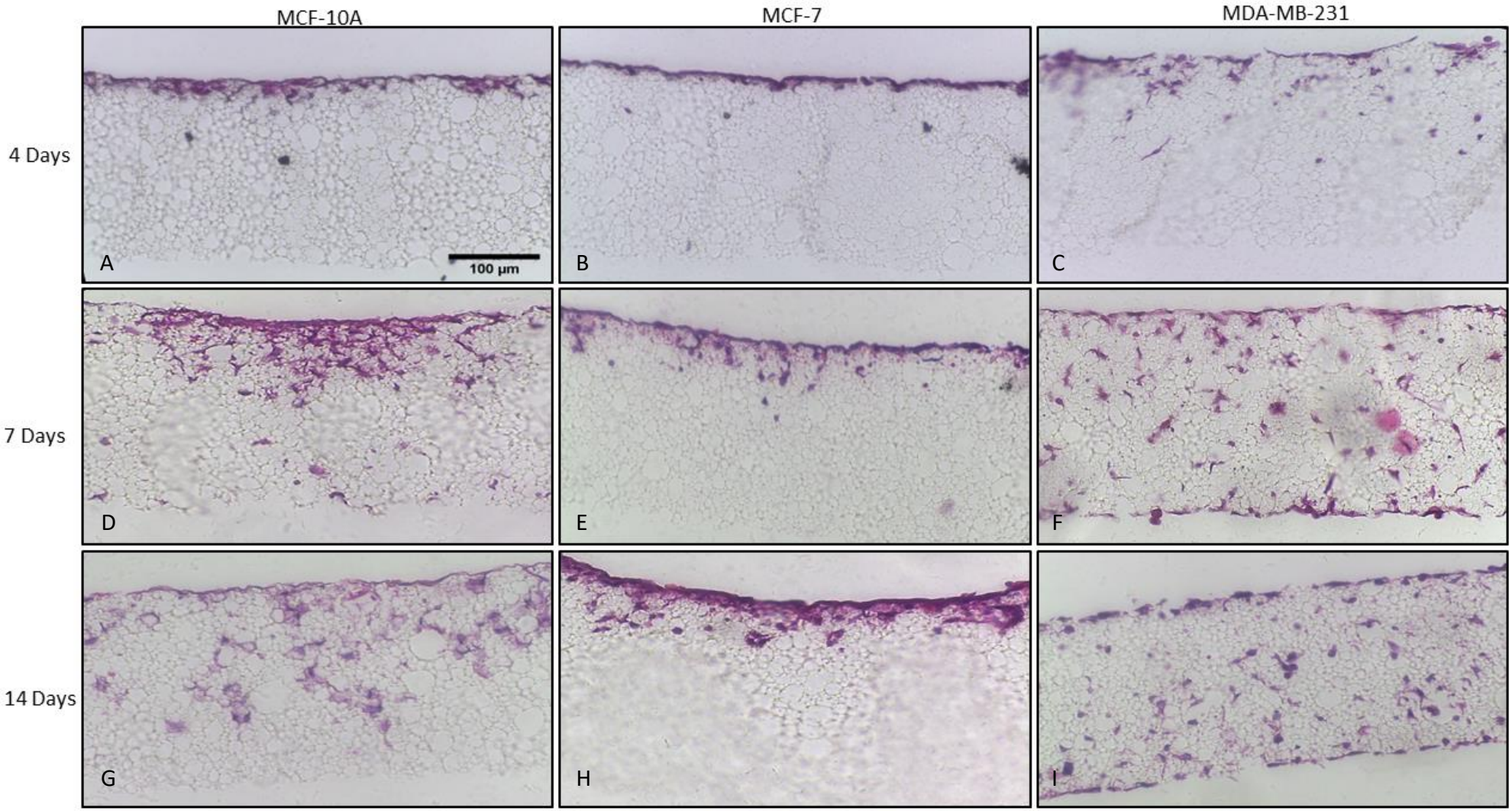

Figure 15: Growth of Immortalised Breast Epithelial Cell Lines on Alvetex® Strata at 4, 7, and 14 days. The seeding of immortalised breast epithelial cell lines showed continuous penetration into the Alvetex® Strata membrane over time, albeit to varying degrees based on cell-line intrinsic and microenvironmental factors.

H&E staining of Alvetex® Strata inserts shows that across all three cell lines as time progresses their depth penetration into the Alvetex® Strata membrane also increases, albeit to varying degrees. When observing the global growth morphology between cell lines, there are apparent differences present. The growth of the MCF-10A cell line is initially confined to the top of the layer by day 4, where it forms a monolayer across the Alvetex® Strata membrane with minimal penetration into the Alvetex® Strata membrane (Figure 16A). As growth in Alvetex® Strata continues over time, the MCF-10A maintains its clear monolayer on top of the membrane, with cell migration occurring underneath this layer (Figure 16B). The underlying migration then forms spiderwebs of cells connected to each other throughout the Alvetex® Strata membrane (Figure 16B).

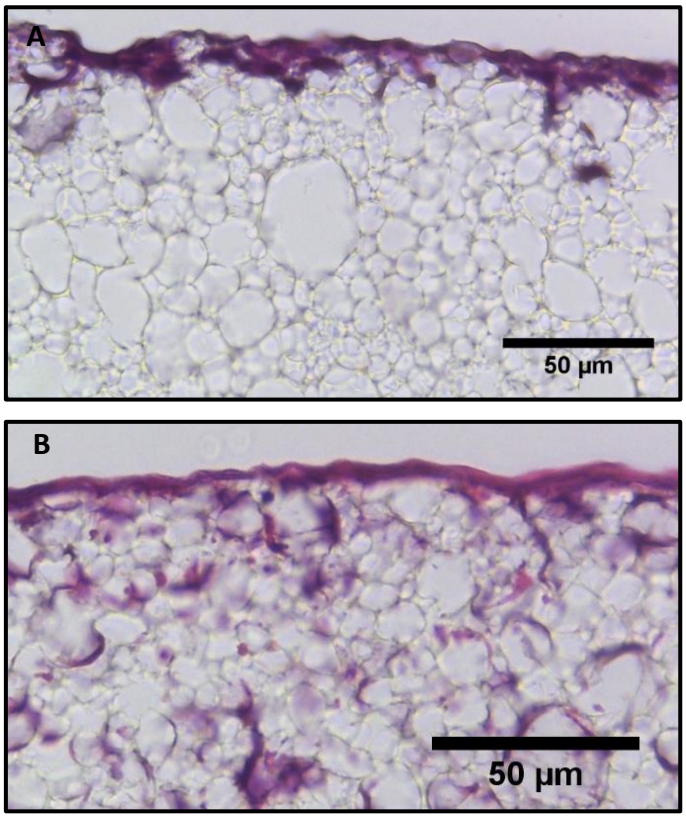

Figure 16: x40 Magnification of MCF-10A Growth in Alvetex® Strata

Similar to the MCF-10A cell line, the MCF-7 cell line at 4 days also has its growth confined to the top of the Alvetex® Strata membrane where it forms a monolayer-like structure (Figure 15B). As growth continues over time, the layer of MCF-7 cells on top of the Alvetex® Strata membrane thickens and minimal penetration of the MCF-7 cells is observed into the membrane (Figure 15E, & H).

In contrast to both the MCF-10A and MCF-7 cell lines, the MDA-MB-231 cell line did not form a monolayer on top of the Alvetex® Strata membrane, instead the cells displayed significant invasion after three days (Figure 15C). Then as the growth period continued, penetration into the membrane continued like the other two cell lines, albeit to a higher degree (Figure 15F & I). Furthermore, the migration pattern differed from the migratory nature of the other two cell lines. While the MCF-10A cell line formed web-like patterns of cell growth and the MCF-7 cell line formed a thickened layer on top of the membrane, the MDA-MB-231 cells migrated as distinct single cells into the membrane (Figure 17).

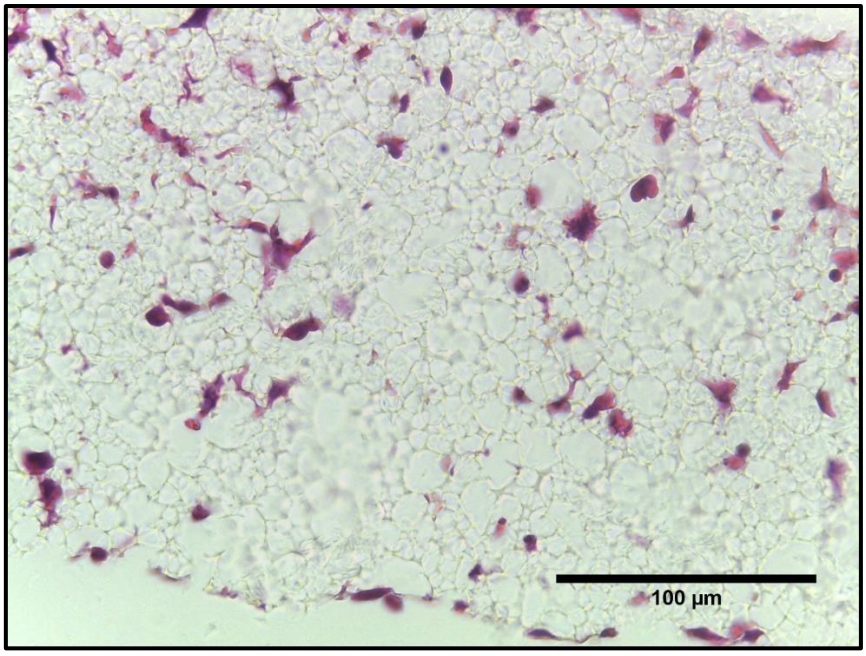

Figure 17: x40 Magnification Image of the growth of MDA-MB-231 cell line in Alvetex® Strata at 7 days.

It is evident that each cell line displays unique growth and invasion characteristics when grown in Alvetex® Strata. In each case, penetration into the membrane was observed to differential degrees, allowing the formation of a novel invasion assay using this platform, whereby % Depth Penetration is a direct indicator of invasive potential of each cell line. Figure 18 shows how % Depth Penetration differs between each cell line, with the MCF-7 cell line penetrating the least, the MDA-MB-231 cell line penetrating the most, and the MCF-10A cell line acting as an intermediate of the two.

The lack of overlap of the SEM bars between cell lines suggests that the differences in depth penetration observed in Figure 18 may be statistically significant. One-way ANOVA testing revealed that there was a statistically significant difference in % Depth Penetration between at least two of the cell lines (F(2, 797) = [760.4], p = <0.0001). Tukey's Post-hoc Test for multiple comparisons between groups found that the differences in mean value of % Depth Penetration between all of the cell lines was statistically significant (p = <0.0001). For in depth results see Table 12.

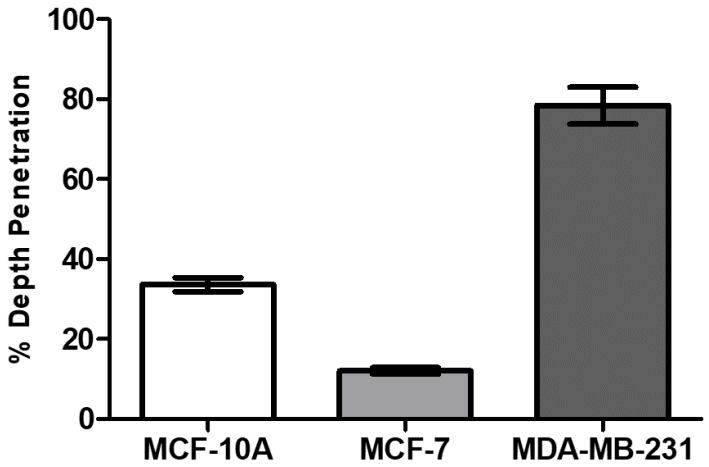

Figure 18: % Depth Penetration of Immortalised Breast Epithelial Cell Lines grown on Alvetex® Strata membrane at 14 days. Error bars represent ± SEM. N = 3 independent repeats, with measurements across three models composing each repeat totalling to $n_{MCF\text{-}10A}$ = 167, $n_{MCF\text{-}7}$ = 138, $n_{MDA\text{-}MB\text{-}231}$ = 495.

Table 12: Table showing the Tukey's Post-hoc test for the One-way ANOVA undertaken between each cell line during Alvetex® Strata experiments.

Tukey's Multiple Comparison Test	Mean Diff.	q	P Value	Summary	95% CI of diff
MCF-10A vs MCF-7	21.42	13.18	<0.0001	***	15.99 to 26.86
MCF-10A vs MDA-MB-231	-45.38	35.89	<0.0001	***	-49.61 to -41.15
MCF-7 vs MDA-MB-231	-66.81	49.12	<0.0001	***	-71.36 to -62.25

6.2.1. Treatment of Commercially Available Breast Cancer Cell Lines with CAPE Inhibited Penetration Into Alvetex® Strata.

It has been demonstrated that each cell line shows statistically significant differences in migration when grown on Alvetex® Strata. The next stage in the development of the Alvetex® Strata breast cancer invasion assay was to test the platforms compatibility with the CAPE inhibitor in line with the 2D scratch assays. Treatment with CAPE was changed to include 6 treatment groups as follows: Control, Vehicle control consisting of treatment with 10 µL DMSO, and then CAPE treatments of 10

μM, 25 μM, 50 μM and 100 μM. If no bar is present, assume that no cells were present in the membrane at this concentration.

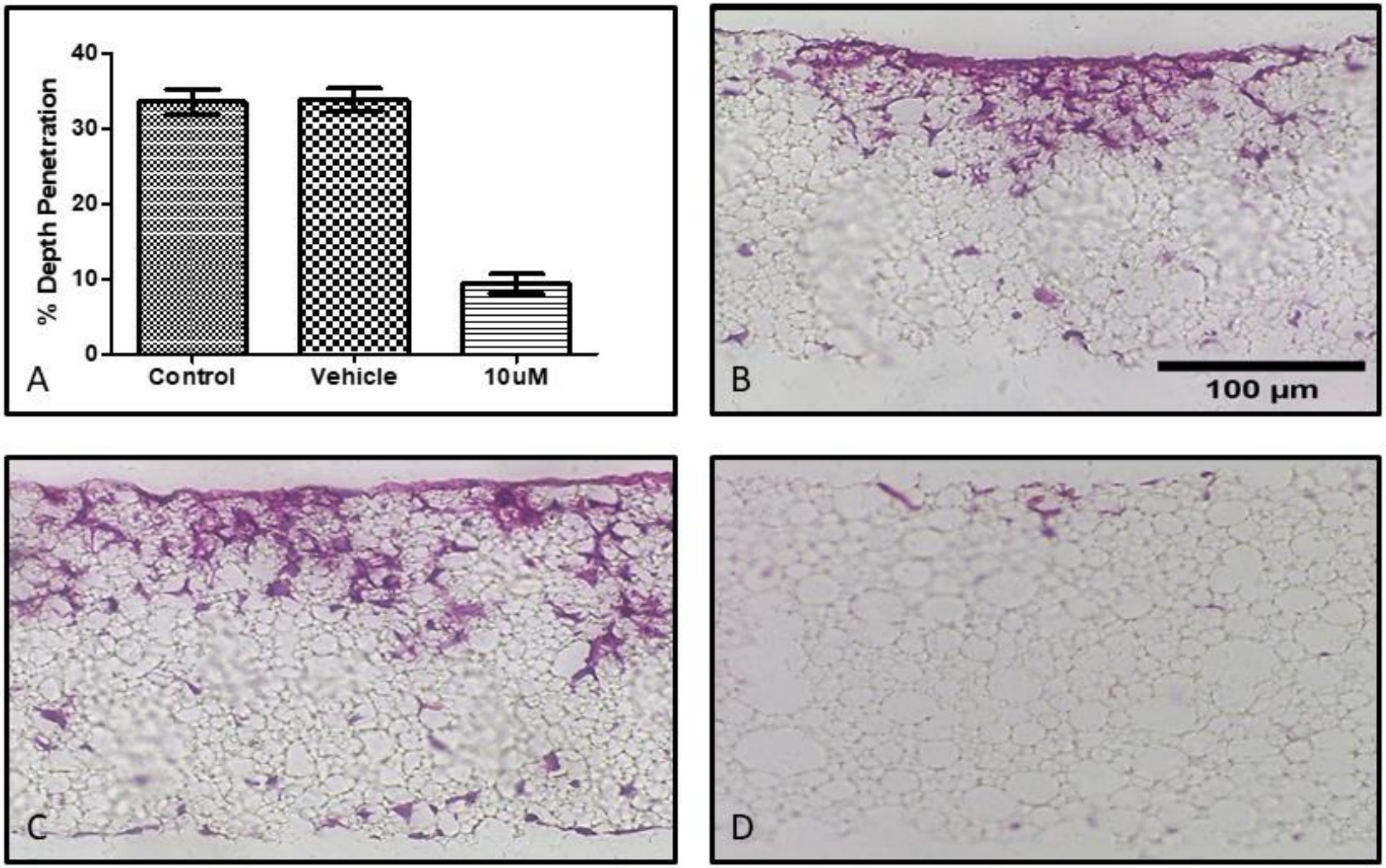

Figure 19: The Invasion Capabilities of MCF-10A 's when seeded onto Alvetex® Strata. A) Graph illustrating the % Depth Penetration of the MCF-10A Cell Line under each experimental condition. B) Control Group. C) Vehicle Control. D) 10 µM CAPE treatment. N = 3, $n_{control}$ = 167, $n_{vehicle}$ = 298, $n_{10\,\mu M}$ = 15. Error bars represent ± SEM. Scale bar = 100 µm.

Treatment of the MCF-10A cell line with the CAPE inhibitor when grown on Alvetex® Strata decreased depth penetration of the cell line, while the vehicle treatment produced similar results to the control group (Figure 19A). One-way ANOVA testing revealed that there was a statistically significant difference in % Depth Penetration between at least two of the treatment groups ($F(2, 477) = [7.303]$, $p = <0.0001$). Dunnett's Post-hoc Test for multiple comparisons between the control group found that the mean value of % Depth Penetrated was not significantly different when comparing the Control and Vehicle groups ($p = >0.05$) but was significantly different when comparing the Control group to the 10 μM CAPE treated group ($p = <0.0001$).

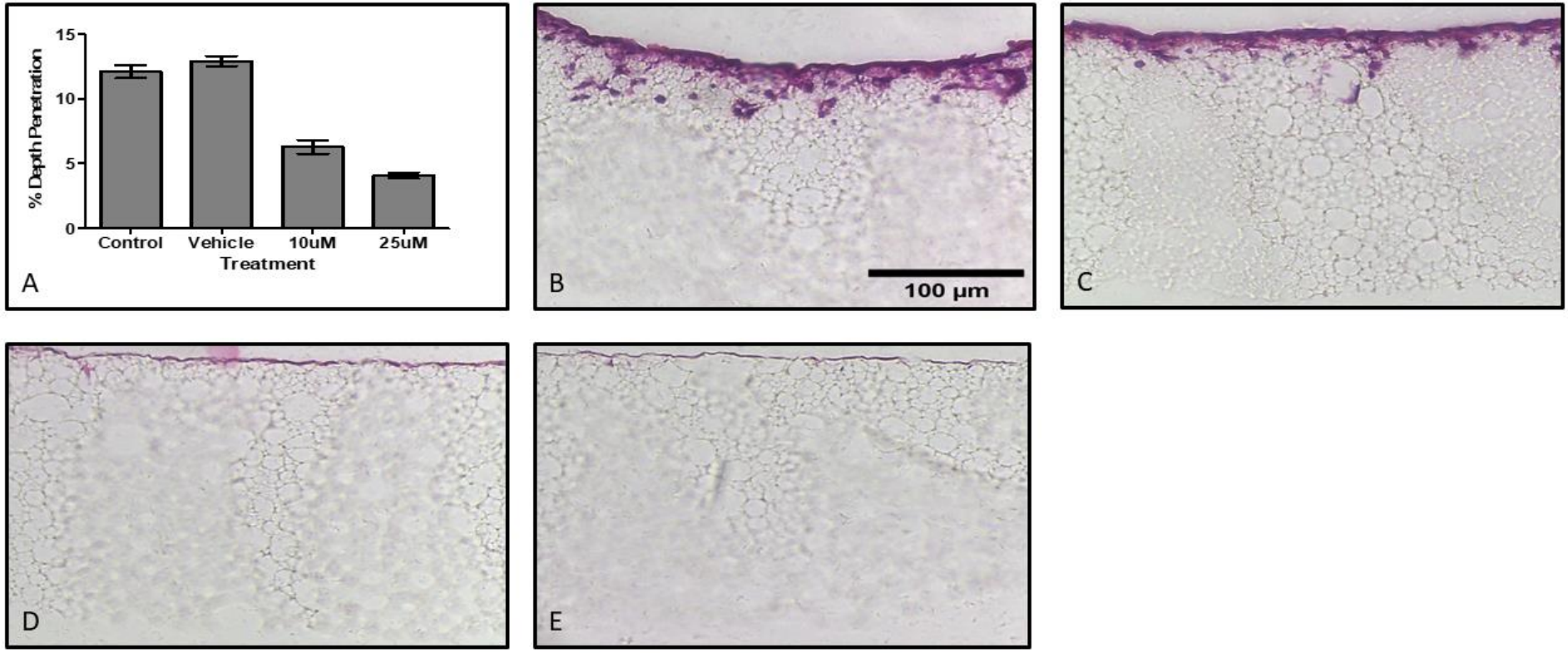

Figure 20: The Invasion Capabilities of MCF-7 's when seeded onto Alvetex® Strata. A) Graph illustrating the % Depth Penetration of the MCF-7 Cell Line under each experimental condition. B) Control Group. C) Vehicle Control. D) 10 µM CAPE treatment. E) 25 µM CAPE treatment. N = 3, $n_{control}$ = 138, $n_{vehicle}$ = 150, $n_{10\ \mu M}$ = 51, $n_{25\ \mu M}$ = 59. Error bars represent ± SEM.

Treatment of the MCF-7 cell line with the CAPE inhibitor when grown on Alvetex® Strata had a similar effect to the MCF-10A cell line, whereby the inhibitor decreased depth penetration of the cell line, while the vehicle treatment produced similar results to the control group (Figure 20A). One-way ANOVA testing revealed that there was a statistically significant difference in % Depth Penetration between at least two of the treatment groups ($F(3, 394) = [66.44]$, $p = <0.0001$). Dunnett's Post-hoc Test for multiple comparisons between the control group found that the mean value of % Depth Penetrated did not show a significant statistical difference when comparing the Control and Vehicle groups ($p = >0.05$), but was significantly different when comparing the Control group to the 10 µM and 25 µM CAPE treated groups ($p = <0.0001$). It was also evident that treatment with CAPE prevented the production of thickened MCF-7 layers on top of the Alvetex® Strata membrane as seen in the control groups (Figure 20B & C), instead thin layers of MCF-7 cells on top of the membrane were produced (Figure 20D & E).

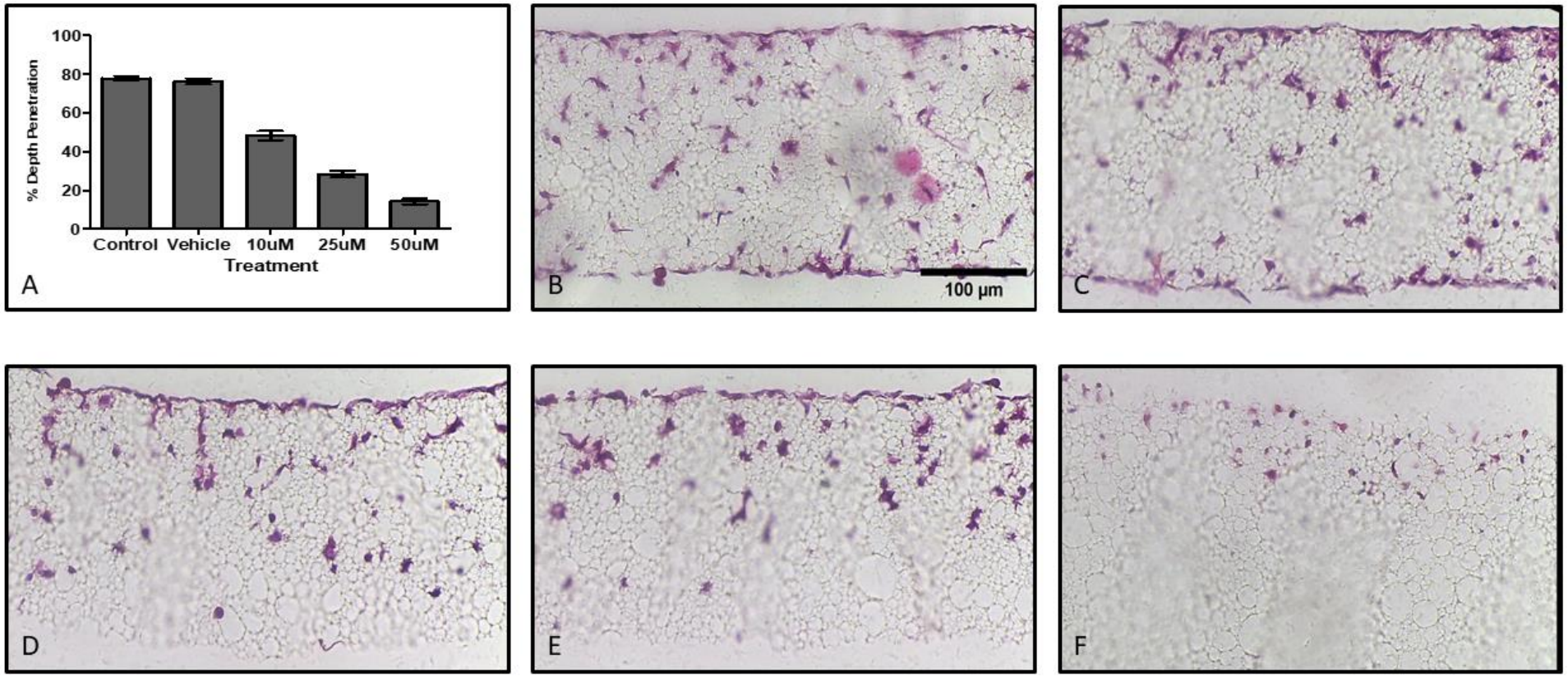

Figure 21: The Invasion Capabilities of MDA-MB-231's when seeded onto Alvetex® Strata. A) Graph illustrating the % Depth Penetration of the MCF-10A Cell Line under each experimental condition. B) Control Group. C) Vehicle Control. D) 10 µM CAPE treatment. E) 25 µM CAPE treatment. F) 50 µM CAPE treatment. N = 3, $n_{control}$ = 396, $n_{vehicle}$ = 286, $n_{10\ \mu M}$ = 91, $n_{25\ \mu M}$ = 146, $n_{50\ \mu M}$ = 44. Error bars represent ± SEM.

Similar to the other two cell lines, treatment of the MDA-MB-231 cell line with the CAPE inhibitor decreased depth penetration of the cell line, while the vehicle treatment produced similar results to the control group (Figure 20A). One-way ANOVA testing revealed that there was a statistically significant difference in % Depth Penetration between at least two of the treatment groups ($F(4, 958) = [205.5]$, $p = <0.0001$). Dunnett's Post-hoc Test for multiple comparisons between the control group found that the mean value of % Depth Penetrated did not show a significant statistical difference when comparing the Control and Vehicle groups ($p = >0.05$), but was significantly different when comparing the Control group to the 10 μM, 25 μM, and 50 μM CAPE treated groups ($p = <0.0001$). CAPE treatment up until 25 μM produced cells with normal H&E staining intensity and global cell morphology when compared to the control groups (Figure 21D & E), however once treated with 50 μM CAPE the cells shrunk and had lower strained intensity when compared to the control groups (Figure 21F).

In addition to the decrease in depth penetration observed in all of the cell lines, each cell line also showed differential tolerance to the CAPE inhibitor when grown on the Alvetex® Strata membrane. The MCF-10A cell line had the weakest tolerance of 10 μM (Figure 19), the MDA-MB-231 cell line had the highest tolerance of 50 μM (Figure 21), and the MCF-7 cell line was an intermediate of the two with a 25 μM tolerance (Figure 20).

Overall, these results show that not only is the use of the CAPE inhibitor compatible with the novel Alvetex® Strata invasion assay, but also treatment with the CAPE inhibitor decreased cell motility, as shown through decreased depth penetration, across all three cell lines to a statistically significant degree when compared to the control groups.

6.3. The Introduction of a Complex and Relevant 3D Microenvironment Through Co-Culture of Breast Cancer Cell Lines with HDFn's Led to the Adoption of Enhanced *In Vivo* Characteristics.

The introduction of a 3D microenvironment when growing the cells on Alvetex® Strata has an obvious effect on cell line behaviour and growth patterns when compared to the 2D scratch assays. However, the physiological relevance of this platform is limited as the cell are being grown in monoculture and without the ECM components present in an *in vivo* system. In the Przyborski lab physiologically relevant and reproducible microenvironments, termed stromal compartments, are able to be created through the culture of HDFn's in the Alvetex® Scaffold platform.

The stromal compartment produced through the culture of HDFn's in Alvetex® Scaffold contain fibroblasts spread throughout the membrane, with a defined fibroblast layer on top and bottom of the scaffold as shown through H&E staining (Figure 22A&D, White Arrow). The localisation of fibroblasts is further confirmed through α-SMA staining of the membrane (Figure 22C). Furthermore, when immunostaining the stromal compartment for ECM components also shows that these compartments contain Fibronectin (Figure 22B), Collagen 1 (Figure 22E), and Collagen IV (Figure 22F).

Once formed, these stromal compartments are then able to have epithelial populations seeded on top of them to build full thickness epithelial models with an *in vivo*-like microenvironment and stromal compartment.

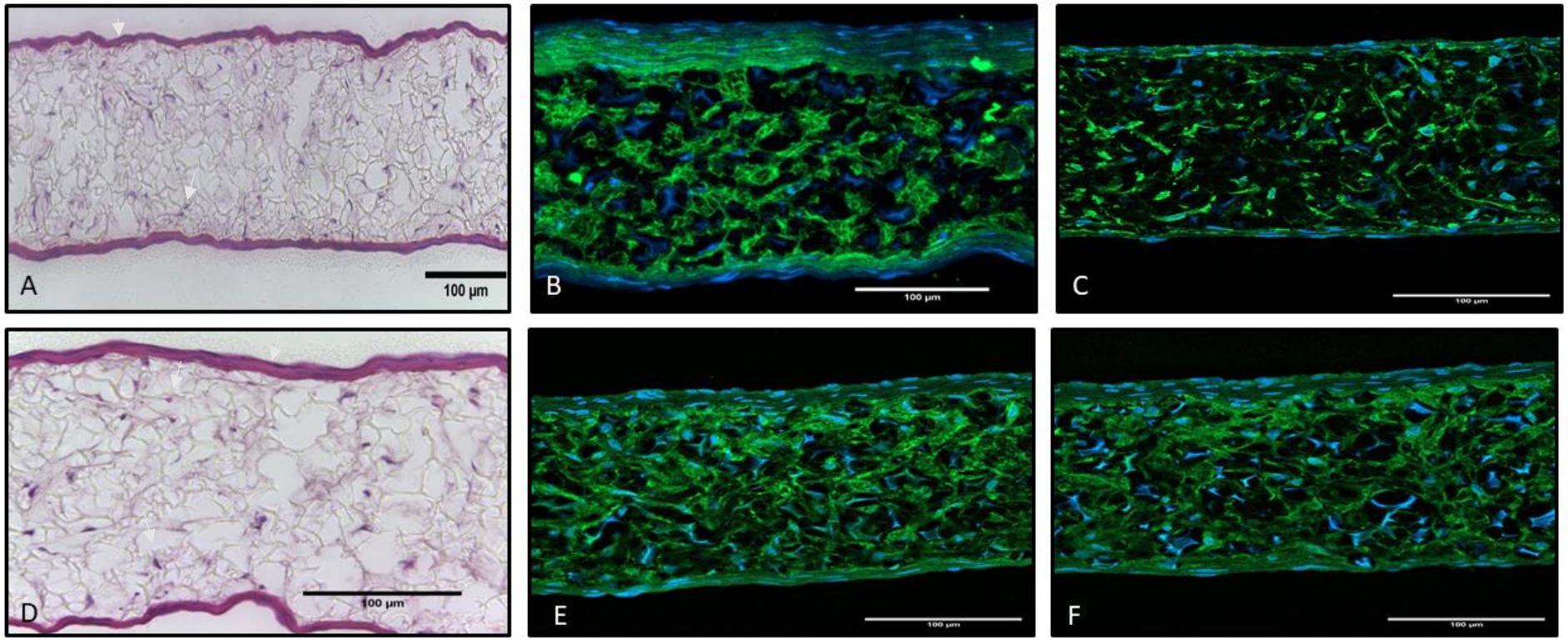

Figure 22: Characterisation of the HDFn-derived stromal compartment in Alvetex® Scaffold. A) x20 H&E image of the stromal compartment, white arrows point to fiobroblast cells. B) Immunostained image of the HDFn compartment for Fibroncectin (Green), with nuclei stained blue using Hoerscht. C) Immunostained image of the HDFn compartment for α-SMA (Green), with nuclei stained blue using Hoerscht. D) x40 H&E image of the stromal compartment, white arrows point to fiobroblast cells. E) Immunostained image of the HDFn compartment for Collagen 1 (Green), with nuclei stained blue using Hoerscht. F) Immunostained image of the HDFn compartment for Collagen IV (Green), with nuclei stained blue using Hoerscht.

6.3.1. The MCF-10A Cells Formed Structures and Invasion Patterns That Highly Represent Healthy Mammary Tissue.

Seeding of the MCF-10A cell line onto the HDFn-derived stromal compartment led to the formation of consistent and reproducible full thickness models with unique characteristics when compared to the other two models. H&E analysis of the MCF-10A models (Figure 23A& D) showed thickening of the top of the stromal compartment where the cells were seeded. The cells composing this thickened layer had elongated nuclei, suggesting that the epithelial cells are stretching out across the fibroblast layer. Immunostaining for CK8 and Vimentin confirmed this observation, and it was found that the MCF-10A cells would grow as a monolayer across the top of the stromal compartment (Figure 23B & E). However, it should be noted that these models contained regions of MCF-10A cells that were either devoid of epithelial cells or contained MCF-10A cells that were CK8 negative, potentially stemming from the mixed cell population found during 2D characterisation. Despite this, growth of the MCF-10A cells was confined to this layer creating clear epithelial and mesenchymal compartments, with little invasion into the stromal compartments by the MCF-10A cells. In terms of ECM components, the MCF-10A full thickness models show Collagen I and IV expression like the original stromal compartments; however, their distribution is much denser than that seen in the other models and standalone stromal compartments (Figure 23C & F).

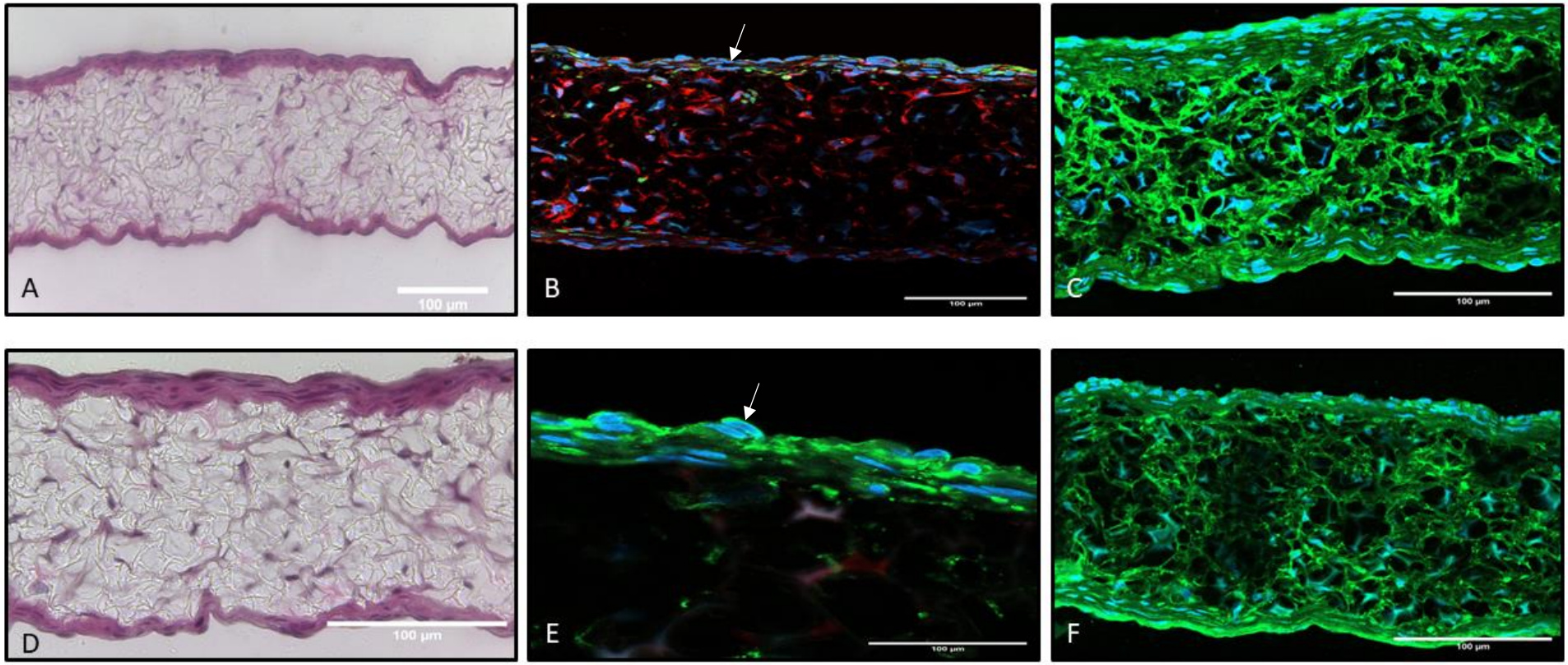

Figure 23: Characterisation of the MCF-10A Full Thickness Model in Alvetex® Scaffold. A) x20 H&E image of the MCF-10A Full Thickness Model. B) Immunostained image of the MCF-10A Full Thickness Model for Cytokeratin 8(Green) and Vimentin (Red), with nuclei stained blue using Hoerscht. White arrows show MCF-10A cells. C) x20 Immunostained image of the MCF-10A Full Thickness Model for Collagen 1 (Green), with nuclei stained blue using Hoerscht. D) x40 H&E image of the MCF-10A Full Thickness Model. E) x63 Immunostained image of the MCF-10A Full Thickness Model for Cytokeratin 8(Green) and Vimentin (Red), with nuclei stained blue using Hoerscht. White arrows show MCF-10A cells. F) Immunostained image of the MCF-10A Full Thickness Model for Collagen IV (Green), with nuclei stained blue using Hoerscht

6.3.2. The MCF-7 Cells Formed Structures and Invasion Patterns That Highly Represent DCIS Lesions.

Seeding of the MCF-7 cell line onto the HDFn-derived stromal compartment led to the formation of a reproducible full thickness model. Initial H&E analysis of the models (Figure 24A & D) showed a thickened layer of cells growing on top of the stromal compartment, with cells spread throughout the membrane in a similar way to the stromal compartments. Immunostaining for MCF-7 and HDFn specific markers (CK8 and Vimentin respectively), showed clear compartmentalisation of the model whereby the MCF-7's growth was confined to the top of the model with the inside of the scaffold being solely occupied by the fibroblast population used to generate the stromal compartment prior to epithelial cell seeding (Figure 24B & E). Higher magnification images show that the MCF-7 cells do not grow as a monolayer as part of this full thickness model, instead they irregularly stack to form a multilayer epithelial compartment with some of the cells directly in contact with the fibroblast layer of the stromal compartment, and others in contact with other MCF-7 cells (Figure 24E). In terms of ECM components, the MCF-7 full thickness models show Collagen I and IV expression much-like the original stromal compartments, whereby their distribution is even across the model (Figure 24C & F).

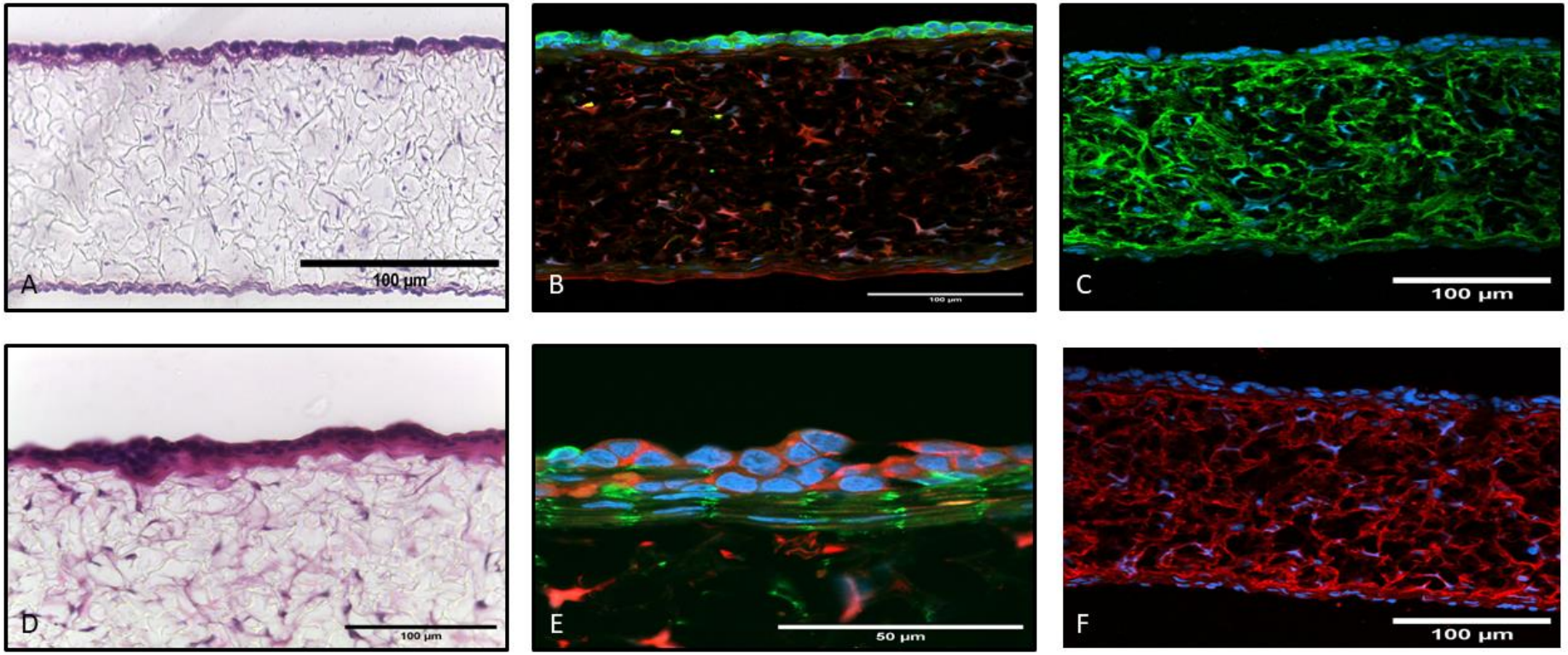

Figure 24: Characterisation of the MCF-7 Full Thickness Model in Alvetex® Scaffold. A) x20 H&E image of the MCF-7 Full Thickness Model. B) Immunostained image of the MCF-7 Full Thickness Model for Cytokeratin 8 (Green) and Vimentin (Red), with nuclei stained blue using Hoerscht. C) x20 Immunostained image of the MCF-7 Full Thickness Model for Collagen 1 (Green), with nuclei stained blue using Hoerscht. D) x40 H&E image of the MCF-7 Full Thickness Model. E) x63 Immunostained image of the MCF-7 Full Thickness Model for Cytokeratin 8 (Green) and Vimentin (Red), with nuclei stained blue using Hoerscht. F) Immunostained image of the MCF-7 Full Thickness Model for Collagen IV (Red), with nuclei stained blue using Hoerscht

6.3.3. The MDA-MB-231 Cells Formed Structures and Invasion Patterns That Highly Represent IDC Lesions.

Similar to the MCF-7 and MCF-10A Full Thickness models, seeding of the MDA-MB-231 cell line onto the HDFn-derived stromal compartment led to the formation of a reproducible full thickness model, however the characteristics of the model differed greatly to the MCF-7 full thickness model. H&E analysis of the MDA-MB-231 models (Figure 25A & D) showed growth of enlarged nuclei, likely to be the MDA-MB-231 cells, spread on top of and throughout the Alvetex® Scaffold with some smaller nuclei, likely to be the fibroblast cells, interspersed between. The mesenchymal profile of the MDA-MB-231 cell line meant that a dual stain of Vimentin and α-SMA had to be used in order to identify the two cell populations specifically, where Vim+/ α-SMA- showed MDA-MB-231 cells and Vim+/ α-SMA+ showed fibroblast cells (Figure 25B & E). This immunostaining confirmed that MDA-MB-231 growth was not confined to one area and was spread throughout the stromal compartment. It is also evident that invasion and growth of the MDA-MB-231 cells into the stromal compartment potentially hindered fibroblast growth due to their decreased number when compared to the original stromal compartments (Figure 22 & Figure 25), with the majority of fibroblasts growing on the non-seeded (bottom) side of the scaffold (Figure 25). In terms of ECM components, the MDA-MB-231 full thickness models show Collagen I and IV expression like the original stromal compartments; however their distribution is less even, whereby sparse regions of collagen can be observed in these models (Figure 25C & F).

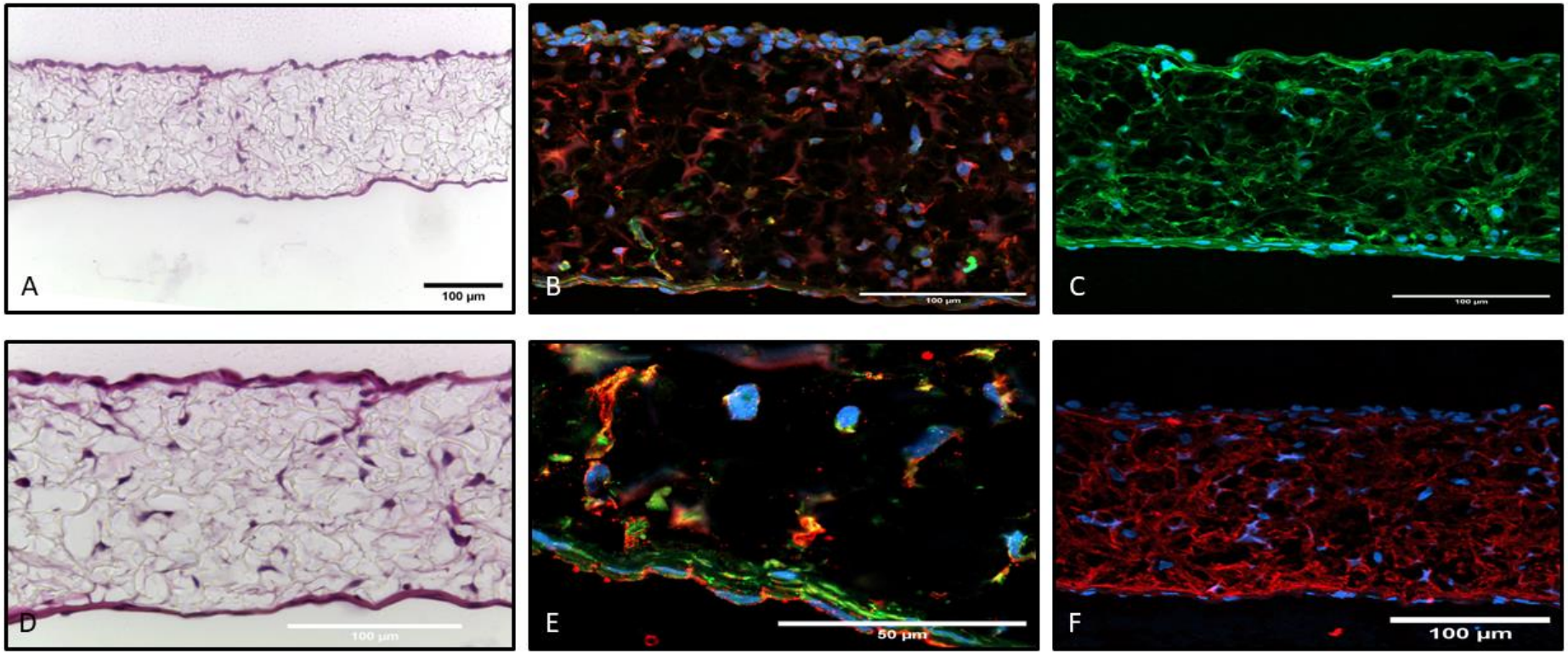

Figure 25: Characterisation of the MDA-MB-231 Full Thickness Model in Alvetex® Scaffold. A) x20 H&E image of the MDA-MB-231 Full Thickness Model. B) Immunostained image of the MDA-MB-231 Full Thickness Model for α-SMA(Green) and Vimentin (Red), with nuclei stained blue using Hoerscht. C) x20 Immunostained image of the MDA-MB-231 Full Thickness Model for Collagen 1 (Green), with nuclei stained blue using Hoerscht. D) x40 H&E image of the MDA-MB-231 Full Thickness Model. E) x63 Immunostained image of the MDA-MB-231 Full Thickness Model for α-SMA (Green) and Vimentin (Red), with nuclei stained blue using Hoerscht. F) Immunostained image of the MDA-MB-231 Full Thickness Model for Collagen IV (Red), with nuclei stained blue using Hoerscht.

6.3.4. Quantification of the Invasion Capabilities of the Commercially Available Breast Cancer Cell Lines in 3D Co-Culture Showed Significant Differences in Invasive Potential.

It is evident that the introduction of a physiologically relevant stromal compartment to the growth of each breast epithelial cell line created changes in epithelial cell morphology and growth behaviour when compared to the other growth platforms. The invasive behaviour of each cell line in this 3D co-culture system was ascertained through the measurement of the average % Depth Penetration of each cell line into the stromal compartment was carried out, whereby a higher % Depth Penetration indicates higher invasive potential of a cell line in this platform that accounts for a physiologically relevant microenvironment.

All three cell lines displayed some invasion into the stromal compartment, with the MDA-MB-231 cell line showing the largest average % Depth Penetration of 61.8% and the MCF-10A and MCF-7 cell lines showing similar low % Depth Penetration of 4.3% and 4.8% respectively (Figure 26). The lack of overlap of the SEM bars between the depth penetration of the three different full thickness models suggests that these observed differences may be statistically significant. One-way ANOVA testing revealed that there was a statistically significant difference in % Depth Penetration between at least two of the cell lines ($F(2, 304) = [305.9]$, $p = <0.0001$). Tukey's Post-hoc Test for multiple comparisons between groups found that the difference observed in the mean value of % Depth Penetration for the MDA-MB-231 full thickness model was statistically significant when comparing against the penetration data for the other two full thickness models ($p = <0.0001$). However, the % Depth Penetration of the MCF-10A and MCF-7 full thickness models was not statistically significant when compared to each other ($p = >0.05$). For in depth post-hoc results see Table 13.

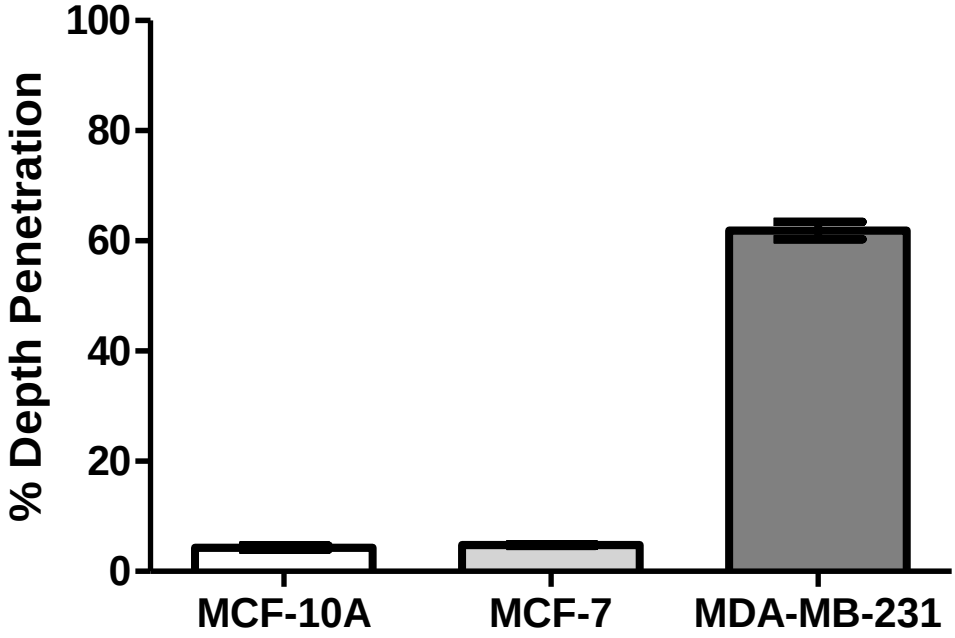

Figure 26: A graph illustrating the % Depth Penetration of the three immortalised cell lines when cultured on the Alvetex® Scaffold platform. Error bars show ± SEM.

Table 13: Tukey's Post Hoc test for multiple comparisons on full thickness model invasion data.

Tukey's Multiple Comparison Test	Mean Diff.	q	Significant? P < 0.05?	Summary	95% CI of diff
MCF-7 vs MDA-MB-231	-57.08	32.07	Yes	***	-63.04 to -51.11
MCF-7 vs MCF-10A	0.4662	0.1419	No	ns	-10.56 to 11.49
MDA-MB-231 vs MCF-10A	57.54	18.83	Yes	***	47.29 to 67.79

6.3.5. Addition of the CAPE Inhibitor to the MDA-MB-231 Models Inhibited their Invasion in 3D Co-Culture.

With the development of a reproducible Alvetex® Scaffold Co-Culture Invasion model for each of the chosen cell lines, it was important to assess the platforms compatibility with the CAPE inhibitor. As a result of low % depth penetration of the MCF-10A and MCF-7 cell lines as part of this platform, experiments were focussed on the highly invasive MDA-MB-231 full thickness models. These experiments involved the creation of three treatment groups: Control, 10 µM CAPE treatment, 20 µM CAPE treatment.

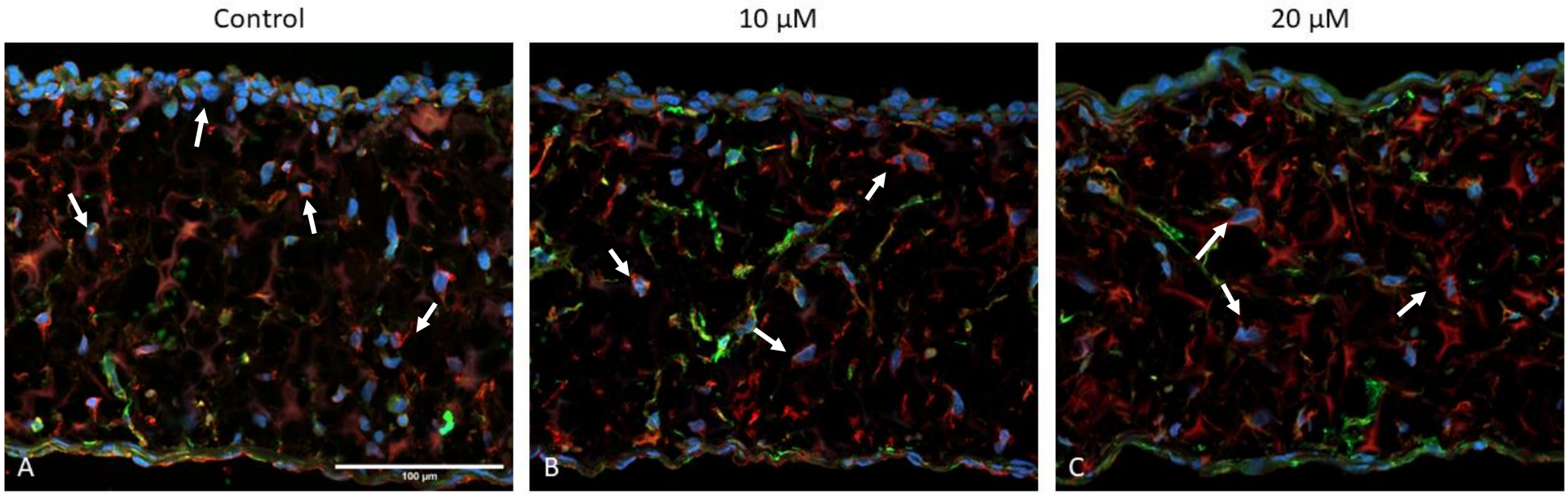

Figure 27: Immunostained images of the MDA-MB-231 HDFn full thcikness models treated with the CAPE inhibitor. All images were stained for Vimentin (Red) and α-SMA (Green) A) Control group. B) Treatment of models with 10 µM CAPE inhibitor. C) Treatment of models with 20 µM CAPE inhibitor. White arrows indicate MDA-MB-231 cells for reference.

Across all three treatment groups MDA-MB-231 growth was observed and similar cell morphologies were maintained across treatment groups (Figure 27). CAPE treatment did seem to reduce the number of MDA-MB-231 cells as its concentration increased. Despite this decrease, invasion of the MDA-MB-231 cells was still observed across all three treatment groups to some degree. Figure 28 confirms this trend and shows that as CAPE is introduced and its concentration increased, the % Depth Penetration of the MDA-MB-231 cells decreases. A one-way ANOVA confirmed that these differences observed were significant between at least two of the treatment groups ($F(2, 908) = [54.19]$, $p = <0.0001$). Dunnet's post-hoc test was used to compare the CAPE treatment groups to the control group, found that both groups shared a statistically significant difference when compared to the control ($p = <0.0001$).

Overall, these results show that not only is the use of the CAPE inhibitor compatible with this novel Alvetex® Scaffold invasion model, but also treatment with the CAPE inhibitor was able to decrease the % depth penetration of the MDA-MB-231 cells when compared to the control groups.

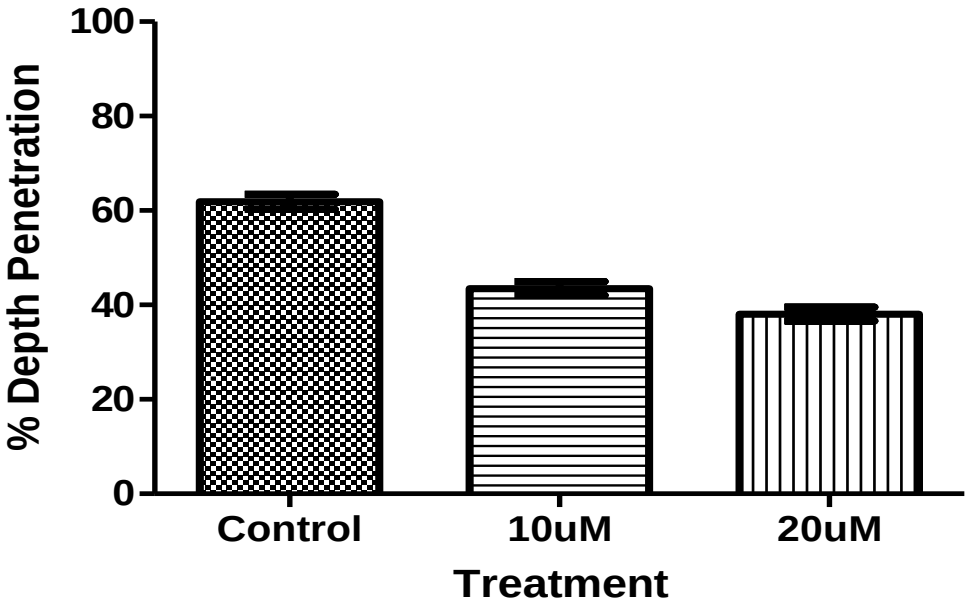

Figure 28: A graph illustrating the % Depth Penetration of the MDA-MB-231 Alvetex® Scaffold model following treatment with 10 µM and 20 µM of the CAPE inhibitor. Error bars show ± SEM. Per condition data was collected from 3 independent experimental repeats (N=3), with 3 technical model repeats per set up. 48 measurements were taken per condition across the 3 models ($n_{control}$=209, $n_{10\ \mu M}$ = 375, $n_{25\ \mu M}$ = 327).

6.4. Physiological Relevance of the Alvetex® Scaffold Models was Increased Through the Seeding of Primary Healthy Breast Epithelium Cells with Human Dermal Fibroblasts

Despite the optimisation of three distinct breast cancer models that are based around the three pathological timepoints of breast cancer progression, the models are based on immortalised cell lines which do not full represent their *in vivo* counterparts. While allowing the production of highly reproducible and consistent models, this becomes a barrier for physiological relevance due to the differences in behaviour that arise when creating immortalised cell lines. Thus, to increase the relevance of the full thickness models, and as a proof of concept for the compatibility of primary epithelial cells with this invasion model, primary healthy mammary epithelial cells (pME) were seeded on top of the HDFn-derived stromal compartment.

Similar to the other three Full Thickness models, seeding of the pME cells onto the HDFn-derived stromal compartment led to the formation of consistent and reproducible full thickness models with unique characteristics. This creation of consistent models confirmed the compatibility of this novel invasion model with primary epithelial cell populations. H&E analysis of the pME full thickness models, showed slight thickening of the top of the stromal compartment where the cells had been seeded (Figure 29A). Immunostaining for epithelial and mesenchymal markers, showed clear confinement of the pME cells to the top of the stromal compartment where they formed a consistent monolayer across the surface Figure 29. Higher magnification images showed that unlike the MCF-10A cells which elongated across the surface of the stromal compartment and formed a sparse monolayer, the primary epithelial cells condensed into a cuboidal epithelial cell morphology (Figure 29D), similar to that seen *in vivo.* Analysis for the presence of ECM components, showed Collagen I and IV in the stromal compartment and it was evenly distributed across the inside of the model.

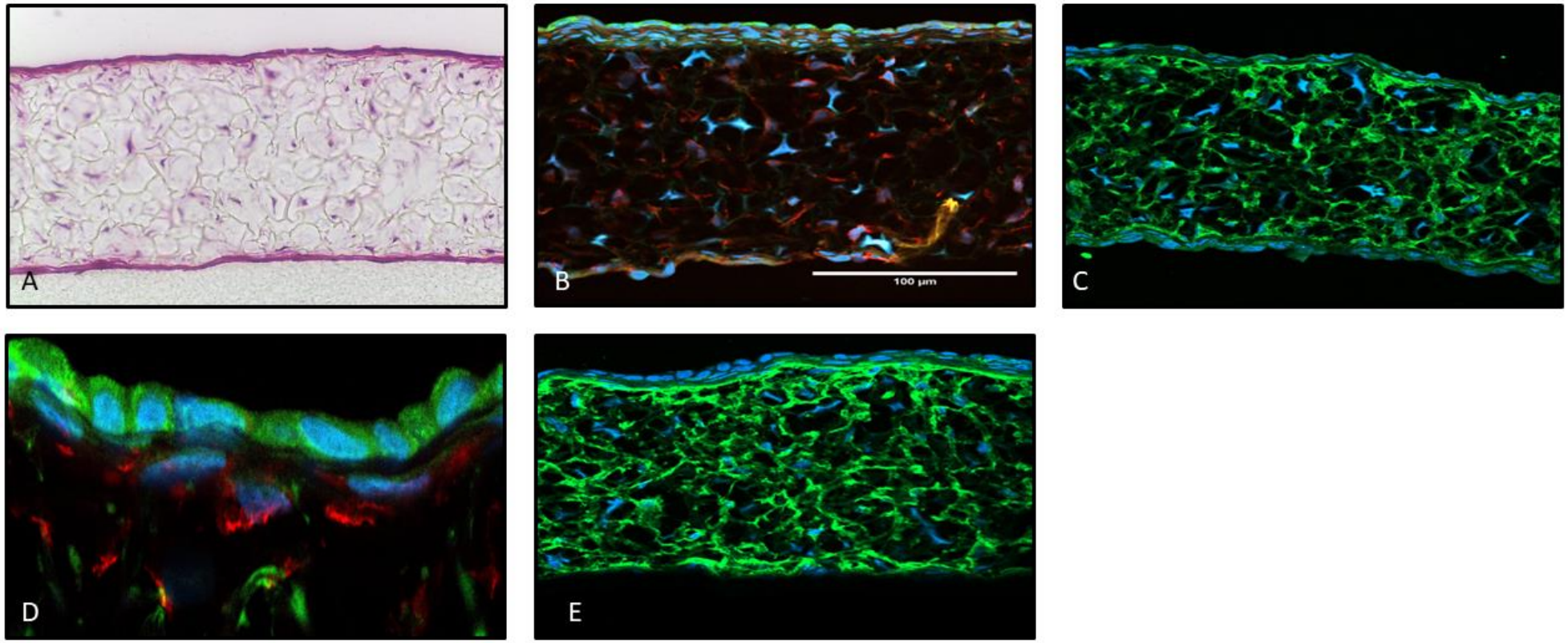

Figure 29: Characterisation of the pME Full Thickness Model in Alvetex® Scaffold. A) x20 H&E image of the pME Full Thickness Model. B) Immunostained image of the MCF-10A Full Thickness Model for Cytokeratin 8(Green) and Vimentin (Red), with nuclei stained blue using Hoerscht. C) x20 Immunostained image of the pME Full Thickness Model for Collagen 1 (Green), with nuclei stained blue using Hoerscht. D) x63 Immunostained image of the pME Full Thickness Model Cytokeratin 8 (Green) and Vimentin (Red), with nuclei stained blue using Hoerscht. F) Immunostained image of the pME Full Thickness Model for Collagen IV (Green), with nuclei stained blue using Hoerscht.

6.5. Growth of Breast Cancer Cell Lines in Alvetex® Scaffold as a co-culture system with Mammary Fibroblasts to Make Models More Representative of Mammary Tissue.

It is evident that the introduction of an *in vivo*-like stromal compartment derived from HDFn's and seeding of various breast epithelial cell populations (immortalised and primary) on top has an obvious effect on cell line invasion behaviour and morphology. However, the physiological relevance of this platform can be further improved, as the ECM's deposited by fibroblasts is tissue specific. The HDFn's used to deposit the stromal compartments used previously, while well-defined and highly proliferative, are derived from skin tissue and thus deposit ECM components in the proportions relevant for skin tissue. Thus, the physiological relevance of these full thickness invasion models can be increased through the formation of stromal compartments derived from mammary fibroblast (MF) populations grown in Alvetex® Scaffold.

The mammary fibroblast derived stromal compartments, much like the HDFn-derived stromal compartments, contain fibroblasts spread throughout the membrane, with a defined fibroblast layer on top and bottom of the scaffold as shown through H&E staining (Figure 30A&D, White Arrow). Comparison of H&E images of HDFn stromal compartments with those generated by MF's showed little histological differences (Figure 22A&D and Figure 30A&D). These similarities in localisation of the MFs was confirmed through α-SMA staining of the membrane (Figure 30C). Furthermore, when immunostaining the stromal compartment for ECM components also shows that ECM components such as Fibronectin (Figure 30B), Collagen 1 (Figure 30E), and Collagen IV (Figure 30F), are deposited by the MFs.

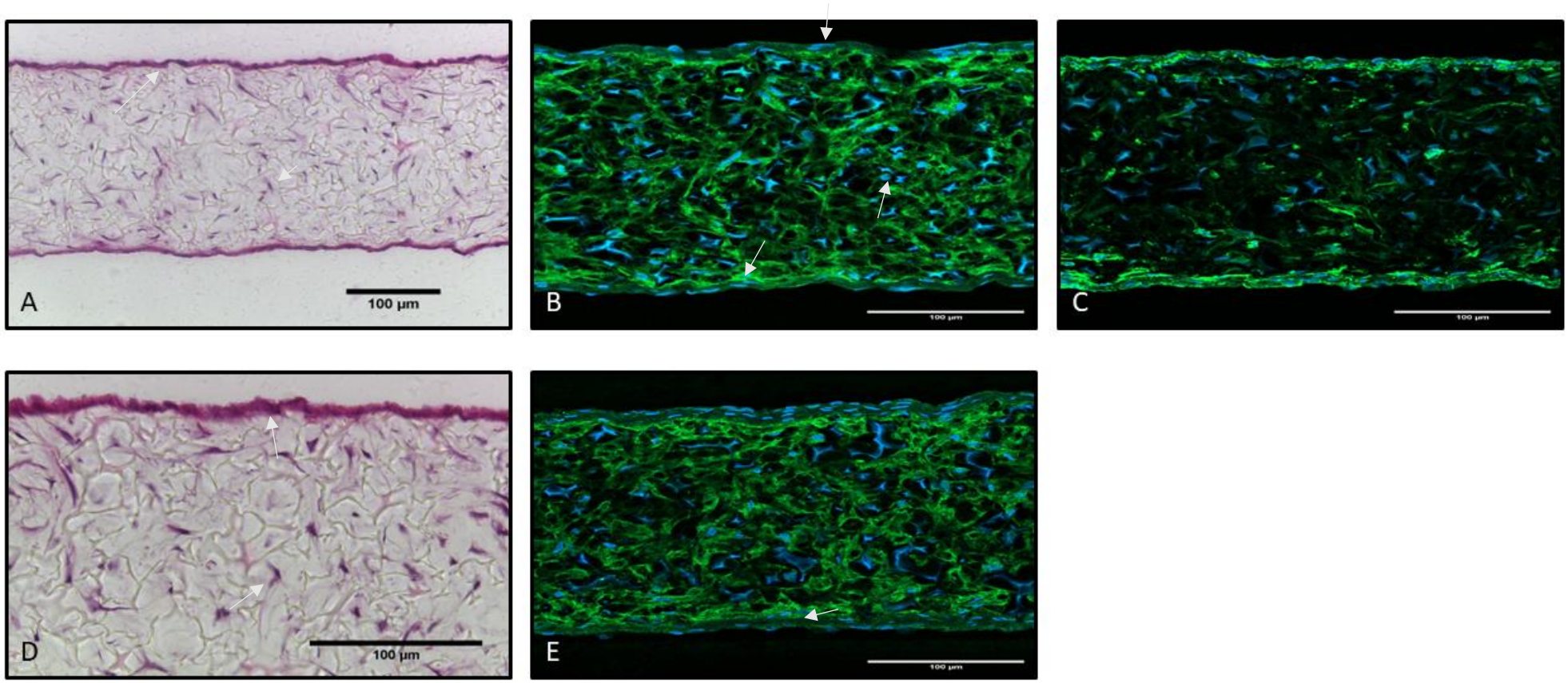

Figure 30: Figure 31: Characterisation of the MF-derived stromal compartment in Alvetex® Scaffold. A) x20 H&E image of the stromal compartment, white arrows point to fiobroblast cells. B) Immunostained image of the MF compartment for Fibroncectin (Green), with nuclei stained blue using Hoerscht. C) Immunostained image of the MF compartment for α-SMA (Green), with nuclei stained blue using Hoerscht. D) x40 H&E image of the stromal compartment, white arrows point to fiobroblast cells. E) Immunostained image of the MF compartment for Collagen 1 (Green), with nuclei stained blue using Hoerscht. F) Immunostained image of the MF compartment for Collagen IV (Green), with nuclei stained blue using Hoersch

6.5.1. Seeding of Immortalised Epithelial Cell Lines Onto the MF Stromal Compartment Maintained The Enhanced *In Vivo* Characteristics Observed in HDFn Co-Culture.

Seeding of all three immortalised cell lines onto MF-derived stromal compartments produced consistent and reproducible models (Figure 32, Figure 33, Figure 34). Analysis of each of the models showed histological similarities to their HDFn-derived counterparts, however key differences were present in the MCF-7 models. H&E analysis of the MCF-7 model showed stacked growth of MCF-7 cells across the top of the stromal compartment (Figure 32A&C), and immunostaining for a MCF-7 specific marker, CK8, confirmed this growth was confined to this area (Figure 32B&D). Furthermore, a layer of fibroblasts was making contact with the MCF-7 cells, with this cell type distributed throughout the scaffold, this was confirmed through vimentin staining (Figure 32B&E). ECM components and their distribution matched their HDFn-derived counterparts whereby Fibronectin and Collagen 1 were present in equal distributions. Despite these apparent similarities, it was evident that there were gaps present across the epithelial layer seeded across the stromal compartment that were not observed in the HDFn models (Figure 32B, white arrows). However, where MCF-7 growth was observed stacking was more frequent than in the HDFn derived models, producing structures similar to those observed in DCIS lesions.

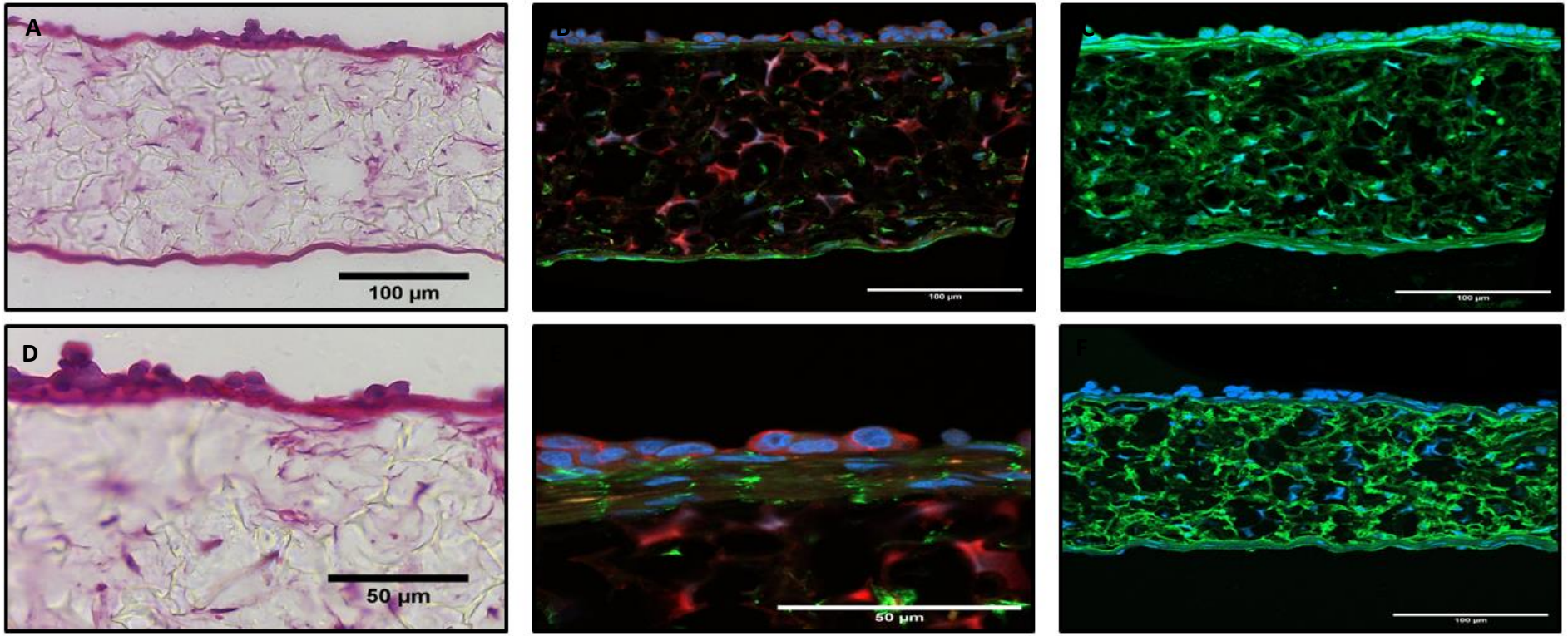

Figure 32: Characterisation of the MCF-7 cells grown on the MF derived stromal compartment in Alvetex® Scaffold. A) x20 H&E image of the MCF-7 Full Thickness Model. B) Immunostained image of the MCF-7 Full Thickness Model for Cytokeratin 8 (Red) and Vimentin (Green), with nuclei stained blue using Hoerscht. C) x20 Immunostained image of the MCF-7 Full Thickness Model for Collagen 1 (Green), with nuclei stained blue using Hoerscht. D) x40 H&E image of the MCF-7 Full Thickness Model. E) x63 Immunostained image of the MCF-7 Full Thickness Model for Cytokeratin 8 (Red) and Vimentin (Green), with nuclei stained blue using Hoerscht. F) Immunostained image of the MCF-7 Full Thickness Model for Collagen IV (Red), with nuclei stained blue using Hoerscht

The MDA-MB-231 MF full thickness model was highly similar to its HDFn derived counterpart. Growth of the MDA-MB-231 cells was observed throughout the model, with MDA-MB-231 cells growing on top of the stromal compartment and within it (Figure 33B&E, white arrows). Fibroblast numbers within the scaffold were reduced, when compared to the other model types, where their growth was confined to the surfaces lining the stromal compartment formed on the Alvetex® Scaffold. In contrast to the HDFn-derived models, Collagen 1 distribution was denser.

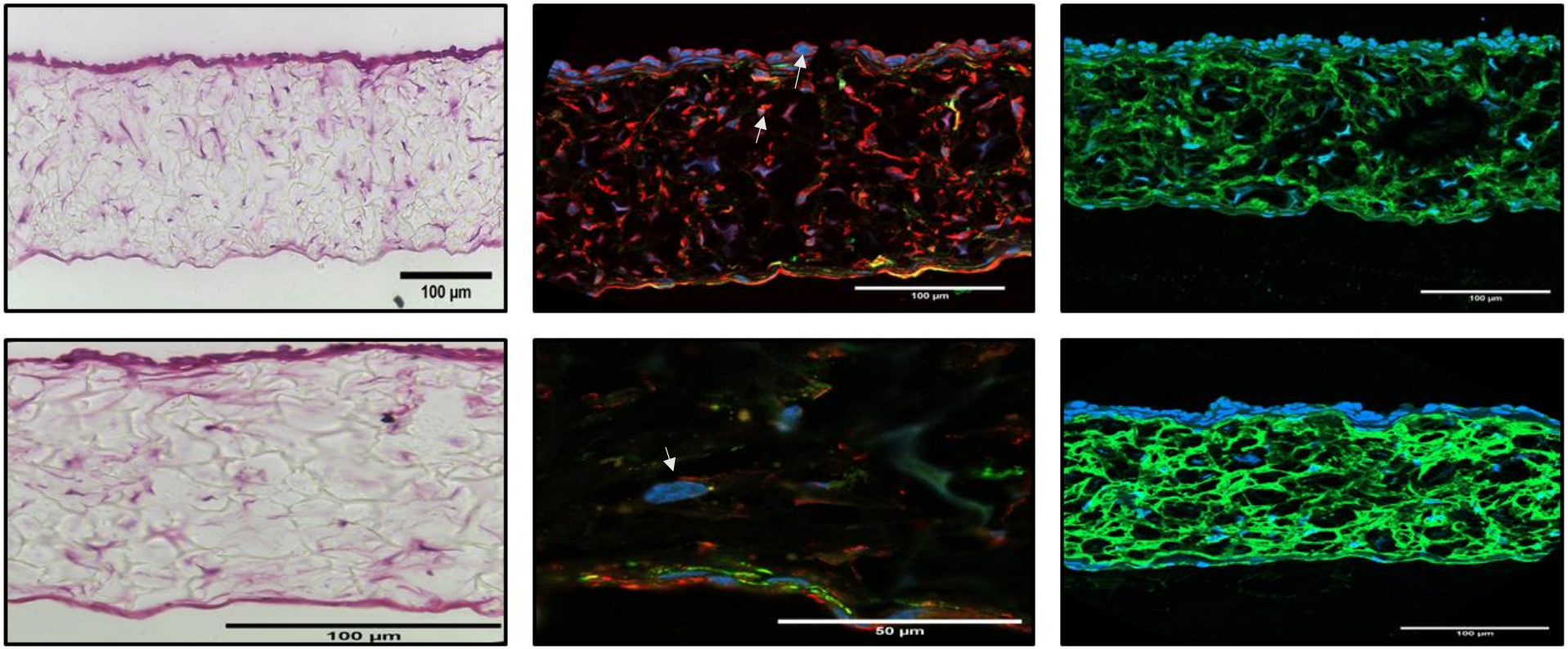

Figure 33: Characterisation of the MDA-MB-231 cells when grown on an MF-derived stromal compartment in Alvetex® Scaffold. A) x20 H&E image of the MDA-MB-231 Full Thickness Model. B) Immunostained image of the MDA-MB-231 Full Thickness Model for α-SMA(Green) and Vimentin (Red), with nuclei stained blue using Hoerscht. White arrows show the MDA-MB-231 cells C) x20 Immunostained image of the MDA-MB-231 Full Thickness Model for Collagen 1 (Green), with nuclei stained blue using Hoerscht. D) x40 H&E image of the MDA-MB-231 Full Thickness Model. E) x63 Immunostained image of the MDA-MB-231 Full Thickness Model for α-SMA (Green) and Vimentin (Red), with nuclei stained blue using Hoerscht. White arrows show the MDA-MB-231 cells F) Immunostained image of the MDA-MB-231 Full Thickness Model for Collagen IV (Red), with nuclei stained blue using Hoerscht

The MCF-10A MF full thickness model also shared many similarities with its HDFn derived counterpart. For example, H&E analysis showed thickening of the seeded layer surface of the stromal compartment (Figure 34A&D). Immunostaining for epithelial marker, CK8, confirmed that the growth of the MCF-10A cells was confined to the top of the model where they formed a flattened and elongated monolayer (Figure 34B&E, white arrows). Fibroblast growth matched both the MF and HDFn-derived stromal compartments, where growth was observed on the surfaces lining the stromal compartment and inside the stromal compartment formed on the Alvetex® Scaffold (Figure 34B&E, white star). Distribution of ECM components Collagen 1 and Fibronectin was even across the whole inside of the model, matching the HDFn derived MCF-10A full thickness models.

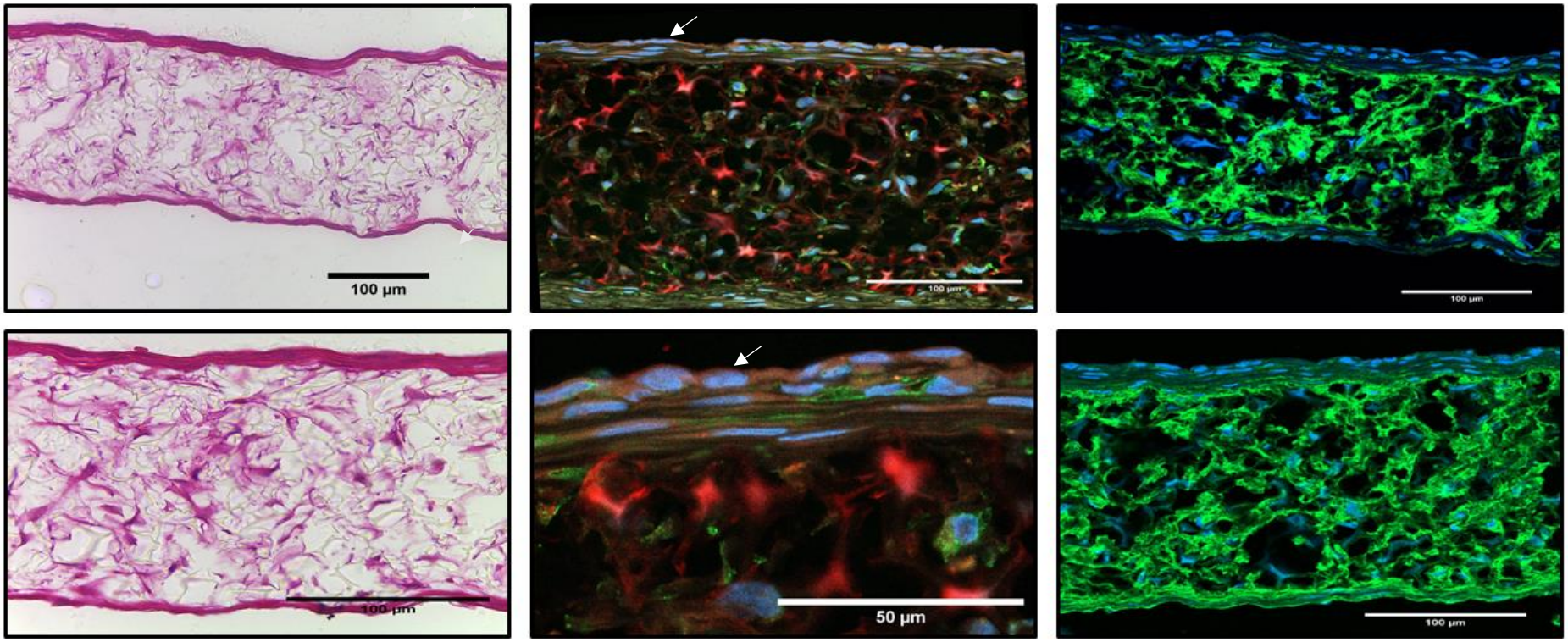

Figure 34: Characterisation of the MCF-10A cells grown on an MF-derived stromal compartment in Alvetex® Scaffold. A) x20 H&E image of the MCF-10A Full Thickness Model. B) Immunostained image of the MCF-10A Full Thickness Model for Cytokeratin 8(Red) and Vimentin (Green), with nuclei stained blue using Hoerscht. White arrows show the MCF-10A cells C) x20 Immunostained image of the MCF-10A Full Thickness Model for Collagen 1 (Green), with nuclei stained blue using Hoerscht. D) x40 H&E image of the MCF-10A Full Thickness Model. White arrows show the MCF-10A cells. E) x63 Immunostained image of the MCF-10A Full Thickness Model for CK8 (Red) and Vimentin (Green), with nuclei stained blue using Hoerscht. F) Immunostained image of the MCF-10A Full Thickness Model for Collagen IV (Green), with nuclei stained blue using Hoerscht

6.6. Growth of pME in a Co-culture system with Mammary Fibroblasts to demonstrate the intrinsic modularity of Alvetex® Scaffold.

Seeding of all pME cells onto the MF-derived stromal compartments produced a consistent and reproducible model (Figure 35). Despite this production of these models, the pME cells had morphological features that were less physiologically relevant when cultured with the MF cells. For example, H&E analysis of the pME model showed marginal thickening of the seeded surface of the stromal compartment (Figure 35A&C). Further immunostaining then showed that unlike the HDFn derived models, where the pME cells condensed into cuboidal cell morphologies highly representing their *in vivo* counterparts, the pME cells elongated and stretched across the top of the stromal compartment. Furthermore, there were gaps present across the monolayer of pME cells. Despite these differences, it should be noted that their growth was still confined to the top of the stromal compartment, creating a compartmentalised model.

There were similarities between the MF and HDFn derived models, especially when analysing MF growth and ECM component distribution as part of this model. For example, a clear layer of MF cells was present on top of the compartment, where the cells were making contact with the pME cells, with more MF cells evenly distributed throughout the stromal compartment, as shown through vimentin staining (Figure 35B&E). Furthermore, the presence of, and distribution of, key ECM components Collagen 1 and Fibronectin matched their HDFn-derived counterparts.

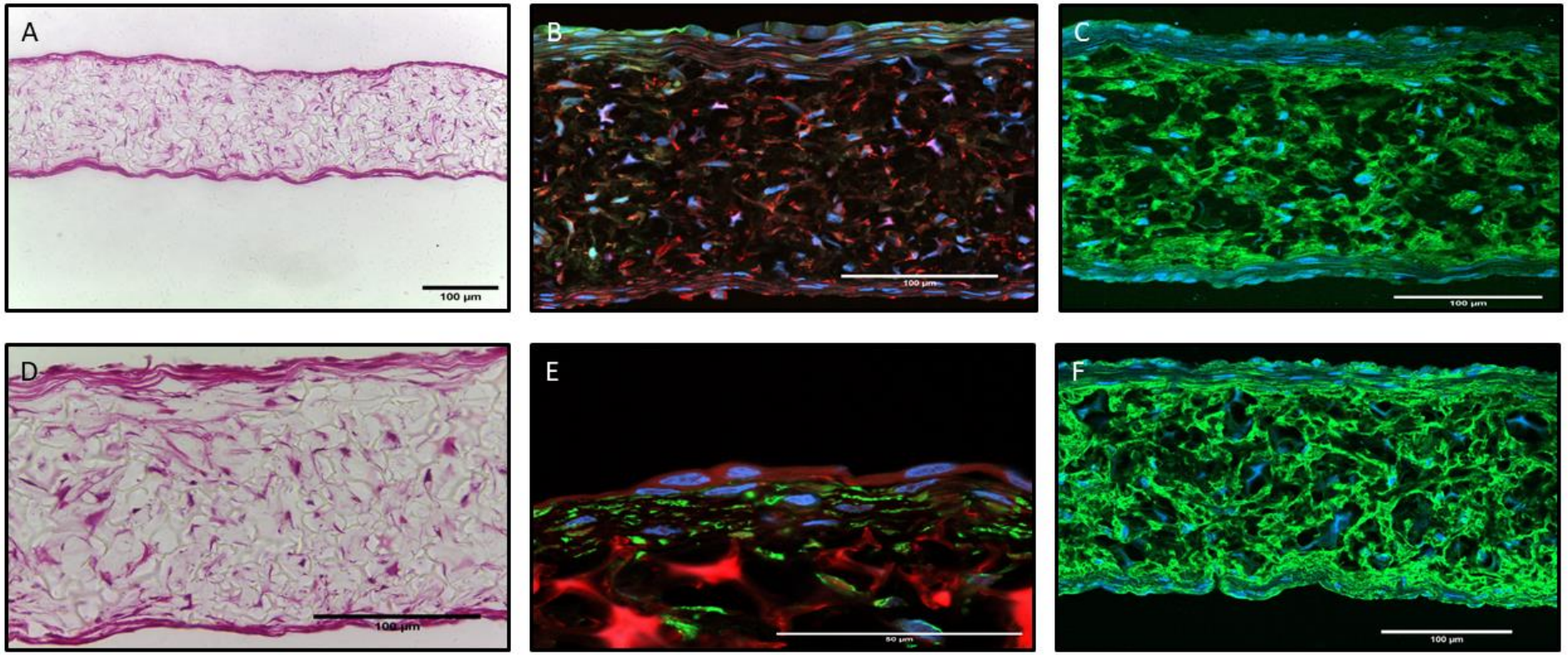

Figure 35: Characterisation of the pME cells seeded onto a MF-derived stromal compartment in Alvetex® Scaffold. A) x20 H&E image of the pME Full Thickness Model. B) Immunostained image of the MCF-10A Full Thickness Model for Cytokeratin 8(Green) and Vimentin (Red), with nuclei stained blue using Hoerscht. C) x20 Immunostained image of the pME Full Thickness Model for Collagen 1 (Green), with nuclei stained blue using Hoerscht. D) x63 Immunostained image of the pME Full Thickness Model Cytokeratin 8 (Green) and Vimentin (Red), with nuclei stained blue using Hoerscht. F) Immunostained image of the pME Full Thickness Model for Collagen IV (Green), with nuclei stained blue using Hoersch

7. Discussion

The lack of understanding of the molecular mechanisms driving breast cancer cell invasion, and how these are coupled with interactions with microenvironmental components, is a major driver in the problems associated with breast cancer treatment, including: poor prognosis; over-diagnosis; over-treatment; and the varying effectiveness of treatment options. The models generated in this thesis start to address this lack of understanding, whereby the models allow the investigation of invasion characteristics in systems that account for 3D microenvironments of varying complexity and physiological relevance. Specifically, the Alvetex® Strata models provide a mono-culture platform that incorporates a simple 3D growth environment to investigate this variable on breast cancer cell invasion. The Alvetex® Scaffold models then build on this, incorporating higher degrees of physiological relevance through the generation of an *in vivo*-like stromal compartment, via co-culture with fibroblasts, and how this interacts with, and drives, breast cancer cell invasion.

Overall, it is evident that the invasion capabilities and morphological features displayed vary and change across the different model platforms as further complexity is introduced. In turn, these morphological and invasion characteristics can not only be compared between the model platforms investigated in this thesis, but their ability to recapitulate *in vivo*-like characteristics can be assessed through comparison with primary patient samples sourced from the literature. This contextualisation can then be taken further, in which the specific uses of these models when compared to other 3D modelling technologies can be assessed. These novel Alvetex® models, both Strata and Scaffold, could act as powerful, highly modular tools that could revolutionise drug development pipelines, personalised medicine, and our understanding of proteolytic dependant and independent invasion mechanisms in a system that better incorporates microenvironment characteristics.

7.1. In 2D Breast Cancer Cell Lines Show Graded Invasion that is Consistent with the Literature

When comparing the invasive potential of each cell line in 2D scratch assays, a graded invasion pattern was seen across the cell lines. In particular, as the modelled developmental timepoint increased, from Healthy to DCIS to IDC, the % scratch closure of each cell line increased (Figure 13 and Figure 14). When considering the invasion characteristics of healthy mammary tissue, the epithelial cells composing the ductal compartment are held in low migratory states to remain within their boundaries during tissue homeostasis [64], [103]. Then once a wound or break of the epithelial monolayer occurs, the cells initiate migratory signalling pathways that allow them to migrate as a collective and close the wound [65], [67], [104]. The MCF-10A cell line, in 2D, display this low migratory phenotype, as shown by the smallest % scratch closure metric. The clumping of MCF-10A cell following the scratch may be some remnant of the wound healing response pathway mentioned previously [104]. This, in conjunction with the migratory behaviour of the MCF-10A cell line, shows that this cell line is retaining some remnants of physiological behaviour when cultured as part of this conventional 2D invasion platform.

This retention of some physiological behaviour is also observed in the MCF-7 cell lines. When considering the invasion characteristics of DCIS, the breast cancer cells have their invasion confined to the ductal space, while maintaining epithelial phenotypes [10], [105]. The MCF-7 cells not only maintained epithelial phenotypes, as shown through CK8+/Vimentin- immunostaining (Figure 12), but they also showed increased % scratch closure when compared to the MCF-10A cells, indicating a higher migratory phenotype. This increase in migratory capabilities is as expected when comparing healthy mammary tissue to DCIS lesions [10], [105], [106].

The MDA-MB-231 cell line also showed some reflection of *in vivo* migratory behaviours in 2D. *In vivo*, as DCIS lesions progress to IDC lesions, the cells adopt mesenchymal phenotypes that promote cell motility and invasion. The MDA-MB-231 cell line matched a mesenchymal profile, whereby the cells adopted spindle-like morphologies in phase contrast and showed CK8-/Vimentin+ immunostaining (Figure

12). This adoption of mesenchymal migratory phenotypes was further supported by the % scratch closed by this cell line, where it had the highest migratory potential.

This trend in invasion capabilities between these immortalised cell lines is highly observed in the literature ([107]–[111]). This alignment with results from the literature generates confidence twofold. First, that the cell line batches used in this thesis are behaving as expected, in a consistent and comparable manner to the literature. This in turn, creates a baseline set of reliable results that can be used to analyse the effectiveness of the novel *in vitro* models developed during this thesis. Second, this alignment and reflection of characteristics of the literature reinforces the selection of each cell line to model its respective developmental timepoint of breast cancer.

7.1.1. Physiological Relevance is Limited in 2D.

Although we are observing differential invasion between the mammary cell lines and the presence of key similarities of invasion and morphological characteristics with their *in vivo* counterparts, there are limitations to the 2D model platform. For example, scratch assays force the cells to form abnormal adhesions to the 2D plasticware which in turn forces unnatural polarisation of the cells, gene expression profiles, cell morphologies, and growth behaviours [112]. Furthermore, this planar growth across the surface of 2D plasticware means all cells have access to 100% nutrient and oxygen supplies in the media. Both of these factors are not observed *in vivo,* where 3D structures restrict nutrient availability and waste accumulation, but they also form adhesions on all surfaces. Thus, the next logical step for model development was to better recapitulate *in vivo* growth spaces and investigate the addition of a 3D growth environment on cell line invasion characteristics and morphology, and how this compares to the cells' behaviour when grown on 2D platforms and their representation of *in vivo* counterparts.

7.2. The introduction of a basic 3D growth environment by Alvetex Strata maintained invasion characteristics of cell lines while enforcing new *in vivo-like* characteristics.

While a 3D environment is pertinent to increasing physiological relevance, it is important to consider the 3D structures of *in vivo* mammary tissue. For example, when analysing the growth and invasion characteristics of breast cancer pathologies, medical practitioners utilise boundaries to determine staging and diagnosis of breast cancers [5], [29], [40]. For example, DCIS lesions and their growth is highly confined to the epithelial compartment, while IDC lesions extend past the epithelial tissue boundaries and into the underlying mesenchymal compartment. This functional compartmentalisation of epithelial and mesenchymal areas of growth plays a substantial role in tumour development and is not accounted for in 2D scratch assays. Alvetex® Strata can start to mimic these 3D *in vivo* compartments. Specifically, the pore size of Alvetex® Strata is small enough to prevent cells passively falling through the membrane, but large enough to allow any penetration to be the result of active migration. Thus, the porosity of Alvetex® Strata allows the membrane to physically compartmentalise the model by acting as a synthetic basement membrane, separating the epithelial compartment (the surface of the Alvetex® Strata), from the stromal compartment (the interior growth space of Alvetex® Strata).

The introduction of a physically compartmentalised 3D growth environment, in the form of cell culture on Alvetex® Strata, had a distinct effect on the cell morphologies and invasion characteristics of all three cell lines. Similar to the 2D scratch assays, the MCF-10A, MCF-7, and MDA-MB-231 cell lines showed differential invasion characteristics that were graded in the same way as the 2D scratch assays (Figure 15 and Figure 18). Specifically with the MDA-MB-231 cells invading the most into the Strata scaffold, the MCF-7's as an intermediate, and the MCF-10A invading the least. Despite this similar grading of invasion characteristics between cell lines, it is evident that the introduction of the physically compartmentalised 3D growth environment by Alvetex® Strata led to the adoption of improved *in vivo*-like characteristics when compared to *in vivo* samples and the 2D scratch assays. For

example, the MCF-7 cells formed a multi-layered layer on the surface of the Alvetex® Strata with minimal invasion into the Alvetex® Strata membrane, while in 2D the cells were confined to a monolayer cobblestone morphology across the surface of the flask (Figure 15 and Figure 20). This layering on the surface of the Alvetex® Strata starts to mimic one of the key characteristics of DCIS lesions, whereby breast cancer cells in this cancer type are confined to and proliferate in the epithelial compartment and form disorganised multi-layered cell structures as shown in Figure 36.

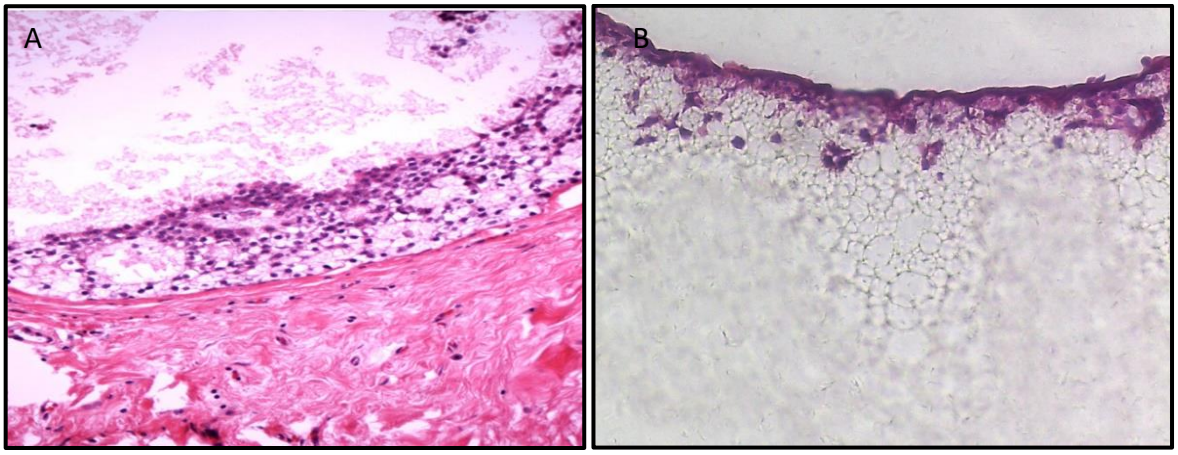

Figure 36: A) Ductal carcinoma in situ *with clear cell features. Magnification, ×20. Figure adopted from Sonati, 2019.* [106]. *B) Growth of the MCF-7 Cell Lines on Alvetex® Strata for 14 days x20 magnification.*

This acquisition of improved *in vivo* -like characteristics is also shown by the MDA-MB-231 cell lines when grown in Alvetex® Strata. In this set of models, the cells showed dispersed growth and high invasion throughout the Alvetex® Strata membrane (Figure 15 and Figure 21). This dispersed growth is highly observed in IDC lesions, where breast cancer cells penetrate throughout the epithelial and stromal compartments in a single cell manner (Figure 37) [52], [105], [106].

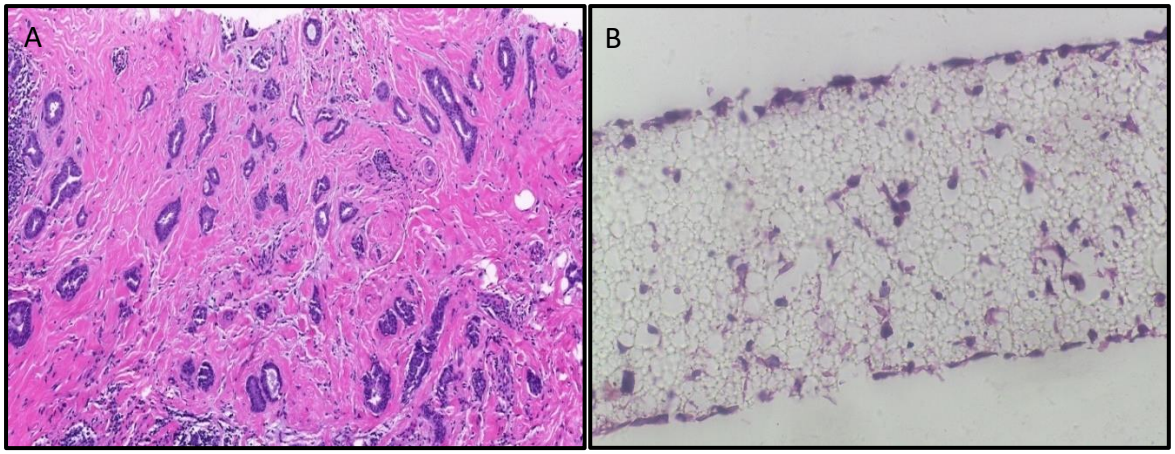

Figure 37: A) Invasive Ductal Carcinoma with *clear cell features. Magnification, ×20. Figure adopted from PathologyOutlines* [113] *B) Growth of the MDA-MB-231 Cell Lines on Alvetex® Strata for 14 days x20 magnification.*

The MCF-10A models also show improved *in vivo*-like characteristics, whereby the cells form monolayers across the epithelial compartment growth zone (Figure 15, Figure 16, and Figure 19). This formation of a monolayer during early growth timepoints (4 days) is highly representative of healthy mammary tissue structures seen *in vivo* (Figure 38).

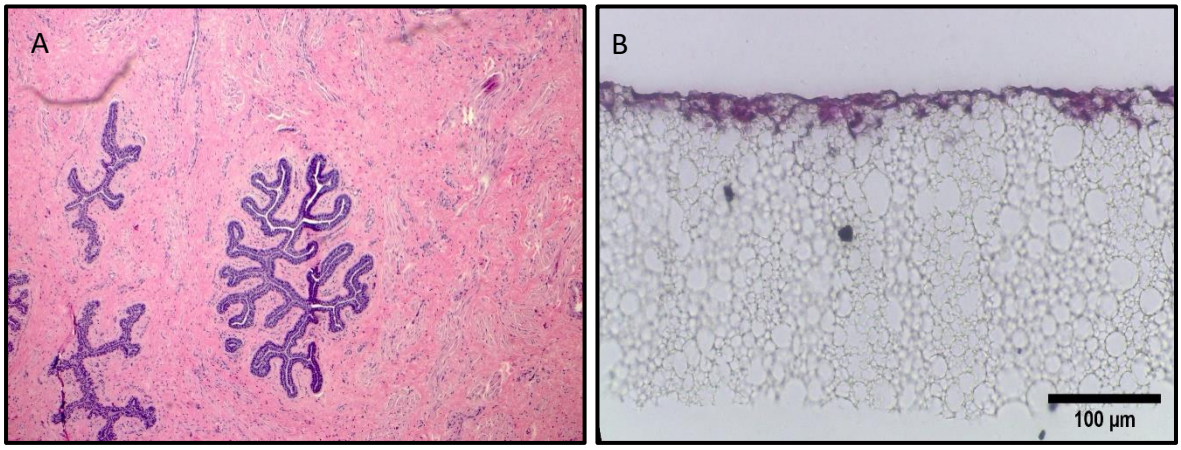

Figure 38: A) Histology section of healthy mammary ductal Magnification, ×20. Figure adopted from PathologyOutlines [113] *B) Growth of the MCF-10A Cell Lines on Alvetex® Strata for 4 days x20 magnification.*

7.2.1. Limitations of the Alvetex® Strata Models

Despite this adoption of improved *in vivo*-like characteristics by the each of the mammary cell lines, the highly proliferative nature of the MCF-10A cell line shows a key limitation of the Alvetex® Strata Models: migration cannot be easily decoupled from proliferation. Although a monolayer is observed across the surface of the Alvetex® Strata membrane, it is evident that as the period of growth increases,

underlying growth into the interior of the membrane is observed. Decoupling of proliferation and migration in this model was attempted through the treatment with Mitomycin C, a proliferation inhibitor, following cell adhesion to the Alvetex® Strata membrane. However, this often led to the formation of models that were either not viable or contained low populations of cells. This could be overcome through further experiments to optimise the use of Mitomycin C with the Strata models might be required. For example, experiments could be designed to test a concentration gradient of mitomycin C, or alternatively the best cell seeding number for use in these migration models.

Despite the incompatibility with Mitomycin C, it has been found *in vivo* that proliferation is tightly coupled to migratory events, whereby switching from a low migratory and proliferative state to a high migratory and proliferative state does play a key role during key migratory processes such as wound healing and tumour invasion ([114], [115]*)*. However, the ability to decouple these events means migration-specific mechanisms can be investigated more easily.

In addition to the inability to decouple proliferation and migration in these models, the physical compartmentalisation and internal microenvironment created in this model type lacks physiological accuracy. For example, the basement membrane mimicked by Alvetex® Strata is a homogenous synthetic material, *in vivo* the basement membrane is composed of a heterogenous mix of collagenous and non-collagenous proteoglycans and glycoproteins, all of which form distinct cell adhesions that signal and modulate cell morphology and invasion characteristics [116], [117]. Furthermore, the stromal compartment of the Alvetex® Strata membrane also lacks physiological relevance. Specifically, the compartment lacks complex features observed *in vivo,* such as fibroblasts, which are key signalling components of tissue homeostasis and cancer development ([63]), and collagenous and non-collagenous ECM components such as collagens I, III, IV, fibronectin, and laminins [65], [66]. Thus, the next logical step in model development is to introduce these components into the 3D breast cancer invasion models, in order to increase physiological relevance of the novel invasion models developed in this thesis.

7.3. The introduction of physiologically relevant microenvironment constituents led to adoption of highly representative *in vivo* characteristics.

A widely accepted problem in the literature when recapitulating the tumour microenvironment and its constituents, is the physiological accuracy and reproducibility when supplementing models with ECM components. In terms of physiological accuracy, it is practically difficult for researchers to deposit ECM components (Collagens, Fibronectin, Laminins, etc), and their isoforms, in the proportions that are found *in vivo* [66], [87], [118]. This is further complexed by differences in ECM densities and proportions found across a tissue, and between tissue types [87], [117], [118]. Furthermore, even when these constituents are deposited, the reproducibility of these systems is hindered because of the large batch-batch variability present in exogenous ECM components [119].

These problems of supplementation and reproducibility of ECM components have been shown to be overcome through the culture of Human Derived Neonatal Fibroblasts (HDFn's) in the Alvetex® Scaffold cell culture platform [100], [120]. These stromal compartments also benefit from the presence of fibroblasts spread throughout the inside of the membrane, in a similar way to that of fibroblasts found *in vivo,* which means the deposited ECM can be actively remodelled and maintained throughout cell culture [99], [121], [122]. Following the derivation of these stromal compartments, epithelial cells can be seeded on top to create a compartmentalised model that builds on the principles of the Alvetex® Strata invasion models.

In a similar way to the Alvetex® Strata models, the Alvetex® Scaffold models are split into two functional zones: The surface of the Alvetex® Scaffold acts as the epithelial compartment; while the interior of the Alvetex® Scaffold model acts as the stromal compartment, which now contains both physiologically relevant ECM components that are deposited in *in vivo*-like proportions and fibroblasts that can actively signal with the epithelial compartment to modulate cell behaviour [100], [120], [121].

The seeding of the immortalised cell lines onto these Alvetex® Scaffold HDFn-derived stromal compartments, led to the acquisition of highly representative *in vivo* morphological and invasion characteristics.

7.3.1. MCF-10A cells seeded onto HDFn-derived stromal compartments displayed key features of Healthy Mammary Tissue.

Seeding of MCF-10A cells onto the HDFn-derived stromal compartments led to the acquisition of enhanced morphological and invasion characteristics. For example, when considering healthy mammary ductal tissue (Figure 38), the epithelial cells are monolayered across the duct, a key feature for its function as an apocrine tissue, and this is recapitulated in the MCF-10A Alvetex® Scaffold model [1], [75], [123]. Specifically, the MCF-10A cells form a consistent monolayer across the surface of the HDFn-derived stromal compartment. This structural similarity is then reinforced by recapitulating the invasive behaviour of healthy mammary tissue, where there is minimal invasion of MCF-10A epithelial cells into the stromal compartment, forming clear epithelial and stromal boundaries (Figure 26) [1], [123]. Immunostaining confirmed the compartmentalisation of the model (Figure 23) with confinement of the MCF-10A cells to the epithelial compartment (the surface of the Alvetex® Scaffold).

This non-invasive behaviour is also observed consistently in the literature. For example, in a study by Guzman *et al.,* the MCF-10A cells did not breach into the basement membrane and associated compartments created in the study [124]. However, the morphologies exhibited by the MCF-10A cells were significantly different to those found in the literature, whereby the MCF-10A cells in 3D culture tended to form cuboidal epithelial structures[75], [124]. This likely is a result of the use of cholera toxin in the culturing media of these experiments, which initiates the accumulation of cAMP and acquisition of epithelial phenotypes, a component that was missing from the culturing media in this thesis due to safety and availability restrictions. Overall, the MCF-10A Alvetex® Scaffold model is highly representative of the invasion characteristics and morphological features of healthy mammary tissue, while also aligning with the associated invasion data and models found in the

literature. However future studies should incorporate the use of cholera toxin with this cell line to enhance epithelial phenotypes.

7.3.2. MCF-7 cells seeded onto HDFn-derived stromal compartments displayed enhanced DCIS features.

As mentioned previously DCIS lesions have their tumour cells retain epithelial phenotypes and have their invasion confined to the epithelial compartment [10], [51], [52], [106]. Morphologically, when seeded onto the HDFn-derived stromal compartments, the MCF-7 cells adopt enhanced characteristics of DCIS lesions. For example, while their growth is confined to the epithelial compartment (Figure 24), the cells do not form a monolayer across the surface of the model. Instead, they start to stack and form multi-layered structures that are reminiscent of tumour cells *in vivo* (Figure 36*)*. Furthermore, expression of CK8+/Vimentin- shows that the MCF-7 cells have retained their epithelial phenotype when cultured in this compartmentalised model, which is a characteristic highly reflected in DCIS lesions.

These observed morphological characteristics also align with those found in the literature. For example, a study by Vantangoli *et al.,* investigated the use of hydrogels to generate MCF-7-derived microtissues [88]. The microtissues derived in this study show identical multi-layered structures and marker expression as the MCF-7 cells seeded onto the HDFn-derived stromal compartments. A similar trend is observed in a study by Yakavets *et al.,* whereby MCF-7 cells were co-cultured with MCR5 fibroblast cells to generate physiologically relevant organoids for the use in fibrosis investigations during breast cancer development [125]. The organoids showed similar MCF-7 morphologies, ECM component distributions, and compartmentalisation observed in the MCF-7 Alvetex® scaffold models [125].

In addition to physiologically relevant morphological features, the MCF-7 model also adopts highly relevant invasion characteristics. When we analyse the Alvetex® Strata models it can be seen that while cell invasion into the membrane is limited, the cells do migrate past the basement membrane substitute of the Alvetex® Strata as the only blocking factor is pore size. However, when observing the Alvetex® Scaffold models, the cells invasion is fully confined to the epithelial compartment (Figure 24 and Figure 26). Overall, the MCF-7 Alvetex® Scaffold model displays

highly representative invasion and morphological features observed in DCIS lesions. These invasion properties are also supported in the literature, namely the study by Yakavets *et al.,* mentioned previously, whereby the MCF-7 cells showed little invasive capacity and clear compartmentalisation away from the fibroblast containing compartment.

7.3.3. The deposition of an ECM physically blocked cell migration in the MCF-7 and MCF-10A models, but not in the MDA-MB-231 model

Both the MCF-10A and MCF-7 models, representing healthy and DCIS tissue respectively, showed limited invasion into the Alvetex® Scaffold. Surveying of the literature showed that ECM components and the basement membrane are able to physically block tumour cells from invading into the stromal compartment [126]. It is only when tumour cells acquire a migratory, metastatic phenotype that they are able to undertake proteolytic degradation, typically through the secretion of Matrix metallopeptidase's (MMP's), and associated migration away from the primary tumour site [53], [65], [67]. When cancer cells are in the pre-metastatic phase of development, they must instead rely on proteolytic independent migration, and instead deform and move through the native pores created by the ECM and basement membrane, however these ECM pores are often too small to allow this kind of migration [53], [65], [67], [126].

Collagen IV is a major constituent of the basement membrane and is degraded by MMP-2 and MMP-9 during proteolytic dependent tumour invasion. Figure 24 and Figure 23 show marked expression of Collagen IV in both the MCF-7 and MCF-10A Alvetex® Scaffold models [126]. Surveying of the literature then showed that both cell lines lack expression of MMP-2 and MMP-9 [127], [128]. It could be speculated that this lack of expression in both cell lines means that they are unable to degrade the underlying collagens and a prevented from invading into the stromal compartment, potentially explaining the invasion results shown in Figure 26. However, additional analyses would be needed to ascertain the MMP statuses of the cells in the Alvetex® Scaffold models.

However, when analysing the Alvetex® Scaffold MDA-MB-231 models, the invasion characteristics of the cell line are maintained across the different platforms developed and investigated in this thesis. The literature shows that this cell line highly expresses a broad range of MMP's, allowing the cell line to degrade collagens in the underlying stromal compartment and invade [129]. It could be speculated that these proteolytic mechanisms exhibited by the MDA-MB-231 cell line explain their maintained invasive potential when compared to the MCF-10A and MCF-7 models (Figure 26). This, in part, is supported by the lower density of collagens in the MDA-MB-231 models when compared to the MCF-7 and MCF-10A models (Figure 24, Figure 25, Figure 23).

7.3.4. MDA-MB-231 cells seeded onto HDFn-derived stromal compartments display enhanced IDC features

This ability to invade through ECM constituents is a key characteristic of IDC lesions, where tumour cells are able to migrate past tissue compartments to sites distinct from the primary tumour site. This enhanced invasion characteristic observed in the MDA-MB-231 cells compared to the MCF-7 cells aligns with data in the literature, whereby MDA-MB-231 cells consistently migrate further into 3D matrixes [130], [131].

Furthermore, the data presented in this thesis starts to show how the Alvetex® Scaffold IDC models are acquiring enhanced IDC features. In particular through the display of mesenchymal phenotypes by the MDA-MB-231 cells, as shown through CK8-/Vimentin+ immunostaining, which is a hallmark of IDC lesions [105], [113], [132]. This adoption of elongated mesenchymal phenotypes is also consistently observed in the literature [133], [134].Overall, the MDA-MB-231 Alvetex® Scaffold model is highly representative of the invasion characteristics and morphological features of IDC lesions.

7.3.5. The Compatibility of the CAPE inhibitor with the Alvetex® models.

The CAPE inhibitor has been extensively investigated in 2D cancer cell systems to ascertain the anti-tumour and anti-migratory properties of propolis, a substance

obtained through extraction from honeybee hives [135]. The molecule has been shown across the literature to inhibit the migratory capabilities of MCF-7 and MDA-MB-231 cells during scratch and wound healing assays in 2D, concurrently aligning with the scratch assay results shown in Figure 13 and Figure 14 [77], [136], [137]. CAPE's use in 3D model systems has been shown in select adenocarcinoma spheroid systems, however its use in 3D has been limited and not widely applied to breast cancer systems [138]. This provided ample opportunity to not only show the compatibility of the Alvetex® models created in this thesis with anti-migratory compounds, but also the models' compatibility with novel compounds.

The anti-migratory effect of CAPE was maintained when treating all 3D models, both Strata and Scaffold derived, with the inhibitor. This shows the intrinsic compatibility of the Alvetex® models developed in this thesis with drug compounds, whereby the Alvetex® models can act as tuneable systems that can allow the investigation of breast cancer invasion in models that can account for 3D microenvironments of varying complexity.

However, the data generated in this thesis showed an increase in sensitivity to CAPE when moving from a 2D to a 3D platform. This is contradictory to trends seen in literature, where often increases in model complexity of breast cancer *in vitro* models (creation of spheroid structures, incorporation into hydrogels, 3D co-culture) tends to lead to increases in resistance, and decreases in sensitivity, of breast cancer cells treated with anti-migratory drugs [139], [140]. It could be that this increase in sensitivity could be a result of the timeframe in which treatment with CAPE was applied. Specifically, CAPE interacts with and inhibits NF-κB, a cell adhesion regulator, it may be that treatment with CAPE occurred too soon after cell seeding, hampering their ability to adhere to the models, thereby reducing cell number in a form that mimicked increased sensitivity [141]. Further optimisation experiments will be required to confirm and potentially overcome this problem.

7.3.6. Overcoming key limitations of the Alvetex® Scaffold model.

Overall, it is evident that as model complexity increased between the conventional 2D platform, Alvetex® Strata, and Alvetex® Scaffold, the models better reflected their *in vivo* counterparts in terms of cell morphology and invasion characteristics. However, the Alvetex® Scaffold models generated in this thesis do possess specific limitations when being utilised to investigate breast cancer cell invasion.

Across the literature it is evident that fibroblasts deposit and remodel ECM's in a tissue dependent manner; whereby skin fibroblasts will manufacture and maintain differently composed ECM's to mammary tissue [99], [122], [126]. The Alvetex® Scaffold models generated in this thesis all utilised dermal fibroblasts when trying to recapitulate breast cancer cell invasion. While the HDFn's provided a highly proliferative and metabolically active population of fibroblasts that deposited reproducible and consistent *in* vivo-like stromal compartments, the physiological accuracy of these models is limited. Thus, to overcome this, the HDFn cells were replaced with adult primary mammary fibroblasts.

The mammary fibroblasts produced comparable stromal compartments that showed deposition of key ECM components such as Collagens I and IV, and fibronectin, all of which are components found in *in vivo* mammary tissue samples [142]. Furthermore, when seeded with immortalised cell lines the models were viable and produced enhanced physiological characteristics that are highly similar to the ones elicited by the HDFn-based models.

Another key limitation of the Alvetex® Scaffold models produced for investigating invasion in this thesis, is the use of immortalised cell lines. Immortalised cell lines have large benefits when considering their intrinsic reproducibility and consistent characteristics, however they do often show limited characteristics of their primary *in vivo* counterparts, partially limiting the conclusions that can be made when utilising them [143], [144]. Thus, it was important to demonstrate the compatibility of the Alvetex® Scaffold models with primary healthy epithelial cells. Not only did the cells produce viable models on both types of stromal compartment, highlighting the high

modularity of the Alvetex® Scaffold models produced in this thesis, but their characteristics differed between them. For example, when cultured on the HDFn stromal compartment, the primary cells produced a more cuboidal epithelial shape (typical of mammary ductal tissue), while when cultured on the mammary fibroblast stromal compartment they elongated and flattened across the surface of the model in a similar way to the MCF-10A models. It could be that the neonatal origins of the HDFn cell population led to a stronger modulatory effects by the cells, however this would need to be investigated further [145].

Overall, the incorporation of primary mammary fibroblast and epithelial cell populations within the Alvetex® Scaffold models show the intrinsic modularity of this platform. A characteristic that is often missing from comparable 3D models found in the literature and limits their investigative power.

7.3.7. Advantages and Potential Uses of Alvetex® Strata derived Breast Cancer Invasion Models

When analysing the Alvetex® Strata models, a major advantage is the relative simplicity of this model compared to other 3D invasion models. The Alvetex® Strata models utilise monoculture regimens on an inert growth substrate, meaning that any observed results are likely to be a direct result of the cell line incorporated into this novel invasion platform and the effect of 3D geometric space, and not a result of anomalous interactions generated from biologically reactive growth substrates, as has been found in some hydrogel and bioprinting techniques [87], [146], [147].

This lack of supplementation of ECM components, combined with the small pore sizes present in Alvetex® Strata platform, makes this model platform an ideal candidate for investigating proteolytic independent migration mechanisms that occur in breast cancer. These mechanisms play a key role in single cell metastasis and are often overlooked in 3D invasion models. This paired with the compatibility of the platform with the CAPE inhibitor mentioned previously, shows that these models are tuneable and could be utilised in drug discovery pipelines that target these processes.

In addition to this, these models are not confined to investigation of proteolytic independent migration, they could also incorporate into the early stages of drug development pipelines as an alternative to 2D invasion assays. Where their ability to account for 3D growth in a technically simple mono-culture regimen could provide better predictive accuracy than conventional 2D invasion assays during the early stages of drug development.

7.3.8. Advantages and Potential Uses of Alvetex® Scaffold derived Breast Cancer Invasion Models

It is highly evident that the Alvetex® Scaffold models have large advantages over the Alvetex® Strata models and conventional 2D invasion assays developed and investigated in this thesis, where they promote the adoption of enhanced *in vivo* characteristics. These advantages also extend across to 3D invasion models present in the literature. For example, the utilisation of fibroblast seeding regimens allows the formation of reproducible and physiologically relevant stromal compartments and microenvironments that contain ECM components in their *in vivo* compositions. This allows the Alvetex® Scaffold models to generate a more holistic investigation into breast cancer cell invasion, one that incorporates microenvironment interactions and signalling from fibroblasts, both of which have been found to be critical in tumour development and metastasis.

This ability of the Alvetex® Scaffold models to generate a more holistic view of breast cancer invasion, is a major advantage of the platform over other 3D technologies found in the literature. For example, when considering hydrogel models, they are often unable to account for the wide range of ECM components found *in vivo*. Often these hydrogel-based models only focus on recapitulating the presence of one major class of ECM component: Collagens [78], [148], Fibronectins [149], Laminins [150], etc. The Alvetex® Scaffold models generated in this thesis are able to replicate the complexity of the mammary tissue microenvironment, where it accounts for multiple ECM components including: Collagen I, Collagen IV, and Fibronectin (Figure 23, Figure 24, Figure 25).

Furthermore, when considering breast cancer spheroid systems, the Alvetex® Scaffold models generated in this thesis are able to better replicate the compartmentalisation observed *in vivo.* For example, many co-culture spheroid models can achieve functional compartmentalisation and create stromal (interior of the spheroid) and epithelial (exterior of the spheroid) compartments. However, the nature of the spheroid structures formed, forces contact between cell types and creates a stromal compartment through dense packing of fibroblast cells [125]. This is not representative of the structures found *in vivo,* where often fibroblasts are interspersed throughout the stromal compartment and signal through both cell-cell contact and paracrine signalling [151], [152]. The models generated in this thesis are thus able to account for both of these signalling types, where fibroblasts are observed throughout the Alvetex® membranes and in contact with the seeded epithelial cells, in a way that aligns with the structures observed *in vivo* (Figure 23, Figure 24, Figure 25).

Given its intrinsic advantages, an Alvetex®-based breast cancer invasion model could have various applications in a clinical context. For example, the ability for Alvetex®-based epithelial models to build both a dermal and epidermal compartment means that an Alvetex® based-breast model could be used to answer biological questions about breast cancer tumour progression. Specifically, these models will take better account for the tumour microenvironment and could be used to better understand how the tumour microenvironment drives metastasis and migration. For example, the models could allow enhanced investigations into the proteolytic mechanisms that drive breast cancer metastasis and invasion.

Furthermore, the compatibility of the Alvetex® scaffold platform with the CAPE inhibitor and 96-well formats mean that these *in vitro* models could be used as part of high throughput screening (HTS) protocols. Specifically, it could be that the generation of reproducible and physiologically relevant ER/PR, HER2, and triple negative breast cancer Alvetex® models (using primary or immortalised cell lines) could be used by pharmaceutical companies in drug discovery and development for invasion specific drugs. Whereby, the potential increased physiological relevance of these models could provide better predicative outcomes for drugs being screened for treatment of various breast cancer phenotypes.

The clinical utilities of an Alvetex® scaffold breast cancer invasion model is not just restricted to HTS drug screening protocols, the modular compatibility of these models with primary cells could also be used within a personalised medicine context. Whereby patient biopsies could be incorporated into the models and allowed to develop to give an idea of prognosis and invasive capacity of the primary tumour. This could also be taken a step further whereby patient primary cells, as part of a Alvetex® Scaffold model, could be exposed to potential treatment options to see which option would be the most effective against the patient's specific cancer cells. As breast cancer is such a highly heterogenous disease, this is the next crucial step towards improving patient quality of life, and in particular improving mortality statistics surrounding breast cancer.

7.3.9. Future Directions

This thesis shows the development of reproducible and physiologically relevant breast cancer invasion models of varying complexity that have large potential for investigating biological questions surrounding breast cancer development and metastasis.

7.3.10. Alvetex® Strata Models: Modelling Metastasis of Complex Tumour Structures.

The Alvetex® Strata models generated in this thesis have the potential to be developed further. In this study, the models were seeded using single cell suspensions, future work could investigate incorporation of spheroids with this scaffold technology. Whereby, seeding of a spheroid collection of breast cancer cells, mimicking a tumour structure, onto the scaffold could be carried out to investigate how tumours disseminate their cells during metastasis.

7.3.11. Alvetex® Scaffold Models: Increasing Complexity and Physiological Relevance to Better Model Tumour Microenvironments.

Future work on the Alvetex® Scaffold models could be centred onto three main routes. The first is the incorporation of cancer-associated fibroblasts (CAFs), to these models and how these cells effect invasion properties of mammary epithelial cells of varying diseased states [63]. Alternatively, future work could be centred on the investigation of proteolytic dependent invasion mechanisms by breast cancer cells. For example, future work could investigate the role of MMP's on ECM remodelling during different stages of breast cancer [127]–[129]. Finally, much-like in the future directions section for the Alvetex® Strata models, spheroids could be incorporated into the Alvetex® Scaffold healthy models to better recapitulate tumour structures, and to investigate how breast cancer tumours remodel healthy tissue and disseminate cells away from the primary tumour site in a model that highly recapitulates the tumour microenvironment.

Overall, the novel invasion models developed in this thesis have the potential to advance our understanding of metastatic processes driving breast cancer development in a modular, highly reproducible way, that accounts for 3D growth and tumour microenvironments.

8. Conclusion

In this thesis three immortalised cell lines MCF-10A, MCF-7, MDA-MB-213, were chosen to mimic the pathological timepoints of breast cancer development: Healthy Tissue, DCIS, and IDC respectively. Each cell line's ability to recapitulate these timepoints, whereby invasive capacity increases with pathological development, was tested using 2D cell culture techniques and invasion assays. Once assessed against the literature and in-house 2D results, it was investigated how Alvetex® platforms (Alvetex® Strata and Alvetex® Scaffold) could be used in conjunction with these cell lines to create novel 3D invasion models of increasing physiological relevance. First, the impact on cell lines invasion characteristics in response to the inclusion of a 3D geometric growth space was investigated by growing the cell lines as a mono-culture regimen in Alvetex® Strata. This was then taken further by incorporating a

physiologically relevant stromal compartment into the 3D growth space through the growth of fibroblasts in Alvetex® Scaffold. Once this compartment had matured, the immortalised epithelial cell lines were seeded on top to create Alvetex® Scaffold co-culture breast mucosal models. Once optimised, the invasion characteristics of the Alvetex® Scaffold co-culture models were assessed, and their physiological relevance increased through the incorporation of primary mammary epithelial and fibroblast cells. Following the development of the Alvetex®-based models, the effectiveness of the models as an invasion assay was compared against conventional 2D invasion assays and each other through treatment with a known migration inhibitor. Overall, this thesis demonstrates the creation of highly modular, novel Alvetex® breast cancer models that can effectively recapitulate the tumour microenvironment to varying degrees of complexity, inducing highly relevant tumour characteristics. The compatibility of these models with migration inhibitors, starts to demonstrate their potential versatility to a clinical environment, whereby they could revolutionise our understanding of breast cancer invasion mechanisms and how these are modulated by the tumour microenvironment.

9. References

[1] Y. Feng *et al.*, “Breast cancer development and progression: Risk factors, cancer stem cells, signaling pathways, genomics, and molecular pathogenesis,” *Genes Dis.*, vol. 5, no. 2, pp. 77–106, May 2018, doi: 10.1016/j.gendis.2018.05.001.

[2] L. Iacoviello, M. Bonaccio, G. de Gaetano, and M. B. Donati, “Epidemiology of breast cancer, a paradigm of the ‘common soil’ hypothesis.,” *Semin. Cancer Biol.*, vol. 72, pp. 4–10, Jul. 2021, doi: 10.1016/j.semcancer.2020.02.010.

[3] S. Loibl, P. Poortmans, M. Morrow, C. Denkert, and G. Curigliano, “Breast cancer,” *Lancet*, vol. 397, no. 10286, pp. 1750–1769, 2021, doi: https://doi.org/10.1016/S0140-6736(20)32381-3.

[4] H. Sung *et al.*, “Global Cancer Statistics 2020: GLOBOCAN Estimates of Incidence and Mortality Worldwide for 36 Cancers in 185 Countries.,” *CA. Cancer J. Clin.*, vol. 71, no. 3, pp. 209–249, May 2021, doi: 10.3322/caac.21660.

[5] S. Łukasiewicz, M. Czeczelewski, A. Forma, J. Baj, R. Sitarz, and A. Stanisławek, “Breast Cancer-Epidemiology, Risk Factors, Classification, Prognostic Markers, and Current Treatment Strategies-An Updated Review.,” *Cancers (Basel).*, vol. 13, no. 17, Aug. 2021, doi: 10.3390/cancers13174287.

[6] A. Hennigs *et al.*, “Prognosis of breast cancer molecular subtypes in routine clinical care: A large prospective cohort study,” *BMC Cancer*, vol. 16, no. 1, pp. 1–9, 2016, doi: 10.1186/s12885-016-2766-3.

[7] F. M. Alkabban and T. Ferguson, “Breast Cancer,” in *StatPearls [Internet]*, Treasure Island (FL): StatPearls Publishing, 2021.

[8] M. I. Nounou, F. ElAmrawy, N. Ahmed, K. Abdelraouf, S. Goda, and H. Syed-Sha-Qhattal, “Breast Cancer: Conventional Diagnosis and Treatment Modalities and Recent Patents and Technologies,” *Breast Cancer (Auckl).*, vol. 9, no. Suppl 2, pp. 17–34, Sep. 2015, doi: 10.4137/BCBCR.S29420.

[9] H. Y. Wen and E. Brogi, “Lobular Carcinoma In Situ.,” *Surg. Pathol. Clin.*, vol. 11, no. 1, pp. 123–145, Mar. 2018, doi: 10.1016/j.path.2017.09.009.

[10] A. Bane, “Ductal carcinoma in situ: what the pathologist needs to know and why.,” *Int. J. Breast Cancer*, vol. 2013, p. 914053, 2013, doi: 10.1155/2013/914053.

[11] C. Petridis, “Molecular genetics of lobular breast cancer ductal carcinoma in situ,” 2018.

[12] F. Lüönd, S. Tiede, and G. Christofori, “Breast cancer as an example of tumour heterogeneity and tumour cell plasticity during malignant progression,” *Br. J. Cancer*, vol. 125, no. 2, pp. 164–175, 2021, doi: 10.1038/s41416-021-01328-7.

[13] C. G. Murphy and M. N. Dickler, “Endocrine resistance in hormone-responsive breast cancer: mechanisms and therapeutic strategies,” *Endocr. Relat. Cancer*, vol. 23, no. 8, pp. R337–R352, 2016, doi: 10.1530/ERC-16-0121.

[14] A. M. Brufsky and M. N. Dickler, “Estrogen Receptor-Positive Breast Cancer: Exploiting Signaling Pathways Implicated in Endocrine Resistance.,” *Oncologist*, vol. 23, no. 5, pp. 528–539, May 2018, doi: 10.1634/theoncologist.2017-0423.

[15] N. Fuentes and P. Silveyra, “Estrogen receptor signaling mechanisms.,” *Adv. Protein Chem. Struct. Biol.*, vol. 116, pp. 135–170, 2019, doi: 10.1016/bs.apcsb.2019.01.001.

[16] C. M. Klinge, “Estrogen receptor interaction with estrogen response

elements.," *Nucleic Acids Res.*, vol. 29, no. 14, pp. 2905–2919, Jul. 2001, doi: 10.1093/nar/29.14.2905.

[17] C. Gutierrez and R. Schiff, "HER2: biology, detection, and clinical implications.," *Arch. Pathol. Lab. Med.*, vol. 135, no. 1, pp. 55–62, Jan. 2011, doi: 10.5858/2010-0454-RAR.1.

[18] D. Harari and Y. Yarden, "Molecular mechanisms underlying ErbB2/HER2 action in breast cancer," *Oncogene*, vol. 19, no. 53, pp. 6102–6114, 2000, doi: 10.1038/sj.onc.1203973.

[19] T. Vu and F. X. Claret, "Trastuzumab: updated mechanisms of action and resistance in breast cancer.," *Front. Oncol.*, vol. 2, p. 62, 2012, doi: 10.3389/fonc.2012.00062.

[20] N. M. Almansour, "Triple-Negative Breast Cancer: A Brief Review About Epidemiology, Risk Factors, Signaling Pathways, Treatment and Role of Artificial Intelligence," *Front. Mol. Biosci.*, vol. 9, 2022, doi: 10.3389/fmolb.2022.836417.

[21] C. Yam, S. A. Mani, and S. L. Moulder, "Targeting the Molecular Subtypes of Triple Negative Breast Cancer: Understanding the Diversity to Progress the Field.," *Oncologist*, vol. 22, no. 9, pp. 1086–1093, Sep. 2017, doi: 10.1634/theoncologist.2017-0095.

[22] E. E. Newton, L. E. Mueller, S. M. Treadwell, C. A. Morris, and H. L. Machado, "Molecular Targets of Triple-Negative Breast Cancer: Where Do We Stand?," *Cancers (Basel).*, vol. 14, no. 3, Jan. 2022, doi: 10.3390/cancers14030482.

[23] W.-J. Ryu and J. H. Sohn, "Molecular Targets and Promising Therapeutics of Triple-Negative Breast Cancer.," *Pharmaceuticals (Basel).*, vol. 14, no. 10, Sep. 2021, doi: 10.3390/ph14101008.

[24] M. Hubalek, T. Czech, and H. Müller, "Biological Subtypes of Triple-Negative Breast Cancer," *Breast Care*, vol. 12, no. 1, pp. 8–14, 2017, doi: 10.1159/000455820.

[25] R. Buisson *et al.*, "Coupling of Homologous Recombination and the Checkpoint by ATR," *Mol. Cell*, vol. 65, no. 2, pp. 336–346, 2017, doi: https://doi.org/10.1016/j.molcel.2016.12.007.

[26] P. M. Schoonen *et al.*, "Premature mitotic entry induced by ATR inhibition potentiates olaparib inhibition-mediated genomic instability, inflammatory signaling, and cytotoxicity in BRCA2-deficient cancer cells," *Mol. Oncol.*, vol. 13, no. 11, pp. 2422–2440, Nov. 2019, doi: https://doi.org/10.1002/1878-0261.12573.

[27] A. Zhang, X. Wang, C. Fan, and X. Mao, "The Role of Ki67 in Evaluating Neoadjuvant Endocrine Therapy of Hormone Receptor-Positive Breast Cancer," *Front. Endocrinol. (Lausanne).*, vol. 12, 2021, doi: 10.3389/fendo.2021.687244.

[28] G. Cserni, E. Chmielik, B. Cserni, and T. Tot, "The new TNM-based staging of breast cancer," *Virchows Arch.*, vol. 472, no. 5, pp. 697–703, 2018, doi: 10.1007/s00428-018-2301-9.

[29] J. Koh and M. J. Kim, "Introduction of a New Staging System of Breast Cancer for Radiologists: An Emphasis on the Prognostic Stage.," *Korean J. Radiol.*, vol. 20, no. 1, pp. 69–82, Jan. 2019, doi: 10.3348/kjr.2018.0231.

[30] S. Kalli, A. Semine, S. Cohen, S. P. Naber, S. S. Makim, and M. Bahl, "American Joint Committee on Cancer's Staging System for Breast Cancer, Eighth Edition: What the Radiologist Needs to Know," *RadioGraphics*, vol. 38, no. 7, pp. 1921–1933, Sep. 2018, doi: 10.1148/rg.2018180056.

[31] N. Rachdaoui and D. K. Sarkar, “Effects of alcohol on the endocrine system.,” *Endocrinol. Metab. Clin. North Am.*, vol. 42, no. 3, pp. 593–615, Sep. 2013, doi: 10.1016/j.ecl.2013.05.008.

[32] N. Zeinomar *et al.*, “Alcohol consumption, cigarette smoking, and familial breast cancer risk: findings from the Prospective Family Study Cohort (ProF-SC).,” *Breast Cancer Res.*, vol. 21, no. 1, p. 128, Nov. 2019, doi: 10.1186/s13058-019-1213-1.

[33] L. S. Mørch, C. W. Skovlund, P. C. Hannaford, L. Iversen, S. Fielding, and Ø. Lidegaard, “Contemporary Hormonal Contraception and the Risk of Breast Cancer,” *N. Engl. J. Med.*, vol. 377, no. 23, pp. 2228–2239, Dec. 2017, doi: 10.1056/NEJMoa1700732.

[34] N. D. White, “Hormonal Contraception and Breast Cancer Risk.,” *Am. J. Lifestyle Med.*, vol. 12, no. 3, pp. 224–226, 2018, doi: 10.1177/1559827618754833.

[35] Y.-S. Sun *et al.*, “Risk Factors and Preventions of Breast Cancer.,” *Int. J. Biol. Sci.*, vol. 13, no. 11, pp. 1387–1397, 2017, doi: 10.7150/ijbs.21635.

[36] M. Kotepui, “Diet and risk of breast cancer.,” *Contemp. Oncol. (Poznan, Poland)*, vol. 20, no. 1, pp. 13–19, 2016, doi: 10.5114/wo.2014.40560.

[37] “Familial breast cancer: collaborative reanalysis of individual data from 52 epidemiological studies including 58 209 women with breast cancer and 101 986 women without the disease,” *Lancet*, vol. 358, no. 9291, pp. 1389–1399, Oct. 2001, doi: 10.1016/S0140-6736(01)06524-2.

[38] G. Tagliabue *et al.*, “Molecular Subtypes, Metastatic Pattern and Patient Age in Breast Cancer: An Analysis of Italian Network of Cancer Registries (AIRTUM) Data.,” *J. Clin. Med.*, vol. 10, no. 24, Dec. 2021, doi: 10.3390/jcm10245873.

[39] D. A. Hill, E. R. Prossnitz, M. Royce, and A. Nibbe, “Temporal trends in breast cancer survival by race and ethnicity: A population-based cohort study.,” *PLoS One*, vol. 14, no. 10, p. e0224064, 2019, doi: 10.1371/journal.pone.0224064.

[40] A. Hennigs *et al.*, “Prognosis of breast cancer molecular subtypes in routine clinical care: A large prospective cohort study,” *BMC Cancer*, vol. 16, no. 1, p. 734, Sep. 2016, doi: 10.1186/s12885-016-2766-3.

[41] F. Lumachi, A. Brunello, M. Maruzzo, U. Basso, and M. M. S. Basso, “Treatment of Estrogen Receptor-Positive Breast Cancer,” *Current Medicinal Chemistry*, vol. 20, no. 5. pp. 596–604, 2013, doi: http://dx.doi.org/10.2174/092986713804999303.

[42] N. P. McAndrew and R. S. Finn, “Clinical Review on the Management of Hormone Receptor–Positive Metastatic Breast Cancer,” *JCO Oncol. Pract.*, vol. 18, no. 5, pp. 319–327, Oct. 2021, doi: 10.1200/OP.21.00384.

[43] M. Shah, M. R. Nunes, and V. Stearns, “CDK4/6 Inhibitors: Game Changers in the Management of Hormone Receptor–Positive Advanced Breast Cancer?,” *Oncology (Williston Park).*, vol. 32, no. 5, pp. 216–222, May 2018.

[44] S. H. Lecker, A. L. Goldberg, and W. E. Mitch, “Protein Degradation by the Ubiquitin–Proteasome Pathway in Normal and Disease States,” *J. Am. Soc. Nephrol.*, vol. 17, no. 7, pp. 1807 LP – 1819, Jul. 2006, doi: 10.1681/ASN.2006010083.

[45] V. R. Gómez Román, J. C. Murray, and L. M. Weiner, “Chapter 1 - Antibody-Dependent Cellular Cytotoxicity (ADCC),” M. E. Ackerman and F. B. T.-A. F. Nimmerjahn, Eds. Boston: Academic Press, 2014, pp. 1–27.

[46] L. Arnould *et al.*, “Trastuzumab-based treatment of HER2-positive breast cancer: an antibody-dependent cellular cytotoxicity mechanism?,” *Br. J.*

Cancer, vol. 94, no. 2, pp. 259–267, Jan. 2006, doi: 10.1038/sj.bjc.6602930.
[47] N. G. Adel, “Current treatment landscape and emerging therapies for metastatic triple-negative breast cancer.,” *Am. J. Manag. Care*, vol. 27, no. 5 Suppl, pp. S87–S96, Apr. 2021, doi: 10.37765/ajmc.2021.88626.
[48] K.-A. Won and C. Spruck, “Triple-negative breast cancer therapy: Current and future perspectives (Review).,” *Int. J. Oncol.*, vol. 57, no. 6, pp. 1245–1261, Dec. 2020, doi: 10.3892/ijo.2020.5135.
[49] E. A. Mittendorf *et al.*, “PD-L1 expression in triple-negative breast cancer.,” *Cancer Immunol. Res.*, vol. 2, no. 4, pp. 361–370, Apr. 2014, doi: 10.1158/2326-6066.CIR-13-0127.
[50] P. Schmid *et al.*, “Atezolizumab and Nab-Paclitaxel in Advanced Triple-Negative Breast Cancer,” *N. Engl. J. Med.*, vol. 379, no. 22, pp. 2108–2121, Oct. 2018, doi: 10.1056/NEJMoa1809615.
[51] J. Kulwatno, X. Gong, R. DeVaux, J. I. Herschkowitz, and K. L. Mills, “An Organotypic Mammary Duct Model Capturing Matrix Mechanics-Dependent Ductal Carcinoma In Situ Progression.,” *Tissue Eng. Part A*, vol. 27, no. 7–8, pp. 454–466, Apr. 2021, doi: 10.1089/ten.TEA.2020.0239.
[52] R. M. Tamimi *et al.*, “Comparison of molecular phenotypes of ductal carcinoma in situand invasive breast cancer,” *Breast Cancer Res.*, vol. 10, no. 4, p. R67, 2008, doi: 10.1186/bcr2128.
[53] J. Wu, J. Jiang, B. Chen, K. Wang, Y. Tang, and X. Liang, “Plasticity of cancer cell invasion: Patterns and mechanisms,” *Transl. Oncol.*, vol. 14, no. 1, p. 100899, 2021, doi: https://doi.org/10.1016/j.tranon.2020.100899.
[54] I. Januškevičienė and V. Petrikaitė, “Heterogeneity of breast cancer: The importance of interaction between different tumor cell populations.,” *Life Sci.*, vol. 239, p. 117009, Dec. 2019, doi: 10.1016/j.lfs.2019.117009.
[55] Y. Guo, C. A. Arciero, R. Jiang, M. Behera, L. Peng, and X. Li, “Different Breast Cancer Subtypes Show Different Metastatic Patterns: A Study from A Large Public Database.,” *Asian Pac. J. Cancer Prev.*, vol. 21, no. 12, pp. 3587–3593, Dec. 2020, doi: 10.31557/APJCP.2020.21.12.3587.
[56] W. Xiao *et al.*, “Breast cancer subtypes and the risk of distant metastasis at initial diagnosis: a population-based study.,” *Cancer Manag. Res.*, vol. 10, pp. 5329–5338, 2018, doi: 10.2147/CMAR.S176763.
[57] Y. Gong, Y.-R. Liu, P. Ji, X. Hu, and Z.-M. Shao, “Impact of molecular subtypes on metastatic breast cancer patients: a SEER population-based study.,” *Sci. Rep.*, vol. 7, p. 45411, Mar. 2017, doi: 10.1038/srep45411.
[58] D. J. P. van Uden *et al.*, “Metastatic behavior and overall survival according to breast cancer subtypes in stage IV inflammatory breast cancer.,” *Breast Cancer Res.*, vol. 21, no. 1, p. 113, Oct. 2019, doi: 10.1186/s13058-019-1201-5.
[59] Q. Wu *et al.*, “Breast cancer subtypes predict the preferential site of distant metastases: a SEER based study.,” *Oncotarget*, vol. 8, no. 17, pp. 27990–27996, Apr. 2017, doi: 10.18632/oncotarget.15856.
[60] J. Fares, M. Y. Fares, H. H. Khachfe, H. A. Salhab, and Y. Fares, “Molecular principles of metastasis: a hallmark of cancer revisited,” *Signal Transduct. Target. Ther.*, vol. 5, no. 1, p. 28, 2020, doi: 10.1038/s41392-020-0134-x.
[61] D. F. Quail and J. A. Joyce, “Microenvironmental regulation of tumor progression and metastasis.,” *Nat. Med.*, vol. 19, no. 11, pp. 1423–1437, Nov. 2013, doi: 10.1038/nm.3394.
[62] A. B. Bloom and M. H. Zaman, “Influence of the microenvironment on cell fate

determination and migration.," *Physiol. Genomics*, vol. 46, no. 9, pp. 309–314, May 2014, doi: 10.1152/physiolgenomics.00170.2013.

[63] M. E. Fiori, S. Di Franco, L. Villanova, P. Bianca, G. Stassi, and R. De Maria, "Cancer-associated fibroblasts as abettors of tumor progression at the crossroads of EMT and therapy resistance.," *Mol. Cancer*, vol. 18, no. 1, p. 70, Mar. 2019, doi: 10.1186/s12943-019-0994-2.

[64] G. W. Pearson, "Control of Invasion by Epithelial-to-Mesenchymal Transition Programs during Metastasis," *J. Clin. Med.*, vol. 8, no. 5, 2019, doi: 10.3390/jcm8050646.

[65] K. M. Yamada and M. Sixt, "Mechanisms of 3D cell migration," *Nat. Rev. Mol. Cell Biol.*, vol. 20, no. 12, pp. 738–752, 2019, doi: 10.1038/s41580-019-0172-9.

[66] P. Lu, K. Takai, V. M. Weaver, and Z. Werb, "Extracellular matrix degradation and remodeling in development and disease.," *Cold Spring Harb. Perspect. Biol.*, vol. 3, no. 12, Dec. 2011, doi: 10.1101/cshperspect.a005058.

[67] V. te Boekhorst and P. Friedl, "Chapter Seven - Plasticity of Cancer Cell Invasion—Mechanisms and Implications for Therapy," in *Molecular and Cellular Basis of Metastasis: Road to Therapy*, vol. 132, D. R. Welch and P. B. B. T.-A. in C. R. Fisher, Eds. Academic Press, 2016, pp. 209–264.

[68] R. Mayor and S. Etienne-Manneville, "The front and rear of collective cell migration," *Nat. Rev. Mol. Cell Biol.*, vol. 17, no. 2, pp. 97–109, 2016, doi: 10.1038/nrm.2015.14.

[69] A. Haeger *et al.*, "Collective cancer invasion forms an integrin-dependent radioresistant niche," *J. Exp. Med.*, vol. 217, no. 1, p. e20181184, Oct. 2019, doi: 10.1084/jem.20181184.

[70] Ş. COMŞA, A. M. CÎMPEAN, and M. RAICA, "The Story of MCF-7 Breast Cancer Cell Line: 40 years of Experience in Research," *Anticancer Res.*, vol. 35, no. 6, pp. 3147 LP – 3154, Jun. 2015.

[71] E. E. Sweeney, R. E. McDaniel, P. Y. Maximov, P. Fan, and V. C. Jordan, "Models and mechanisms of acquired antihormone resistance in breast cancer: significant clinical progress despite limitations," *Horm. Mol. Biol. Clin. Investig.*, vol. 9, no. 2, pp. 143–163, 2012, doi: doi:10.1515/hmbci-2011-0004.

[72] Ş. COMŞA, A. M. CÎMPEAN, and M. RAICA, "The Story of MCF-7 Breast Cancer Cell Line: 40 years of Experience in Research," *Anticancer Res.*, vol. 35, no. 6, pp. 3147 LP – 3154, Jun. 2015.

[73] S. Borges, E. A. Perez, E. A. Thompson, D. C. Radisky, X. J. Geiger, and P. Storz, "Effective Targeting of Estrogen Receptor-Negative Breast Cancers with the Protein Kinase D Inhibitor CRT0066101," *Mol. Cancer Ther.*, vol. 14, no. 6, pp. 1306–1316, Jun. 2015, doi: 10.1158/1535-7163.MCT-14-0945.

[74] H. Huang, Y. Ding, X. S. Sun, and T. A. Nguyen, "Peptide Hydrogelation and Cell Encapsulation for 3D Culture of MCF-7 Breast Cancer Cells," *PLoS One*, vol. 8, no. 3, p. e59482, Mar. 2013.

[75] Y. Qu *et al.*, "Evaluation of MCF10A as a Reliable Model for Normal Human Mammary Epithelial Cells.," *PLoS One*, vol. 10, no. 7, p. e0131285, 2015, doi: 10.1371/journal.pone.0131285.

[76] G. Martínez-Revollar *et al.*, "Heterogeneity between triple negative breast cancer cells due to differential activation of Wnt and PI3K/AKT pathways," *Exp. Cell Res.*, vol. 339, no. 1, pp. 67–80, 2015, doi: https://doi.org/10.1016/j.yexcr.2015.10.006.

[77] A. Kabała-Dzik *et al.*, "Migration Rate Inhibition of Breast Cancer Cells Treated

by Caffeic Acid and Caffeic Acid Phenethyl Ester: An In Vitro Comparison Study.," *Nutrients*, vol. 9, no. 10, Oct. 2017, doi: 10.3390/nu9101144.

[78] A. J. Berger *et al.*, "Scaffold stiffness influences breast cancer cell invasion via EGFR-linked Mena upregulation and matrix remodeling.," *Matrix Biol.*, vol. 85–86, pp. 80–93, Jan. 2020, doi: 10.1016/j.matbio.2019.07.006.

[79] M. Kapałczyńska *et al.*, "2D and 3D cell cultures - a comparison of different types of cancer cell cultures," *Arch. Med. Sci.*, vol. 14, no. 4, pp. 910–919, Jun. 2018, doi: 10.5114/aoms.2016.63743.

[80] C.-P. Segeritz and L. Vallier, "Cell Culture: Growing Cells as Model Systems In Vitro," *Basic Sci. Methods Clin. Res.*, pp. 151–172, 2017, doi: 10.1016/B978-0-12-803077-6.00009-6.

[81] F. G. Kern *et al.*, "Transfected MCF-7 cells as a model for breast-cancer progression.," *Breast Cancer Res. Treat.*, vol. 31, no. 2–3, pp. 153–165, 1994, doi: 10.1007/BF00666149.

[82] K. M. Yamada and E. Cukierman, "Modeling Tissue Morphogenesis and Cancer in 3D," *Cell*, vol. 130, no. 4, pp. 601–610, 2007, doi: 10.1016/j.cell.2007.08.006.

[83] I. Holen, V. Speirs, B. Morrissey, and K. Blyth, "In vivo models in breast cancer research: progress, challenges and future directions," *Dis. Model. Mech.*, vol. 10, no. 4, pp. 359–371, Apr. 2017, doi: 10.1242/dmm.028274.

[84] L. E. Dobrolecki *et al.*, "Patient-derived xenograft (PDX) models in basic and translational breast cancer research.," *Cancer Metastasis Rev.*, vol. 35, no. 4, pp. 547–573, Dec. 2016, doi: 10.1007/s10555-016-9653-x.

[85] T. Murayama and N. Gotoh, "Patient-Derived Xenograft Models of Breast Cancer and Their Application," *Cells*, vol. 8, no. 6, p. 621, Jun. 2019, doi: 10.3390/cells8060621.

[86] T. F. Vandamme, "Use of rodents as models of human diseases," *J. Pharm. Bioallied Sci.*, vol. 6, no. 1, pp. 2–9, Jan. 2014, doi: 10.4103/0975-7406.124301.

[87] M. W. Tibbitt and K. S. Anseth, "Hydrogels as extracellular matrix mimics for 3D cell culture," *Biotechnol. Bioeng.*, vol. 103, no. 4, pp. 655–663, Jul. 2009, doi: 10.1002/bit.22361.

[88] M. M. Vantangoli, S. J. Madnick, S. M. Huse, P. Weston, and K. Boekelheide, "MCF-7 Human Breast Cancer Cells Form Differentiated Microtissues in Scaffold-Free Hydrogels," *PLoS One*, vol. 10, no. 8, pp. e0135426–e0135426, Aug. 2015, doi: 10.1371/journal.pone.0135426.

[89] Y. Wang *et al.*, "3D hydrogel breast cancer models for studying the effects of hypoxia on epithelial to mesenchymal transition," *Oncotarget*, vol. 9, no. 63, pp. 32191–32203, Aug. 2018, doi: 10.18632/oncotarget.25891.

[90] H. Huang, Y. Ding, X. S. Sun, and T. A. Nguyen, "Peptide Hydrogelation and Cell Encapsulation for 3D Culture of MCF-7 Breast Cancer Cells," *PLoS One*, vol. 8, no. 3, p. e59482, Mar. 2013.

[91] J. Kim, B.-K. Koo, and J. A. Knoblich, "Human organoids: model systems for human biology and medicine," *Nat. Rev. Mol. Cell Biol.*, vol. 21, no. 10, pp. 571–584, 2020, doi: 10.1038/s41580-020-0259-3.

[92] F. Schutgens and H. Clevers, "Human Organoids: Tools for Understanding Biology and Treating Diseases," *Annu. Rev. Pathol. Mech. Dis.*, vol. 15, no. 1, pp. 211–234, Jan. 2020, doi: 10.1146/annurev-pathmechdis-012419-032611.

[93] M. Hofer and M. P. Lutolf, "Engineering organoids," *Nat. Rev. Mater.*, vol. 6, no. 5, pp. 402–420, 2021, doi: 10.1038/s41578-021-00279-y.

[94] A. Bruna *et al.*, “A Biobank of Breast Cancer Explants with Preserved Intra-tumor Heterogeneity to Screen Anticancer Compounds,” *Cell*, vol. 167, no. 1, pp. 260-274.e22, Sep. 2016, doi: 10.1016/j.cell.2016.08.041.
[95] S. Andrew Octavian and W. Ying Pei, “Organoids as Reliable Breast Cancer Study Models: An Update,” *Int. J. Oncol. Res.*, vol. 1, no. 2, pp. 1–11, 2018, doi: 10.23937/ijor-2017/1710008.
[96] J. M. Rosenbluth *et al.*, “Organoid cultures from normal and cancer-prone human breast tissues preserve complex epithelial lineages,” *Nat. Commun.*, vol. 11, no. 1, p. 1711, 2020, doi: 10.1038/s41467-020-15548-7.
[97] J. Stingl, C. J. Eaves, I. Zandieh, and J. T. Emerman, “Characterization of bipotent mammary epithelial progenitor cells in normal adult human breast tissue.,” *Breast Cancer Res. Treat.*, vol. 67, no. 2, pp. 93–109, May 2001, doi: 10.1023/a:1010615124301.
[98] M. Huch, J. A. Knoblich, M. P. Lutolf, and A. Martinez-arias, “The hope and the hype of organoid research,” pp. 938–941, 2017, doi: 10.1242/dev.150201.
[99] M. Roger *et al.*, “Bioengineering the microanatomy of human skin,” *J. Anat.*, vol. 234, no. 4, pp. 438–455, 2019, doi: 10.1111/joa.12942.
[100] N. J. Darling, C. L. Mobbs, A. L. González-Hau, M. Freer, and S. Przyborski, “Bioengineering Novel in vitro Co-culture Models That Represent the Human Intestinal Mucosa With Improved Caco-2 Structure and Barrier Function ,” *Frontiers in Bioengineering and Biotechnology* , vol. 8. p. 992, 2020.
[101] E. J. Davies *et al.*, “Capturing complex tumour biology in vitro: histological and molecular characterisation of precision cut slices,” *Sci. Rep.*, vol. 5, no. 1, p. 17187, 2015, doi: 10.1038/srep17187.
[102] F. Kottakis, C. Polytarchou, P. Foltopoulou, I. Sanidas, S. C. Kampranis, and P. N. Tsichlis, “FGF-2 regulates cell proliferation, migration, and angiogenesis through an NDY1/KDM2B-miR-101-EZH2 pathway.,” *Mol. Cell*, vol. 43, no. 2, pp. 285–298, Jul. 2011, doi: 10.1016/j.molcel.2011.06.020.
[103] J. Liang, S. Balachandra, S. Ngo, and L. E. O’Brien, “Feedback regulation of steady-state epithelial turnover and organ size,” *Nature*, vol. 548, no. 7669, pp. 588–591, 2017, doi: 10.1038/nature23678.
[104] P. Lu and Y. Lu, “Born to Run? Diverse Modes of Epithelial Migration,” *Front. Cell Dev. Biol.*, vol. 9, 2021, doi: 10.3389/fcell.2021.704939.
[105] J. M. Guinebretière, E. Menet, A. Tardivon, P. Cherel, and D. Vanel, “Normal and pathological breast, the histological basis,” *Eur. J. Radiol.*, vol. 54, no. 1, pp. 6–14, 2005, doi: https://doi.org/10.1016/j.ejrad.2004.11.020.
[106] S. Sanati, “Morphologic and Molecular Features of Breast Ductal Carcinoma in Situ,” *Am. J. Pathol.*, vol. 189, no. 5, pp. 946–955, 2019, doi: https://doi.org/10.1016/j.ajpath.2018.07.031.
[107] Y. Zhang, G. S. Chia, C. Y. Tham, and S. Jha, “Live-imaging of Breast Epithelial Cell Migration After the Transient Depletion of TIP60.,” *J. Vis. Exp.*, no. 130, Dec. 2017, doi: 10.3791/56248.
[108] M. Botlagunta, P. Winnard, and V. Raman, “Neoplastic transformation of breast epithelial cells by genotoxic stress,” *BMC Cancer*, vol. 10, p. 343, Jun. 2010, doi: 10.1186/1471-2407-10-343.
[109] A. Vanlaeys *et al.*, “Cadmium exposure enhances cell migration and invasion through modulated TRPM7 channel expression,” *Arch. Toxicol.*, vol. 94, no. 3, pp. 735–747, 2020, doi: 10.1007/s00204-020-02674-w.
[110] N. H. Barrak, M. A. Khajah, and Y. A. Luqmani, “Hypoxic environment may enhance migration/penetration of endocrine resistant MCF7- derived breast

cancer cells through monolayers of other non-invasive cancer cells in vitro," *Sci. Rep.*, vol. 10, no. 1, p. 1127, 2020, doi: 10.1038/s41598-020-58055-x.

[111] C. Furtado, M. Marcondes, M. Sola-Penna, S. Maisa, and P. Zancan, "Clotrimazole Preferentially Inhibits Human Breast Cancer Cell Proliferation, Viability and Glycolysis," *PLoS One*, vol. 7, p. e30462, Feb. 2012, doi: 10.1371/journal.pone.0030462.

[112] M. Kapałczyńska *et al.*, "2D and 3D cell cultures - a comparison of different types of cancer cell cultures," *Arch. Med. Sci.*, vol. 14, no. 4, pp. 910–919, Jun. 2018, doi: 10.5114/aoms.2016.63743.

[113] I. Agarwal and L. Blanco, "Breast General Histology," *Histology. PathologyOutlines.com*. [Online]. Available: https://www.pathologyoutlines.com/topic/breastnormal.html. [Accessed: 16-Jan-2023].

[114] K. R. Ammann, K. J. DeCook, M. Li, and M. J. Slepian, "Migration versus proliferation as contributor to in vitro wound healing of vascular endothelial and smooth muscle cells.," *Exp. Cell Res.*, vol. 376, no. 1, pp. 58–66, Mar. 2019, doi: 10.1016/j.yexcr.2019.01.011.

[115] X. Zhang, Y. Luo, and Q. Li, "TMED3 Promotes Proliferation and Migration in Breast Cancer Cells by Activating Wnt/β-Catenin Signaling.," *Onco. Targets. Ther.*, vol. 13, pp. 5819–5830, 2020, doi: 10.2147/OTT.S250766.

[116] S. F. Ghannam, C. S. Rutland, C. Allegrucci, N. P. Mongan, and E. Rakha, "Defining invasion in breast cancer: the role of basement membrane," *J. Clin. Pathol.*, vol. 76, no. 1, pp. 11–18, 2023, doi: 10.1136/jcp-2022-208584.

[117] M. A. Morrissey and D. R. Sherwood, "An active role for basement membrane assembly and modification in tissue sculpting.," *J. Cell Sci.*, vol. 128, no. 9, pp. 1661–1668, May 2015, doi: 10.1242/jcs.168021.

[118] C. Frantz, K. M. Stewart, and V. M. Weaver, "The extracellular matrix at a glance," *J. Cell Sci.*, vol. 123, no. Pt 24, pp. 4195–4200, Dec. 2010, doi: 10.1242/jcs.023820.

[119] E. A. Aisenbrey and W. L. Murphy, "Synthetic alternatives to Matrigel.," *Nat. Rev. Mater.*, vol. 5, no. 7, pp. 539–551, Jul. 2020, doi: 10.1038/s41578-020-0199-8.

[120] M. Roger *et al.*, "Bioengineering the microanatomy of human skin," *J. Anat.*, vol. 234, no. 4, pp. 438–455, Apr. 2019, doi: https://doi.org/10.1111/joa.12942.

[121] D. S. Hill *et al.*, "A Novel Fully Humanized 3D Skin Equivalent to Model Early Melanoma Invasion," *Mol. Cancer Ther.*, vol. 14, no. 11, pp. 2665–2673, Nov. 2015, doi: 10.1158/1535-7163.MCT-15-0394.

[122] R. T. Kendall and C. A. Feghali-Bostwick, "Fibroblasts in fibrosis: novel roles and mediators.," *Front. Pharmacol.*, vol. 5, p. 123, 2014, doi: 10.3389/fphar.2014.00123.

[123] A. C. Degnim *et al.*, "Histologic findings in normal breast tissues: comparison to reduction mammaplasty and benign breast disease tissues.," *Breast Cancer Res. Treat.*, vol. 133, no. 1, pp. 169–177, May 2012, doi: 10.1007/s10549-011-1746-1.

[124] A. Guzman, V. Sánchez Alemany, Y. Nguyen, C. R. Zhang, and L. J. Kaufman, "A novel 3D in vitro metastasis model elucidates differential invasive strategies during and after breaching basement membrane," *Biomaterials*, vol. 115, pp. 19–29, 2017, doi: https://doi.org/10.1016/j.biomaterials.2016.11.014.

[125] I. Yakavets, A. Francois, A. Benoit, J.-L. Merlin, L. Bezdetnaya, and G. Vogin, "Advanced co-culture 3D breast cancer model for investigation of fibrosis

induced by external stimuli: optimization study," *Sci. Rep.*, vol. 10, no. 1, p. 21273, 2020, doi: 10.1038/s41598-020-78087-7.

[126] J. Chang and O. Chaudhuri, "Beyond proteases: Basement membrane mechanics and cancer invasion.," *J. Cell Biol.*, vol. 218, no. 8, pp. 2456–2469, Aug. 2019, doi: 10.1083/jcb.201903066.

[127] A. Köhrmann, U. Kammerer, M. Kapp, J. Dietl, and J. Anacker, "Expression of matrix metalloproteinases (MMPs) in primary human breast cancer and breast cancer cell lines: New findings and review of the literature.," *BMC Cancer*, vol. 9, p. 188, Jun. 2009, doi: 10.1186/1471-2407-9-188.

[128] E.-S. Kim, M.-S. Kim, and A. Moon, "TGF-β-induced upregulation of MMP-2 and MMP-9 depends on p38 MAPK, but not ERK signaling in MCF10A human breast epithelial cells," *Int J Oncol*, vol. 25, no. 5, pp. 1375–1382, 2004, doi: 10.3892/ijo.25.5.1375.

[129] M. Endres, S. Kneitz, M. F. Orth, R. K. Perera, A. Zernecke, and E. Butt, "Regulation of matrix metalloproteinases (MMPs) expression and secretion in MDA-MB-231 breast cancer cells by LIM and SH3 protein 1 (LASP1).," *Oncotarget*, vol. 7, no. 39, pp. 64244–64259, Sep. 2016, doi: 10.18632/oncotarget.11720.

[130] H. Eslami Amirabadi *et al.*, "Characterizing the invasion of different breast cancer cell lines with distinct E-cadherin status in 3D using a microfluidic system," *Biomed. Microdevices*, vol. 21, no. 4, p. 101, 2019, doi: 10.1007/s10544-019-0450-5.

[131] D. F. Quail, T. J. Maciel, K. Rogers, and L. M. Postovit, "A Unique 3D In Vitro Cellular Invasion Assay," *SLAS Discov.*, vol. 17, no. 8, pp. 1088–1095, 2012, doi: https://doi.org/10.1177/1087057112449863.

[132] X. Catteau, P. Simon, M. Vanhaeverbeek, and J.-C. Noël, "Variable Stromal Periductular Expression of CD34 and Smooth Muscle Actin (SMA) in Intraductal Carcinoma of the Breast," *PLoS One*, vol. 8, no. 3, p. e57773, Mar. 2013.

[133] L. P. Ivers *et al.*, "Dynamic and influential interaction of cancer cells with normal epithelial cells in 3D culture," *Cancer Cell Int.*, vol. 14, no. 1, p. 108, 2014, doi: 10.1186/s12935-014-0108-6.

[134] P. A. Kenny *et al.*, "The morphologies of breast cancer cell lines in three-dimensional assays correlate with their profiles of gene expression," *Mol. Oncol.*, vol. 1, no. 1, pp. 84–96, 2007, doi: https://doi.org/10.1016/j.molonc.2007.02.004.

[135] P. Zhang, Y. Tang, N.-G. Li, Y. Zhu, and J.-A. Duan, "Bioactivity and chemical synthesis of caffeic acid phenethyl ester and its derivatives.," *Molecules*, vol. 19, no. 10, pp. 16458–16476, Oct. 2014, doi: 10.3390/molecules191016458.

[136] A. Kabała-Dzik, A. Rzepecka-Stojko, R. Kubina, R. D. Wojtyczka, E. Buszman, and J. Stojko, "Caffeic Acid Versus Caffeic Acid Phenethyl Ester in the Treatment of Breast Cancer MCF-7 Cells: Migration Rate Inhibition.," *Integr. Cancer Ther.*, vol. 17, no. 4, pp. 1247–1259, Dec. 2018, doi: 10.1177/1534735418801521.

[137] S. P. Fraser, F. Hemsley, and M. B. A. Djamgoz, "Caffeic acid phenethyl ester: Inhibition of metastatic cell behaviours via voltage-gated sodium channel in human breast cancer in vitro," *Int. J. Biochem. Cell Biol.*, vol. 71, pp. 111–118, 2016, doi: https://doi.org/10.1016/j.biocel.2015.12.012.

[138] H. Sonoki *et al.*, "Caffeic acid phenethyl ester down-regulates claudin-2 expression at the transcriptional and post-translational levels and enhances

chemosensitivity to doxorubicin in lung adenocarcinoma A549 cells," *J. Nutr. Biochem.*, vol. 56, pp. 205–214, 2018, doi: https://doi.org/10.1016/j.jnutbio.2018.02.016.

[139] M. Muguruma *et al.*, "Differences in drug sensitivity between two-dimensional and three-dimensional culture systems in triple-negative breast cancer cell lines," *Biochem. Biophys. Res. Commun.*, vol. 533, no. 3, pp. 268–274, 2020, doi: https://doi.org/10.1016/j.bbrc.2020.08.075.

[140] S. Breslin and L. O'Driscoll, "The relevance of using 3D cell cultures, in addition to 2D monolayer cultures, when evaluating breast cancer drug sensitivity and resistance.," *Oncotarget*, vol. 7, no. 29, pp. 45745–45756, Jul. 2016, doi: 10.18632/oncotarget.9935.

[141] T. Yamada *et al.*, "Receptor activator of NF-κB ligand induces cell adhesion and integrin α2 expression via NF-κB in head and neck cancers," *Sci. Rep.*, vol. 6, no. 1, p. 23545, 2016, doi: 10.1038/srep23545.

[142] P. M. Angel *et al.*, "Extracellular Matrix Imaging of Breast Tissue Pathologies by MALDI-Imaging Mass Spectrometry.," *Proteomics. Clin. Appl.*, vol. 13, no. 1, p. e1700152, Jan. 2019, doi: 10.1002/prca.201700152.

[143] G. Kaur and J. M. Dufour, "Cell lines: Valuable tools or useless artifacts.," *Spermatogenesis*, vol. 2, no. 1, pp. 1–5, Jan. 2012, doi: 10.4161/spmg.19885.

[144] C. Pan, C. Kumar, S. Bohl, U. Klingmueller, and M. Mann, "Comparative proteomic phenotyping of cell lines and primary cells to assess preservation of cell type-specific functions.," *Mol. Cell. Proteomics*, vol. 8, no. 3, pp. 443–450, Mar. 2009, doi: 10.1074/mcp.M800258-MCP200.

[145] R. Weinmüllner *et al.*, "Organotypic human skin culture models constructed with senescent fibroblasts show hallmarks of skin aging," *npj Aging Mech. Dis.*, vol. 6, no. 1, p. 4, 2020, doi: 10.1038/s41514-020-0042-x.

[146] E. Jabbari, J. Leijten, Q. Xu, and A. Khademhosseini, "The matrix reloaded: the evolution of regenerative hydrogels," *Mater. Today*, vol. 19, no. 4, pp. 190–196, 2016, doi: https://doi.org/10.1016/j.mattod.2015.10.005.

[147] Ž. P. Kačarević *et al.*, "An Introduction to 3D Bioprinting: Possibilities, Challenges and Future Aspects.," *Mater. (Basel, Switzerland)*, vol. 11, no. 11, Nov. 2018, doi: 10.3390/ma11112199.

[148] E. E. Antoine, P. P. Vlachos, and M. N. Rylander, "Review of collagen I hydrogels for bioengineered tissue microenvironments: characterization of mechanics, structure, and transport.," *Tissue Eng. Part B. Rev.*, vol. 20, no. 6, pp. 683–696, Dec. 2014, doi: 10.1089/ten.TEB.2014.0086.

[149] S. K. Seidlits, C. T. Drinnan, R. R. Petersen, J. B. Shear, L. J. Suggs, and C. E. Schmidt, "Fibronectin–hyaluronic acid composite hydrogels for three-dimensional endothelial cell culture," *Acta Biomater.*, vol. 7, no. 6, pp. 2401–2409, 2011, doi: https://doi.org/10.1016/j.actbio.2011.03.024.

[150] D. Barros *et al.*, "Engineering hydrogels with affinity-bound laminin as 3D neural stem cell culture systems.," *Biomater. Sci.*, vol. 7, no. 12, pp. 5338–5349, Nov. 2019, doi: 10.1039/c9bm00348g.

[151] T. Alkasalias, L. Moyano-Galceran, M. Arsenian-Henriksson, and K. Lehti, "Fibroblasts in the Tumor Microenvironment: Shield or Spear?," *Int. J. Mol. Sci.*, vol. 19, no. 5, May 2018, doi: 10.3390/ijms19051532.

[152] F. Wu *et al.*, "Signaling pathways in cancer-associated fibroblasts and targeted therapy for cancer.," *Signal Transduct. Target. Ther.*, vol. 6, no. 1, p. 218, Jun. 2021, doi: 10.1038/s41392-021-00641-0.